Engineering

U.S.
f

Journal of Research

of the

National Bureau of Standards

MARCH 1938

VOLUME 20 NUMBER 3

U. S. DEPARTMENT OF COMMERCE
Daniel C. Roper, Secretary
NATIONAL BUREAU OF STANDARDS
A. V. Astin, Director

MARCH • 1934
VOLUME • 12
NUMBER • 3

JOURNAL OF RESEARCH

of the

NATIONAL BUREAU OF STANDARDS

PERIODICALS OF THE NATIONAL BUREAU OF STANDARDS

The National Bureau of Standards is engaged in fundamental and applied research in physics, chemistry, mathematics, and engineering. Projects are conducted in [illegible] fields: electricity, optics and metrology, heat and power, atomic and radiation physics, chemistry, mechanics, organic and fibrous materials, metallurgy, mineral products, building technology, applied mathematics, aeronautics, and radio propagation. The Bureau has custody of the national standards of measurement and conducts research leading to the improvement of scientific and engineering standards and of techniques and methods of measurement. Testing methods and instruments are developed; physical constants and properties of materials are determined; and technical processes are investigated.

JOURNAL OF RESEARCH

Internationally known as a leading scientific periodical, the Journal presents research papers by authorities in the specialized fields of physics, mathematics, chemistry, and engineering. Complete details of the work are presented, including laboratory data, experimental procedures, and theoretical and mathematical analyses. Annual subscription: domestic, $5.00; foreign, $6.00.

TECHNICAL NEWS BULLETIN

Summaries of current research at the National Bureau of Standards are published each month in the Technical News Bulletin. The articles are brief, with emphasis on the results of research, given on the basis of their scientific or technologic importance. Lists of all [illegible] publications during the preceding month are given, including Research Papers, Handbooks, Applied [illegible] Series, [illegible] and Miscellaneous Reports. [illegible] issue contains 12 [illegible] pages [illegible]. Annual subscription, domestic, $1.00; foreign, $1.25.

SPECIAL RADIO PROPAGATION [illegible]

This publication provides information necessary for [illegible] the best frequencies for communication between any two points on the world at any time during the month. The data are important to all [illegible] communications and navigation, including broadcasting, aeronautics, commercial, and [illegible], as well as to investigators of [illegible] and [illegible]. Issued [illegible], covering a period of [illegible] three months in advance. Subscription 10 cents per copy, [illegible] postpaid. Annual subscription: [illegible].

[illegible] Sections [illegible] of Government Printing Office, Washington, D. C.

[illegible] has been approved [illegible]

Journal of Research of the National Bureau of Standards Vol. 52, No. 3, March 1954 Research Paper 2479

Precise Measurements With Bingham Viscometers and Cannon Master Viscometers

J. F. Swindells, R. C. Hardy, and R. L. Cottington

A critical study has been made of the techniques used at the National Bureau of Standards with Bingham viscometers and Cannon kinematic viscometers. All corrections applicable to measurements with these instruments were critically examined. Instruments of each type were calibrated using the viscosity of water at 20° C as the primary viscosity standard. The viscometers were used to determine the viscosities of four hydrocarbon liquids in the range 0.4 to 40 centipoises. With each liquid, the values obtained in the two types of viscometers were in agreement by 0.05 percent or better, indicating that no gross error was involved in the use of either instrument. It is considered, however, that the inherent relative simplicity of operation of the kinematic viscometer makes it a preferable instrument for this type of measurement.

1. Introduction

As the result of a recent determination [1] [1], the National Bureau of Standards on July 1, 1953, adopted the value of 1.002 centipoises (cp) for the absolute viscosity of water at 20° C as the primary standard for viscosity determinations. The American Society for Testing Materials, The National Physical Laboratory in England, and the Physikalisch Technischen Bundesanstalt in Germany have concurred in this action. Previous to this, the values of the secondary standards of viscosity issued by the Bureau were based upon 1.005 cp for the viscosity of water at 20° C. In connection with the reevaluation of the secondary standards on the basis of the new value for water, a comparative study has been made of the use of two types of viscometers for relating the viscosities of other liquids to that of water as a primary standard. Bingham viscometers and Cannon viscometers were used, and comparisons were made of the viscosities of four hydrocarbon liquids in the range 0.4 to 40 cp and of the viscosity of each liquid as determined in each type of instrument. This paper presents in some detail the techniques used in making these determinations to describe the methods employed in evaluating the National Bureau of Standards standard viscosity samples and to call attention to the magnitude of certain corrections often neglected in viscometry. The extension of these techniques to the calibration of viscometers with larger capillaries suitable for the measurement of the viscosities of more viscous liquids is relatively simple and involves the same methods as are covered here.

2. The Bingham Viscometer

2.1. General

A short treatment of the use of the Bingham viscometer, shown diagrammatically in figure 1, has been given previously [2], and it will be assumed that the reader has some familiarity with the instrument. With the usual procedure, pressure is applied to the right limb of the viscometer, and the rate of flow is determined by measuring the time required for the meniscus in the left limb to pass from the fiducial mark d to mark c. To avoid the necessity for drainage corrections, each determination is made with the bulb A initially dry. This is accomplished by introducing the sample into bulb B with a special pipet, sufficient liquid being added to fill the viscometer between the marks d and g at the test temperature. With the exception of certain calibration runs with water, the viscometer is cleaned and a fresh sample is introduced for each measurement. By this procedure the volume of flow is kept constant for each instrument regardless of the viscosity or rate of flow.

Pressure is applied to the liquid in the viscometer by air supplied from a tank having a capacity (about 60,000 cm^3) sufficiently large that the increase in volume (about 4 cm^3) in the pressure system during the flow of liquid from bulb B causes no significant reduction in pressure. The tank is thermally insulated to prevent rapid changes in its temperature

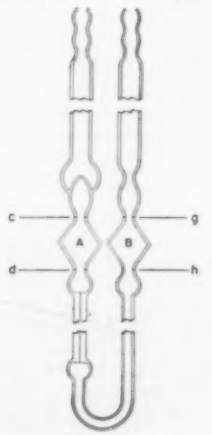

FIGURE 1. *Bingham viscometer.*

[1] Figures in brackets indicate the literature references at the end of this paper.

with fluctuations in the ambient temperature. In general, pressures above 150 mm Hg are read with a mercury manometer, a water manometer being used for lower pressures; differences in liquid levels in the manometer up to 600 mm are read with a cathetometer and greater differences are read by using a calibrated steel tape and reading telescopes. The heights were read to about 0.02 mm with the cathetometer and 0.1 mm with the steel tape.

Times of flow are measured using a stopclock operated from a constant-frequency source of power.

All of the flow measurements reported here were made with the viscometers immersed in a well-stirred, 30-gal oil bath whose temperature was controlled by supplying a heater from the output of a manually adjusted variable transformer. When operating below ambient temperature, heat was taken from the bath through cooling coils in which cold water was circulated at a constant rate. Temperatures were measured with a resistance thermometer, and their recorded values are believed to be accurate to $\pm 0.002°$ C.

2.2. Calibration

The usual form of the modified Poiseuille equation for the calculation of viscosity by the capillary method is

$$\eta = \frac{\pi r^4 P t}{8V(l+nr)} - \frac{m\rho V}{8\pi(l+nr)t}, \tag{1}$$

where

r = radius of capillary
P = mean effective pressure drop through the capillary
V = volume between fiducial marks
t = time for volume V to flow
l = length of capillary
m, n = coefficients associated with the flow at the ends of the capillary
η, ρ = the absolute viscosity and density of the liquid whose viscosity is to be determined;

As over a considerable range of rates of flow, m and n can be taken as constant for capillaries having square-cut ends [3], certain of the quantities in eq (1) are usually grouped to give two constants for the instrument. Equation (1) then takes the form

$$\eta = CPt - C'\rho/t, \tag{2}$$

where

$$C = \frac{\pi r 4}{8V(l+nr)} \text{ and } C' = \frac{mV}{8\pi(l+nr)}.$$

With viscometers having capillary bores small enough for calibration with water, these two constants are commonly evaluated by measuring the times of flow of water at 20° C for various applied pressures. The product Pt is plotted against $1/t$, and C and C' are evaluated from the resulting straight line by introducing known values for η and ρ. For the two water-calibrated viscometers used in the work reported here, however, it was found that such plots did not yield straight lines over the complete range of rates of flow in which the instruments were to be used, indicating that m and n were both varying, and consequently C and C' could not be treated as constants. For this reason and for simplicity, the purely empirical formula,

$$\eta = fPt, \tag{3}$$

was used with the viscometers. In this equation, f is a multiplying factor that varies with the conditions of flow. It is convenient to assume that the conditions peculiar to a given rate of flow are characterized by the corresponding value of the Reynolds number as calculated for the flow in the capillary ($R = 2V\rho/\pi r\eta t$), and therefore f will have a definite value for each value of the Reynolds number. The calibration of these instruments, then, consists of determining the value of f as a function of the Reynolds number.

Although the Bingham viscometer is designed to minimize the effect of hydrostatic head in the instrument, actually small head corrections to an applied external pressure, p_0, are necessary to give an exact value of P. The first correction, which will be called the level head, arises from the fact that, despite careful construction, the two bulbs (A and B in fig. 1) will not be geometrically identical and at the same level. This condition results in a residual hydrostatic head that is of the same magnitude but opposite sign for flow right to left (R-L) and left to right (L-R) in the viscometer. The correction is largely independent of the magnitude of the applied external pressure but is proportional to the density of the liquid. The level head was evaluated in this work by making flow measurements in the L-R direction and then repeating in the R-L direction, using approximately the same applied pressure. The runs were made at the lowest applied pressure that could be accurately measured, and under conditions chosen to insure that the volume of flow was the same in each direction. Under these conditions, the difference in the time of flow for the two directions was attributed to a corresponding difference in pressure. Then, knowing the applied pressures, the magnitude of the correction was calculated.

A second head correction, which becomes very significant at low values of the applied pressure, is the commonly termed logarithmic head correction. If we neglect for the moment the level head discussed above, the initial pressure drop through the capillary is p_0+x, where x is the initial hydrostatic head of liquid, and the final pressure is p_0-x, but the mean effective pressure is not exactly p_0, the arithmetic mean of the two, since the higher pressures during the first part of the run cause more rapid flow and are therefore effective for a proportionately shorter

ume. For bulbs of regular shape, however, the effective pressure is readily calculable. For this work, the calculations were made by using Barr's equation [4]. This equation is written $P(1+y^2/10+y^4/35+\ldots)=p_0$, [approximately, where $y=P/p_0$. Barr states that this equation is derived "for a bulb that has the form of a pair of opposed cones, each of a height equal to the radius of the common base, discharging into air, or for such a bulb discharging symmetrically into a similar one, as in Bingham's viscometer". The correctness of this expression was verified in an independent derivation, but because the radius of the common base dropped out in the derivation, it is concluded that the expression holds for cones of any height-to-base ratio. It is of importance to note in connection with runs at low pressures, that the logarithmic head is a function of the ratio of the initial and final pressures, and therefore it increases in absolute magnitude as the applied pressure is reduced. The sign of the correction is always negative, no matter which direction of flow is being used in the viscometer, and therefore it does not affect the determination of the level head, as described above.

The design of the Bingham viscometer is such as to minimize the effect of surface tension upon P. Calculations of the net contribution of surface tension to the mean effective pressure indicate a maximum correction of about 0.001 mm Hg, which was neglected in this work.

A more complete discussion of the above corrections is given by Barr [3, chap. 3].

The three Bingham viscometers used are identified in table 1. Of these, viscometers 1 and 20 were calibrated with water, whereas number 5 was calibrated subsequently by using two hydrocarbon oils whose viscosities were determined in viscometers 1 and 20. In making the calibration runs with water an exception was made to the usual procedure of flowing into a dry bulb, most of the runs being made with the fiducial bulb wet. Following each R-L run, the liquid was drawn back at such a rate as to require about 80 sec with viscometer No. 1, and 120 sec with No. 20 for the fiducial bulb to empty. After allowing about 18 min for further drainage from the walls of the bulb, another R-L run was started. In this manner a reproducible volume of flow was obtained without the necessity of drying the instrument between runs. The difference between the volume of flow under this wet-bulb condition and the true volume of the fiducial bulb was obtained from the differences in the product Pt between wet and dry-bulb runs made with the same applied pressure. On this basis, all the wet-bulb runs were corrected to dry-bulb conditions.

TABLE 1. *Essential dimensions of Bingham viscometers*

Viscometer	Capillary		Volume of flow
	Radius	Length	
	cm	*cm*	*cm*^{3}
1	0.012	10.2	3.96
20	.011	12.3	5.07
5	.017	10.0	4.00

The calibration data obtained with water at 20° C for viscometers 1 and 20 are given in appendices 7.1 and 7.2. All runs were made in the R-L direction, except for the few special runs made for the determination of the level head corrections. From these data the plots of Pt versus R given in figures 2 and 3 were constructed. Each plotted point represents the mean of at least two runs made at approximately the same pressure. For each viscometer, it is seen that the plot is not linear at certain values of R, as was mentioned previously. Since the data are not adequate to position accurately the curves at the lowest Reynolds numbers, the lines were drawn horizontal in this region on the basis of theoretical considerations [5]. From these curves values of Pt corresponding to selected values of R were obtained and, taking $\eta=0.01002$ poise, were substituted

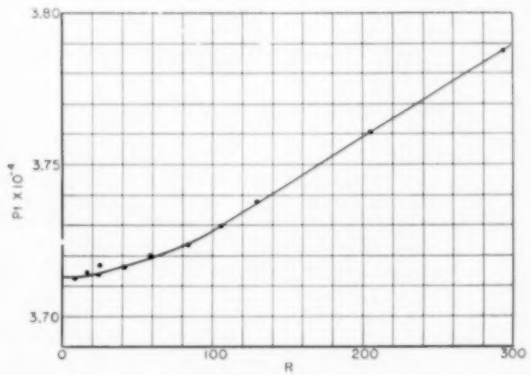

FIGURE 2. *Pt as a function of Reynolds number for Bingham viscometer number 1.*

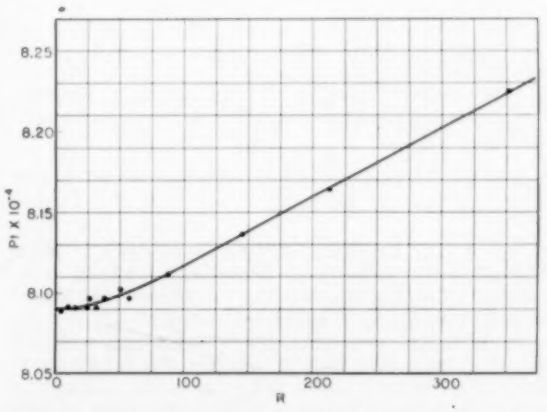

FIGURE 3. *Pt as a function of Reynolds number for Bingham viscometer number 20.*

FIGURE 4. *Calibration curve for Bingham viscometer number 1.*

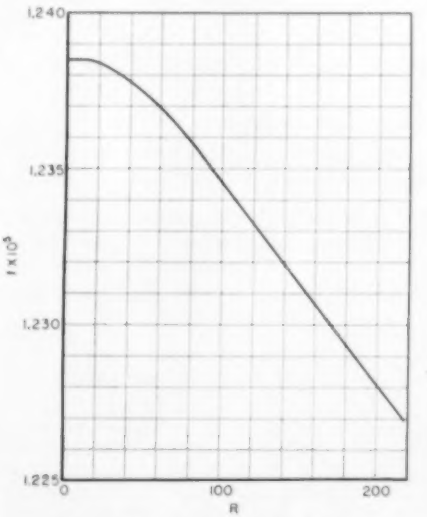

FIGURE 5. *Calibration curve for Bingham viscometer number 20.*

in eq (3) to calculate corresponding values of f. The values of f were then plotted as a function of R, yielding the calibration curves for viscometers 1 and 20 shown in figures 4 and 5, respectively.

To calculate the unknown viscosity of a liquid from flow data obtained in one of these viscometers, it is necessary to choose a value f from the calibration curve corresponding to a tentative value of the Reynolds number based on an estimate of the viscosity of the unknown. If the viscosity value calculated by substituting this value of f, together with the measured values of P and t, in eq (3) differs materially from the first estimate of the viscosity, a second calculation is required.

Viscometer No. 5 was calibrated with oils A and B (to be identified later), using values of their viscosities as determined in viscometers 1 and 20. These calibration data are given in appendix 7.3. As all calibrating runs and viscosity measurements made in viscometer 5 were at Reynolds numbers less than 10, it was assumed that f in eq (3) was constant for this viscometer under these conditions. The level head was measured and the logarithmic head calculated for this viscometer as outlined previously.

2.3. Results with Bingham Viscometers

The viscosities of normal heptane and three additive-free hydrocarbon oils were measured at 20° C. The mean results are given in table 2, and

TABLE 2. *Results at 20° C with Bingham viscometers*

Oil	Viscometer	R	η	η, mean
			cp	*cp*
n-Heptane	1	98.9	0.4112	0.4111
Do	20	154.3	.4110	
A	1	28.2 and 2.4	1.250	1.9250
A	20	18.1	1.9251	
B	1	2.4	7.609	7.610
B	20	1.5	7.610	
C	5	0.2 and 0.5	42.82	42.82

data from individual runs in appendix 7.4. Normal heptane was included to furnish comparative results with a liquid whose viscosity is less than that of water. The heptane was not of highest purity, but was taken from a lot which met specifications for a primary reference fuel for the determination of octane number [6] and was at least 99.5 percent pure. The viscosities of *n*-heptane and oils A and B were determined in viscometers 1 and 20, employing the normal procedure of running in the R-L direction with the fiducial bulb initially dry. Oil A was run at as high and as low Reynolds numbers as was practical. Higher applied pressures were avoided because experience has shown that oils as light as A dissolve air rather rapidly under these conditions, with a consequent lowering of their viscosities. Conditions for the other runs were chosen to strike a balance between optimum conditions for accurate measurement of pressure and of time. In calculating the viscosities, small corrections were made to account for the change of viscosity of the oils with pressure. Observed viscosities were reduced to a pressure of 1 atm, as described elsewhere [2], by adding a second term to eq (3), which then becomes

$$\eta = fPt - FP\eta, \tag{4}$$

where F is a factor representing the fractional change in η for unit change in pressure. Good agreement was found between results obtained in the two viscometers 1 and 20, the largest discrepancy being 0.05 percent with n-heptane. In addition, results obtained with oil A in viscometer 1 at R=28.2 and R=2.4 were in equally good agreement (see appendix 7.4), which tends to confirm the shape of the calibration curve at the lower range of Reynolds numbers (fig. 4).

Runs made with oil C in viscometer 5 at high and at low pressures were in good agreement (see appendix 7.4), indicating that the corrections applied for change of viscosity with pressure are not in serious error.

3. The Cannon Viscometer

3.1. General

In outline, the techniques used at the National Bureau of Standards with the Cannon viscometers, shown in figure 6, are substantially as described by Cannon [7], the principal differences consisting of a more rigorous treatment of the various corrections to be applied to the observed data. With instruments of the kinematic type the value of P applicable to eq (1), neglecting surface tension effects, is given by

$$P=hg(\rho-\rho_a), \tag{5}$$

in which h is the mean effective head, ρ is the liquid density, and ρ_a is the mean density of the air column in the left arm of the viscometer, as shown in figure 6. For application to the Master viscometers, eq (1) then becomes

$$\frac{\eta}{\rho}=\frac{\pi r^4 g}{8V(l+nr)}\,h\left(1-\frac{\rho_a}{\rho}\right)t-\frac{mV}{8\pi(l+nr)t}. \tag{6}$$

If we let

$$\frac{\pi r^4 g}{8V(l+nr)}\,h\left(1-\frac{\rho_a}{\rho}\right)=K$$

and

$$\frac{mV}{8\pi(l+nr)}=B,$$

eq (6) becomes

$$\frac{\eta}{\rho}=Kt-\frac{B}{t}. \tag{7}$$

It is apparent that K and B will not be constant for all test conditions, but their values will reflect any variations in m and n with Reynolds number. As is done with the Bingham viscometers, these changes in m and n are implicitly determined experimentally as a part of the viscometer calibration. In addition, the value of K changes with any change in h or $(1-\rho_a/\rho)$, and a small correction for variation in the value of g may be required if the instrument is used

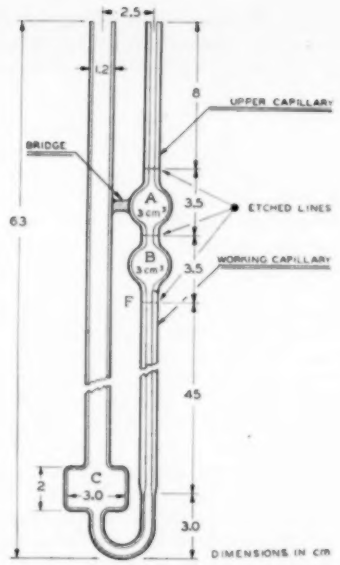

FIGURE 6. *Cannon Master viscometer.*

at a location other than where it is calibrated. If we let K_c be the determined value of K under the particular hydrostatic head at calibration, we can find from it the value of K under other test conditions by calculating changes in h and $(1-\rho_a/\rho)$. Since a change in $(1-\rho_a/\rho)$ is equivalent to a change in h, it is grouped with the other factors which affect h. For any test condition, eq (7) may then be written

$$\frac{\eta}{\rho}=K_c\left(1+\frac{\Delta h}{h}\right)t-\frac{B}{t}, \tag{8}$$

in which Δh is the difference in effective head between test and calibrating conditions, and is made up of the sum of Δh_1, Δh_2, etc., arising from the several factors involved. In practice it is convenient to treat K as a constant equal to K_c, and to apply the corrections to the time of flow t. The viscosity is calculated by means of the equation

$$\frac{\eta}{\rho}=K_c t_c-\frac{B}{t}, \tag{9}$$

in which $t_c=t(1+\Delta h/h)$.

Of the factors affecting h, the filling volume will be considered first. To introduce a reproducible volume of liquid into the viscometer, the viscometer and the liquid must both be at some standard temperature (20° C for this work) each time the viscometer is charged. To obviate the inconvenience of this procedure, fillings are made at ambient temperature, which is observed, and an appropriate correction, Δh_1, is then calculated to account for

any difference between the filling at the observed temperature and a standard filling at a temperature of 20° C. The calculation of this correction is similar to that of Δh_2, which follows.

A second factor affecting h, which gives rise to a correction Δh_2, is the change in effective head with differences between the calibration temperature and that of subsequent runs. The calculation of this correction is based on the cubical expansion of the viscometer and test liquid, together with the mean diameter of the working part of reservoir C, figure 6, [8]. For the most precise work an accurate knowledge of the internal diameter of C is necessary. This measurement was made by plugging the lower end of the capillary with wax and then filling the bottom part of the viscometer with mercury to a low level in C. Weighed increments of mercury were added, and the resulting increases in level in C were measured with a depth gage, from which data a mean internal diameter was calculated.

From differences in the factor $(1-\rho_a/\rho)$ between calibrating and operating conditions a Δh_3 is calculated. The density of the air in the viscometer is a function of the temperature and amount of water vapor present, neither of which is known accurately, but no serious errors are introduced by assuming the air to be 50-percent saturated and at the test temperature.

The factor most difficult to evaluate is the variation of the mean head with surface tension. In the work reported here, viscosity measurements of oils made in water-calibrated viscometers required the most careful estimates of the effects of surface tension. In the case of water, the contribution of surface effects to the effective head was determined experimentally and also calculated. The experimental determination was made with a glass bulb blown as nearly as possible to the size and shape of the fiducial bulb in the viscometer. The bulb was connected through a U-shaped tube to a cylindrical glass tube about 1 cm in diameter and held vertically close to the side of the bulb. The bulb and tube were then mounted in a small bath of oil having close to the same index of refraction as the bulb. Water was introduced into the tube until the level stood in the neck at the bottom of the bulb. The difference between the liquid levels in bulb and tube was then measured with a micrometer microscope mounted for vertical measurements. From this difference and a calculated value for the capillary rise in the cylindrical tube, the rise at this particular level in the bulb was obtained. The calculation of the rise in the cylindrical tube was made by using Sugden's table [9]. A known volume of water was then added and the measurements repeated. The portion of the added volume going into the bulb was the difference between the added volume and the volume increase in the tube as calculated from the change in level in the tube. This process was repeated, taking about 20 increments of volume to fill the bulb. From these data and a measured value of the head in the viscometer at a known level in the bulb, a value of the mean head in an interval, h_t, was estimated for each of the 20 intervals. Then, knowing the volume, ΔV, and the capillary rise, h_γ, for each interval, terms of the form $\Delta V h_\gamma/h_t$ were calculated for each interval. The quotient

$$\frac{\Sigma \frac{\Delta V}{h_t} h_\gamma}{\Sigma \frac{\Delta V}{h_t}}$$

then gave a time-weighted mean value for the capillary rise in the bulb as a whole. The rise in the cylindrical lower reservoir was calculated by using Sugden's table and subtracted from the mean value for the bulb to get a net effect for water in the viscometer. The same techniques were used to determine a net value of the surface tension for each of the oils tested. From the difference between water and oil, a correction, Δh_4, was calculated for application to data obtained with oil.

The net surface tension effect for water in the viscometer was also obtained by calculation alone. For this purpose, a vertical section through the fiducial bulb was plotted on a large scale as accurately as possible. The bulb was then divided into 13 sections, and a value of $\Delta V h_\gamma/h_t$ was calculated for each. With the aid of Bashforth and Adams' tables [10], each value of ΔV was calculated by using the geometry of the bulb as plotted and the calculated change in meniscus volume between the top and bottom of the section. The tables were also used in calculating h_γ for each section. This method has been given in more detail by Barr [11]. The mean value for the bulb was obtained weighting each section with respect to time, as was done in the experimental method. The calculations yielded a value within 0.01 percent of the experimental result, which lent confidence to both methods. Because of limited range of Bashforth and Adams' tables, the calculation could not be made for the oils.

Thus far in the treatment of the factors affecting K in eq (7), it has been assumed that the volume of flow, V, is constant under all conditions. For application to the work reported here, the validity of this assumption was carefully tested. Bulbs similar in size and shape to the fiducial bulbs in the Cannon viscometers were blown with capillary stems about 1 cm long above and below the bulb. To detect differences in the volume of flow of water and the several oils from a bulb, a capillary was attached below the bulb with neoprene tubing so that the bulb could be quickly disconnected. The capillary bore was selected to give about the same time of flow for a particular liquid as was found in the Cannon viscometer. By weighing the test bulb empty and again after a liquid had been run from it at the rate controlled by the resistance of the capillary, the volume of liquid remaining on the walls of the bulb was obtained. From the difference between results obtained with

a calibrating liquid and a test liquid, a correction to K_c could be calculated. Only one instance of a correction as large as 0.01 percent was found, and this so-called drainage correction was applied.

The viscometer is filled by holding it in an inverted position with the end of the upper capillary immersed in the liquid under test. Liquid is drawn into the viscometer by applying suction to the other arm until the level reaches a position slightly beyond the mark F (fig. 6). Applying just enough suction to hold the liquid level at approximately this position, the upper capillary is lifted from the liquid and the operator's finger is placed over its end. With the instrument still inverted, excess liquid is carefully bled out of the capillary past the finger tip until the liquid level reaches F. The viscometer is then returned to its normal upright position, and the finger is removed with a gentle wiping action. In this manner a reproducible filling volume is introduced. After filling the viscometer it is mounted in its bath, and sufficient time is allowed for the fiducial bulb B to empty and for the sample to come to the bath temperature before starting a test. To make a determination, the liquid is pushed up under 17-mm-Hg air pressure until the upper meniscus stands about 5 mm above the mark at the top of bulb B. The air pressure is then released, and the time for bulb B to empty is observed. With relatively low viscosity oils, raising the liquid with vacuum at the start of a run sometimes results in a time of flow slightly higher than when air pressure is used. Such differences are attributed to the removal of air from the sample under reduced pressure. It is therefore considered better technique to use air pressure as any change in the amount of air dissolved in the oil will start at the surface farthest removed from the liquid passing through the capillary.

When the liquid is pushed up at the start of a run, the meniscus level in reservoir C is lowered, leaving some liquid behind on the walls. The amount of liquid left on the walls influences the level in C and hence the value of h. By always using the same pressure in pushing the liquid up, the level in C is lowered at a rate inversely proportional to the liquid viscosity, which leaves about the same amount of liquid on the walls for each test. Calculations indicate that this procedure eliminates significant variations in h.

3.2. Calibration and Results

The calibration of the Cannon viscometers consists in evaluating K_c and B in eq (9). To illustrate the method, eq (9) is rewritten

$$\frac{\eta}{\rho t_c}=K_c-\frac{B}{t_c^2}, \tag{10}$$

in which t_c^2 is substituted for $t_d t$ without detectable error. Liquids having different kinematic viscosities (η/ρ) are run in the viscometer, and values of $\eta/(\rho t_c)$ are plotted against $1/t_c^2$. Values of K_c and B are then obtained from the resulting curve. As unpublished results in this and other laboratories have shown that B may not remain constant over the useful range of Reynolds numbers for this type of viscometer, the calibration must embrace the range in which the instrument is to be used. In practice, therefore, the calibration curve consists of a plot of $\eta/(\rho t_c)$ as a function of $1/t_c^2$ or R, and for a particular viscosity determination values of K_c and B are obtained from the curve at the appropriate value of $1/t_c^2$ or R.

The four Cannon viscometers used in this work are identified in table 3. Of these, M25–1 and M25–2 were calibrated with water, whereas M104 and M105 were calibrated subsequently with two hydrocarbon oils whose viscosities were determined in M25–1 and M25–2. The calibration data obtained with M25–1 and M25–2 are given in appendix 7.5, and from these data the calibration curves in figure 7 were plotted.

The curves were arbitrarily drawn through the values of $\eta/(\rho t_c)$ at Reynolds numbers of about 15, which were obtained with water at 20° C, because a value for the viscosity of water at 20° C was taken as the primary standard for calibration. The points at higher Reynolds numbers were obtained with water at 40°, 60°, and 80° C. The values used for the properties of water at these temperatures are given in appendix 7.6. As K_c refers to the conditions existent with water at 20° C, times of flow obtained at the higher temperatures were corrected by appropriate values of the factor $(1+\Delta h/h)$ in eq (8).

It is evident that the value of B is zero ($m=0$) for these two viscometers up to a Reynolds number of at least 110. Because they were used at values of R never exceeding 50, the determinations made in these instruments were calculated by means of the equation

$$\frac{\eta}{\rho}=K_c t_c. \tag{11}$$

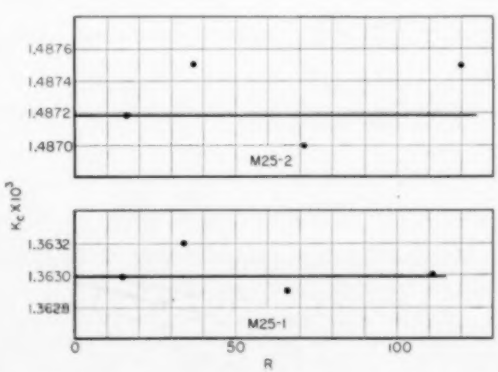

FIGURE 7. *Calibration curves for Cannon viscometers numbers M25–1 and M25–2.*

TABLE 3. *Essential dimensions of Cannon viscometers*

Viscometer	l	r	V	h	Filling volume	Radius of reservoir
	cm	*cm*	cm^3	*cm*	cm^3	*cm*
M25–1	44.5	0.0180	3.11	46.5	6.85	1.52
M25–2	44.5	.0185	3.13	46.3	6.77	1.50
M104	44.3	.0294	3.64	46.6	7.68	1.53
M105	44.5	.0292	3.54	46.6	7.53	1.55

Viscometers M104 and M105 were calibrated with oils A and B, using values of their viscosities as determined in M25–1 and M25–2. The calibration data are given in appendix 7.7. These viscometers were calibrated and used at $R<10$, and hence it was assumed that $B=0$ and eq (11) was applicable. For consistency, the values of K_e for these viscometers were also calculated for the conditions that would exist with water, even though water was never run in these viscometers. The values of the viscosites of *n*-heptane and the three mineral oils, as determined in the Cannon viscometers, are given in table 4. Detailed calculations are given in appendix 7.8. In table 4, kinematic viscosities are converted to absolute units for comparison with the measurements made in the Bingham viscometers. The results obtained independently in the two types of viscometers are in good agreement, the largest discrepancy being 1 part in 2,000 in the case of *n*-heptane. As the techniques employed and the nature of the corrections applied are quite different with the two types of instruments, it is not likely that similar errors are involved in both methods. Hence, there is indication that the treatments of the data obtained in both types of viscometers are free of gross error.

TABLE 4. *Results at 20° C with Cannon viscometers compared with Bingham results*

Oil	Viscometer	η/ρ	η/ρ mean	ρ	η	η, by Bingham
		cs	*cs*	g/cm^3	*cp*	*cp*
n-Heptane	M25–1	0.60070	0.60070	0.6841	0.4109	0.4111
Do	M25–2	.60069				
A	M25–1	2.4641	2.4643	.78110	1.9249	1.9250
A	M25–2	2.4645				
B	M25–1	9.1809	9.1812	.82907	7.612	7.610
B	M25–2	9.1815				
C	M104	49.583	49.584	.8637	42.83	42.82
C	M105	49.585				

4. Discussion of Results

4.1. Sources of Error in Using Bingham Viscometers

From a thorough examination of the various factors involved in the use of the Bingham viscometers, it appears that the greatest source of uncertainty arises from the unavoidable use of relatively low pressures in establishing the portion of the calibration curve corresponding to low Reynolds numbers. The lower pressures are more difficult to maintain relatively steady and measure with a given relative precision, and larger errors are introduced for given uncertainties in the values of the head corrections. This point is illustrated from the data for viscometer number 1 by a comparison of run 1–24, made at a Reynolds number of 8.5, with run 1–38 made at $R=41$ (see appendix 7.1). For run 1–38, with an applied pressure of 73 mm Hg (100 cm H_2O), the level head correction is 0.07 percent, and the logarithmic head correction is 0.01 percent, whereas for run 1–24 with an applied pressure of 15 mm Hg (21 cm H_2O), the level head correction is 0.31 percent, and the logarithmic head correction is 0.24 percent. Thus in the necessary extension of the calibration curve from $R=41$ down to $R=8.5$, the sum of the head corrections is increased from 0.08 percent to 0.55 percent of the applied pressure. For each of the three Bingham viscometers used in this work the value of the level head was determined experimentally, as described previously, the accuracy of the determinations being limited chiefly by the precision with which the pressures could be measured. The experimental evaluation of the logarithmic head corrections with sufficient accuracy, however, was not found feasible, and hence, the corrections were calculated, use being made of an equation given by Barr [4], by which the mean effective pressure for a run is calculated from the known initial and final pressures. This equation was developed on the assumption that each bulb of the viscometer had the shape of two cones placed base-to-base. Although this simple geometry is not exactly realized in any of these viscometers, the correction is not very sensitive to instrument dimensions. Further confidence is lent to the calculations by the fact that good agreement is always found between viscosity measurements made first under conditions where the correction is relatively large and again when the correction is small. This is shown to some extent by the viscosity determinations made on oil A in viscometer 1 (see appendix 7.4). This oil was run first at a pressure of 20 mm Hg, with a logarithmic head correction of 0.08 percent, and then at a pressure of 237 mm Hg, where the correction is negligible. The agreement between these runs is very good, which indicates that the shape of the calibration curve, and the values of the head corrections applied are essentially correct.

It has been shown [12] that the viscosity of water is not significantly affected either by change in the amount of air in solution or by change in pressure under the conditions of these tests. Although the viscosities of the hydrocarbon liquids are more sensitive to these variables, the experimental conditions were chosen such that the variations in the dissolved air under the different test conditions would not be expected to have measurable effects. Furthermore, unpublished experiments at the Bureau have shown that the corrections as applied for the change of viscosity of these hydrocarbon liquids with pressure [2] are probably not in error by more than 30 percent. In the tests recorded in Appendix 7.4, the largest correction occurs with runs 5–17 and

18 on oil C, with an applied pressure of 595 mm Hg. As the pressure correction for these runs is 0.08 percent, an error of 30 percent in the correction will amount to only 0.02 percent in the viscosity determination.

4.2. Sources of Error in Using Cannon Viscometers

The first considerations are concerned with the establishment of the calibration curves given in figure 7 for the two viscometers calibrated with water. In the work reported here these viscometers were used at Reynolds numbers in the range 0.03 to 42, and hence only factors affecting this portion of each curve will influence the results. As the determinations in the viscometers were to give results based on a value for the viscosity of water at 20° C, each calibration curve was arbitrarily put through the point at a Reynolds number of about 15, which represents the data obtained at this temperature. At this point, uncertainties in the value of K_c, which is equal to $\eta/\rho t_c$, will depend only on errors in t_c, as the value of η is taken without error and ρ is known with high accuracy. With reference to appendix 7.5, it is seen that for the data at 20° C, t_c is obtained from the observed time of flow t, by applying only a relatively small correction for filling temperature. This correction is readily calculable and is not considered as a source of error. Of the factors affecting t, the effects of errors in temperature measurement, or of temperature variations, are probably small. Both the platinum resistance thermometer and the Mueller G–2 bridge used for measuring temperature were calibrated shortly before or after tests were made, so that no error larger than 0.001 deg C is expected in the measured temperatures. Observed temperature variations during the tests were 0.002 deg C or less, with the mean temperature closer than is indicated by this spread. It is probable that the actual bath temperatures were within 0.002 deg of 20° C, which is equivalent to an uncertainty of only 0.005 percent in the viscosity of water. Calculations [2] of the precision of the mean values of t as recorded in appendix 7.5 indicate an uncertainty in the mean time of flow for viscometer M25–1 of ±0.03 percent and for viscometer M25–2 an uncertainty of ±0.007 percent. These limits reflect errors due to variations in filling the viscometers, bath temperature, timing, and unrecognized factors. From the above considerations, the values of K_c at $R=15$ for the two viscometers are probably within ±0.03 percent of their true values.

Having established one point on each calibration curve, the other important factor is the shape of the curves in the range $R<50$. From theoretical considerations [3], with increasing values of R these curves should be horizontal lines until some value of R is exceeded and a gradually increasingly negative slope begins to develop. No known theory can account for a positive slope at these Reynolds numbers. The values of $\eta/\rho t_c$ for water at 40°, 60°, and 80° C were therefore obtained and plotted to indicate whether the curves could be assumed to have zero slope up to $R=50$. These values of $\eta/\rho t_c$ were computed by using the values of η/ρ given in appendix 7.5 and are believed to be accurate within 0.1 percent. It is seen that zero slope is indicated in the range of Reynolds numbers covered, and unreasonably large errors in the values of $\eta/\rho t_c$ for water at 40°, 60°, and 80° C would be required to change the positions of the calibration curves at $R<50$ by as much as 0.01 percent.

The calculations of the viscosities of n-heptane and oils A and B from the data obtained with these two water-calibrated viscometers are recorded in appendix 7.8. These data show that the times of flow for repeat fillings of a given viscometer with a given oil are in even better agreement than was the case with repeat fillings with water. It is estimated that the mean times of flow for the two fillings with each oil should be within ±0.01 percent of their true values, based upon 99-percent confidence limits.

In appendix 7.8 the values of t_e are obtained by applying at least three corrections to the observed times of flow. Of these, $\Delta h_1/h$ is calculated without significant error. With reference to section 3.1 it is seen that $\Delta h_3/h$ is dependent upon differences in ρ air/ρ liquid between calibrating and test conditions. The values of $\Delta h_3/h$ were calculated by assuming the air in the viscometers to be 50-percent saturated under all conditions, which was not always the case. No significant error is introduced by this assumption, however, as the difference between the values of $\Delta h_3/h$, assuming dry air and again assuming saturation, affects t_e by only 2 parts in 100,000. The third correction, $\Delta h_4/h$, which is applied to account for the difference in head caused by the difference in surface tension between water and the oils, is perhaps the greatest source of uncertainty. As described previously, the calculated value of the effect of surface tension for water at 20° C was in good agreement with the experimental value, but both calculations and experiments were sufficiently complex as to make it difficult to estimate the accuracy of either. It is believed no error greater than ±0.02 percent is introduced by this correction, but this can not be said with certainty.

The drainage factors recorded in appendix 7.8 based upon experiments described in section 3.1, are believed to be known to about 0.002 percent and are therefore not significantly in error. No satisfactory explanation has been found for the different behavior of oil A, as compared with n-heptane and the other two oils, in bulbs of similar shape and volume to the fiducial bulbs of viscometers M25–1 and M25–2 (see fig. 6). Oil A did not show this different behavior in a somewhat more elongated bulb similar to the fiducial bulbs of viscometers M104 and M105.

In the calibration of viscometers M104 and M105 with oils A and B and the subsequent determinations of the viscosity of oil C, the sources and magnitudes of error are essentially the same as described above for the oil runs in viscometers M25–1 and M25–2.

[2] The calculations were made by the American Society for Testing Materials' methods [13], assuming that the true value of the mean will lie within the limits given 99 times in 100.

286398—54——2

4.3. Heating Effects in Capillaries

So far in the treatment of the data it has been assumed that, once the liquid under test has reached the temperature of the bath in which the viscometer is immersed, it remains at this temperature during the measurement. Because heat is generated in the liquid as it is sheared in the capillary, it is obvious that this assumption cannot be strictly true. As the temperature will vary from point-to-point within the capillary, the viscosity will vary accordingly, and what is measured is a mean value of the viscosity corresponding to some effective mean value of the temperature within the capillary. In attempting to calculate this mean effective temperature, one is unable to postulate what conditions of temperature distribution and heat transfer exist for a given flow condition. Hersey [14] and Hersey and Zimmer [15] have derived equations for calculating the mean effective temperature rise, first assuming conditions of adiabatic flow and then for conditions of thermal equilibrium in the liquid flowing in the capillary. Corrections based on these equations have been calculated for the data in both the Bingham and Cannon viscometers. Referring to appendices 7.4 and 7.8 it is seen that oil C was run in a Bingham viscometer at pressures of 595 mm Hg (runs 5–17 and 5–18) and 303 mm Hg (runs 5–15 and 5–16), and also in Cannon viscometers at 29 mm Hg. If we should assume the conditions defined by Hersey and Zimmer as incomplete adiabatic flow and calculate corrections, using their eq (5) [15], we get a viscosity correction of +0.70 percent for the tests in the Bingham viscometer at 595 mm Hg, and a correction of +0.02 percent for the tests in the Cannon viscometers. On this basis the tests at 595 mm Hg uncorrected, should be about 0.7 percent lower than the runs at 29 mm Hg. As the results recorded in table 4 and appendix 7.4 are in good agreement at all three pressures without these corrections, it must be concluded that conditions of incomplete adiabatic flow are not approximated in these tests. Calculations based on Hersey's eq (13) [13], which assumes flow under the conditions of thermal equilibrium, yield negligibly small corrections, in agreement with the evidence of the tests referred to above.

It should be noted that the effects of heating in the capillary are not only probably negligibly small under the conditions of the tests reported here, but in addition, through the course of calibration and use of a viscometer, the effects tend to be minimized. In the calibration of an instrument, heating effects result in a negative correction to the calibration constant, while in a subsequent determination made in the viscometer the effects result in a positive correction to the time of flow. Thus, even though no corrections are applied, the product of the instrument constant and the time of flow tends to yield a correct result in the viscosity determination. Of course this will only be strictly true when the pressure drop through the capillary is the same for both the calibration and the determination, and when the liquid whose viscosity is being determined and the calibrating liquid have the same heat capacity and temperature coefficient of viscosity. The pertinent physical properties of the liquids involved will usually be sufficiently alike, however, to minimize an accumulation of errors in the usual laboratory practice of calibrating a series of viscometers, graduated as to capillary diameter, by calibrating a larger capillary with an oil whose viscosity has been determined in a smaller one.

4.4. Variability of End Corrections With Reynolds Number

The possible existence of curvature in Pt versus R plots for viscometers of the Bingham type, such as shown in figures 2 and 3, has not been generally recognized. Most observers have confined their calibrations to the higher rates of flow in order to obtain more accurate pressure measurements, and in addition, there has often existed a disregard or inaccurate estimation of the level head and logarithmic head corrections, which may mask the true nature of the calibration curve at the lower Reynolds numbers. The curvature found in the plots for viscometers 1 and 20, however, is not inconsistent with the theory of end corrections and may be explained through a consideration of the nature of the coefficients m and n in eq (1).

The value of m is dependent upon the work done in accelerating the liquid from essential rest to the parabolic distribution of velocities existing after a sufficient entrance length has been traversed. This work is done not against viscous forces, but only imparts kinetic energy to the flowing liquid at the expense of the applied pressure. The value of n arises in part from the excess work done against viscous forces in the entrance length as compared with an equivalent length where the distribution of velocities is parabolic throughout. At sufficiently high Reynolds numbers the kinetic energy of the liquid streaming out of the exit end of the capillary is dissipated as heat [16] in the enlarged part of the viscometer past the capillary. For this condition, the phenomena at the exit end will make a negligible contribution to the values of m and n. At lower Reynolds numbers, however, part or all of the kinetic energy may be expended against viscous resistance close to the exit of the capillary. The value of m for a given Reynolds number will then depend upon the difference between the work done in acceleration at the entrance end and the amount of kinetic energy used in overcoming viscous resistance at the exit end. The magnitude of n will be the sum of the extra work done against viscous resistance at the two ends. It follows then that higher values of m correspond to lower values of n and conversely. Also, when m is constant over a range of Reynolds numbers, n should also be constant. Dorsey [5] has treated this subject at some length and concludes that, for capillaries with square-cut ends, m is zero, and n has a constant value of 1.14 up to a Reynolds number of 10, while at higher Reynolds numbers, $m=1$ and n has a constant value of 0.57. He

recognizes, however, that the values of m and n will be affected by the geometry of the entrance and exit ends of the bore. In the construction of the Bingham viscometers some glass blowing was done at the ends of the capillaries so that they are not precisely square-cut, but evidence slight fire polishing at the edge of the bore. With this geometry it is not surprising that these viscometers show an extended transition region (approximately $R=10$ to 60) between the range where $m=0$ and the range above $R=60$ where m becomes constant.

For Bingham viscometer 1 the constant value of m is 1.12, which is in agreement with values reported by others for capillaries with squarecut ends [3]. The lower value of $m=0.95$ found for Bingham No. 20, may be the result of some peculiarity in the shape of the ends of the capillary bore as a result of glass blowing. With the Cannon viscometers M25–1 and M25–2, it was found that $m=0$ up to at least a Reynolds number of 120, which is as high as the calibration was carried. This condition is undoubtedly associated with the gradual tapers through which the bores of these capillaries expand. It is probable that at sufficiently higher rates of flow these calibration curves would also pass through a transition region and then assume a constant slope corresponding to a value of m which is close to one.

5. Conclusion

In making the measurements reported here, every reasonable precaution was taken so that the results would reflect the accuracy of which each viscometric method was capable. The viscosity values of the four liquids as determined independently by the two methods were in better agreement than was anticipated, and hence it is believed that both methods are relatively free of error. Reviewing the techniques and sources of error critically, however, it is apparent that the necessary steps in calibrating the Bingham viscometers are more complicated and contain more possibilities of uncertainty than are present in calibrating the Cannon viscometers. The experimental difficulties in establishing the calibration curve with water at low Reynolds numbers and the uncertain effects of heating in the capillary are perhaps the weakest points in the method. On the other hand, the relative simplicity of the method with the Cannon viscometers makes this method singularly attractive and inherently more accurate. The greatest difficulty with this method seems to lie in adequately correcting the head for the difference in the surface tensions of water and oil. The procedures described here for evaluating this correction are cumbersome and time consuming to the extent that less accurate estimates of the correction are resorted to in most laboratories. It is possible that a redesign of the shape of the fiducial bulb of the viscometer would simplify the evaluation of this correction. For example, a cylindrical bulb with a conical top and bottom would present simple geometric shapes for which surface tension effects are readily calculable by Barr's method [11]. Any redesign of this nature, however, would have to be accompanied by considerations of the drainage characteristics of the bulb as well.

6. References

[1] J. F. Swindells, J. R. Coe, Jr., and T. B. Godfrey, J. Research NBS **48,** (1952) RP2279.
[2] J. F. Swindells, J. Colloid Sci. **2,** 177 (1947).
[3] G. Barr, A monograph of viscometry, chap. 2 (Humphrey Milford, New York, N. Y., 1931).
[4] G. Barr, J. Chem. Soc., London, 1793 (1935).
[5] N. E. Dorsey, Phys. Rev. **28,** 833 (1926).
[6] 1952 Am. Soc. Testing Materials, Manual of engine test methods for rating fuels, Supp. II, Sec. 217 (a).
[7] M. R. Cannon, Ind. Eng. Chem. **16,** 708 (1944).
[8] M. R. Cannon and M. R. Fenske, Ind. Eng. Chem., An. Ed. **10,** 297 (1938).
[9] S. Sugden, J. Chem. Soc., London, **119,** 1483 (1921).
[10] F. Bashforth and J. C. Adams, Capillary action (University Press, Cambridge, 1883).
[11] G. Barr, Proc. Phys. Soc., London, **58,** 575 (1946).
[12] R. C. Hardy and R. L. Cottington, J. Research NBS **42,** 573 (1949) RP1994 (see p. 575).
[13] Am. Soc. Testing Materials, Manual on presentation of data (1945 printing).
[14] M. D. Hersey, Physics **7,** 403 (1936).
[15] M. D. Hersey and J. C. Zimmer, J. Appl. Phys. **8,** 359 (1937).
[16] S. Erk, J. Rheol. **2,** 205 (1931).

7. Appendices

7.1. Calibration of Bingham Viscometer 1 with Water at 20° C

Run	Direction of flow	Condition of bulb	P_b	Level head	Log head	P	t	Pt Wet bulb	Correction wet to dry	Pt Dry bulb	Pt Dry bulb Mean	F Mean
1	2	3	4	5	6	7	8	9	10	11	12	13
			mm Hg	*mm* Hg	*mm* Hg	*mm* Hg	*sec*					
1-24	R-L	Wet	15.093	+0.047	−0.036	15.104	2456.00	37095.4	+24.0	37119.4	37124	8.5
1-25	R-L	Wet	14.835	+.047	−.036	14.846	2498.71	37095.8	+24.0	37119.8		
1-34	R-L	Wet	15.132	+.047	−.036	15.143	2450.62	37109.7	+24.0	37133.7		
1-31	L-R	Wet	15.225	−.047	−.036	15.142	2448.02	37067.9	+24.0	37091.9	37125	8.5
1-32	L-R	Wet	15.161	−.047	−.036	15.078	2460.65	37101.7	+24.0	37125.7		
1-33	L-R	Wet	15.005	−.047	−.036	14.922	2486.90	37109.5	+24.0	37133.5		
1-35	L-R	Wet	15.244	−.047	−.036	15.161	2448.81	37126.4	+24.0	37150.4		
1-26	R-L	Wet	29.335	+.047	−.018	29.364	1264.24	37123.1	+24.0	37147.1	37143	16.5
1-27	R-L	Wet	29.313	+.047	−.018	29.342	1264.81	37112.1	+24.0	37136.1		
1-42	R-L	Wet	29.142	+.047	−.018	29.171	1272.52	37120.7	+24.0	37144.7		
1-40	R-L	Wet	42.970	+.047	−.013	43.004	862.94	37109.9	+24.0	37133.9	37135	24.2
1-41	R-L	Wet	43.029	+.047	−.013	43.063	861.81	37112.1	+24.0	37136.1		
1-28	R-L	Wet	43.199	+.047	−.013	43.233	859.04	37138.9	+24.0	37162.9	37170	24.6
1-29	R-L	Wet	43.805	+.047	−.013	43.839	847.51	37154.0	+24.0	37178.0		
1-38	R-L	Wet	72.831	+.047	−.007	72.871	509.55	37131.4	+24.0	37155.4	37161	41.4
1-39	R-L	Wet	73.846	+.047	−.007	73.886	502.71	37143.2	+24.0	37167.2		
1-36	R-L	Dry	104.169	+.047	−.005	104.211	356.94			37197.1	37200	58.6
1-37	R-L	Wet	104.169	+.047	−.005	104.211	356.77	37179.4	+24.0	37203.4		
1-15	R-L	Wet	149.480	+.047	−.004	149.523	248.89	37214.8	+24.0	37238.8	37237	84.2
1-16	R-L	Wet	150.074	+.047	−.004	150.117	247.88	37211.0	+24.0	37235.0		
1-1	R-L	Dry	187.703	+.047	−.003	187.747	198.64			37284.1	37296	106.0
1-5	R-L	Dry	187.270	+.047	−.003	187.314	199.08			37280.5		
1-7	R-L	Dry	187.832	+.047	−.003	187.876	198.57			37300.5		
1-9	R-L	Dry	190.737	+.047	−.003	190.781	195.48			37293.9		
1-11	R-L	Dry	190.678	+.047	−.003	190.722	195.51			37288.1		
1-23	R-L	Dry	188.862	+.047	−.003	188.906	197.48			37305.2		
1-2	R-L	Wet	187.480	+.047	−.003	187.524	198.78	37276.0	+24.0	37300.0	37296	106.0
1-6	R-L	Wet	187.039	+.047	−.003	187.083	199.27	37280.0	+24.0	37304.0		
1-8	R-L	Wet	187.655	+.047	−.003	187.699	198.54	37265.8	+24.0	37289.8		
1-10	R-L	Wet	191.037	+.047	−.003	191.081	194.97	37255.1	+24.0	37279.1		
1-12	R-L	Wet	190.810	+.047	−.003	190.854	195.36	37285.2	+24.0	37309.2		
1-17	R-L	Wet	232.251	+.047	−.002	232.296	160.79	37350.9	+24.0	37374.9	37378	130.0
1-18	R-L	Wet	232.011	+.047	−.002	232.056	160.98	37356.4	+24 0	37380.4		
1-19	R-L	Wet	368.515	+.047	−.001	368.561	101.97	37582.2	+24.0	37606.2	37604	205.2
1-20	R-L	Wet	368.476	+.047	−.001	368.522	101.97	37578.2	+24.0	37602.2		
1-21	R-L	Wet	531.552	+.047	−.001	531.598	71.22	37860.4	+24.0	37884.4	37875	293.7
1-22	R-L	Wet	531.285	+.047	−.001	531.331	71.22	37841.4	+24.0	37865.4		

7.2. Calibration of Bingham Viscometer 20 with Water at 20° C

Run	Direction of flow	Condition of bulb	P_0	Level head	Log head	P	t	Pt Wet bulb	Correction wet to dry	Pt Dry bulb	Pt Dry bulb Mean	R Mean
1	2	3	4	5	6	7	8	9	10	11	12	13
			mm Hg	mm Hg	*mm* Hg	*mm* Hg	*sec*					
20-26	R-L	Wet	14.914	−0.097	−0.034	14.783	5470.29	80867	+33	80900	80893	5.2
20-27	R-L	Wet	14.229	−.097	−.035	14.097	5735.43	80852	+33	80885		
20-28	L-R	Wet	15.255	+.097	−.033	15.319	5276.28	80827	+33	80860	80893	5.5
20-29	L-R	Wet	15.207	+.097	−.033	15.271	5299.55	80927	+33	80960		
20-30	L-R	Wet	15.189	+.097	−.033	15.253	5299.06	80827	+33	80860		
20-31	R-L	Wet	28.974	−.097	−.017	28.860	2803.05	80896	+33	80929	80916	10.5
20-32	R-L	Wet	29.190	−.097	−.017	29.076	2782.02	80890	+33	80923		
20-51	R-L	Wet	28.910	−.097	−.017	28.796	2808.12	80863	+33	80896		
20-52	R-L	Wet	29.098	−.097	−.017	28.984	2790.56	80882	+33	80915		
20-33	R-L	Wet	43.374	−.097	−.012	43.265	1869.48	80883	+33	80916	80913	15.6
20-34	R-L	Wet	43.191	−.097	−.012	43.082	1877.25	80876	+33	80909		
20-43	R-L	Wet	74.965	−.097	−.007	74.861	1081.15	80936	+33	80969	80966	27.0
20-44	R-L	Wet	74.714	−.097	−.007	74.610	1084.69	80929	+33	80962		
20-37	R-L	Wet	69.628	−.097	−.007	69.524	1163.14	80866	+33	80899	80910	25.2
20-38	R-L	Wet	69.853	−.097	−.007	69.749	1159.70	80887	+33	80920		
20-35	R-L	Wet	87.942	−.097	−.006	87.839	920.63	80867	+33	80900	80910	31.7
20-36	R-L	Wet	87.731	−.097	−.006	87.628	923.06	80886	+33	80919		
20-39	R-L	Wet	105.450	−.097	−.005	105.348	768.21	80929	+33	80962	80963	38.0
20-40	R-L	Wet	105.919	−.097	−.005	105.817	764.80	80929	+33	80962		
20-41	R-L	Dry	105.452	−.097	−.005	105.350	768.40			80950		
20-42	R-L	Wet	105.196	−.097	−.005	105.094	770.22	80946	+33	80979		
20-45	R-L	Wet	140.328	−.097	−.004	140.227	577.66	81004	+33	81037	81027	50.5
20-46	R-L	Wet	140.074	−.097	−.004	139.973	578.56	80983	+33	81016		
20-15	R-L	Wet	159.491	−.097	−.003	159.391	507.81	80940	+33	80973	80961	57.4
20-16	R-L	Wet	158.835	−.097	−.003	158.735	509.75	80915	+33	80948		
20-17	R-L	Wet	244.479	−.097	−.002	244.380	331.89	81107	+33	81140	81115	88.0
20-18	R-L	Wet	244.589	−.097	−.002	244.490	331.68	81092	+33	81125		
20-25	R-L	Wet	244.963	−.097	−.002	244.864	331.05	81062	+33	81095		
20-47	R-L	Wet	244.297	−.097	−.002	244.198	332.05	81086	+33	81119		
20-48	R-L	Wet	243.924	−.097	−.002	243.825	332.53	81079	+33	81112		
20-24	R-L	Dry	245.341	−.097	−.002	245.242	330.68			81097		
20-2	R-L	Wet	400.796	−.097	−.001	400.698	202.94	81317	+34	81351	81363	144.9
20-4	R-L	Wet	410.912	−.097	−.001	410.814	198.05	81362	+34	81396		
20-6	R-L	Wet	406.918	−.097	−.001	406.820	199.97	81352	+34	81386		
20-8	R-L	Wet	404.893	−.097	−.001	404.795	200.89	81319	+34	81353		
20-10	R-L	Wet	404.433	−.097	−.001	404.335	201.12	81320	+34	81354		
20-12	R-L	Wet	403.796	−.097	−.001	403.698	201.36	81288	+34	81322		
20-49	R-L	Wet	403.883	−.097	−.001	403.785	201.43	81334	+34	81368		
20-50	R-L	Wet	403.961	−.097	−.001	403.863	201.40	81338	+34	81372		
20-1	R-L	Dry	400.860	−.097	−.001	400.762	202.97			81343	81362	145.4
20-3	R-L	Dry	410.850	−.097	−.001	410.752	198.18			81403		
20-5	R-L	Dry	407.486	−.097	−.001	407.388	199.76			81380		
20-7	R-L	Dry	404.853	−.097	−.001	404.755	200.94			81331		
20-9	R-L	Dry	404.632	−.097	−.001	404.534	201.13			81364		
20-11	R-L	Dry	404.078	−.097	−.001	403.980	201.38			81353		
20-19	R-L	Wet	595.256	−.097	−.001	595.158	137.12	81608	+34	81642	81642	212.9
20-20	R-L	Wet	595.038	−.097	−.001	594.940	137.17	81608	+34	81642		
20-21	R-L	Wet	994.445	−.097		994.348	82.67	82203	+34	82237	82250	353.2
20-22	R-L	Wet	995.422	−.097		995.325	82.64	82254	+34	82288		
20-23	R-L	Wet	994.676	−.097		994.579	82.64	82192	+34	82226		

7.3. Calibration of Bingham Viscometer 5 with Oils at 20° C

Run	Oil	Direction of flow	Condition of bulb	p_0	Level head	Log head	P	t	Pt	Pt Mean	R	η	C_1P_0	f
1	2	3	4	5	6	7	8	9	10	11	12	13	14	15
				mm Hg	*mm* Hg	*mm* Hg	*mm* Hg	*sec*				*cp*		
5-3	A	R-L	Wet	20.069	−0.045	−0.017	20.007	884.28	17691.8	17690.6	----	------	------	------
5-6	A	R-L	Wet	20.679	−.045	−.017	20.617	857.90	17687.3		----	------	------	------
5-9	A	R-L	Wet	19.883	−.045	−.017	19.821	892.62	17692.6					
5-2	A	L-R	Wet	20.029	+.045	−.017	20.057	881.80	17686.3	17691.2	----	------	------	------
5-5	A	L-R	Wet	20.589	+.045	−.017	20.617	858.30	17695.6					
5-8	A	L-R	Wet	19.973	+.045	−.017	20.001	884.54	17691.7					
5-1	A	R-L	Dry	19.946	−.045	−.017	19.884	889.86	17694.0	17692.1	6.8	1.9250	0.00003	1.0881×10^{-4}
5-4	A	R-L	Dry	20.285	−.045	−.017	20.223	874.32	17681.4					
5-7	A	R-L	Dry	19.996	−.045	−.017	19.904	889.03	17695.3					
5-14	A	R-L	Dry	19.940	−.045	−.017	19.878	890.32	17697.8					
5-10	B	R-L	Dry	296.132	−.048	−.001	296.083	236.36	69982	69946	6.9	7.6997	.00224	1.0883
5-11	B	R-L	Dry	296.112	−.048	−.001	296.063	236.22	69936					
5-12	B	R-L	Dry	296.924	−.048	−.001	296.875	235.63	69953					
5-13	B	R-L	Dry	296.722	−.048	−.001	296.673	235.66	69914					

7.4. Determinations in Bingham Viscometers

Oil	Viscometer	Run	p_0	Level head	Log head	P	t	Pt	Pt Mean	f	fPt	C_1P_0	η	R
1	2	3	4	5	6	7	8	9	10	11	12	13	14	15
			mm Hg	*mm* Hg	*mm* Hg	*mm* Hg	*sec*						*cp*	
n-Heptane	1	1-52	43.133	+0.032	−0.006	43.159	354.51	15300.3	15299.1	2.6878×10^{-4}	0.41121	0.00001	0.41120	98.9
Do	1	1-53	42.902	+.032	−.006	43.018	355.65	15299.4						
Do	1	1-54	43.310	+.032	−.006	43.336	353.00	15297.6						
Do	1	1-55	43.321	+.032	−.006	43.347	352.95	15299.3						
Do	20	20-60	106.122	−.066	−.002	106.054	314.75	33380.5	33386.8	1.2310	.41099	.00002	.41097	154.3
Do	20	20-61	106.025	−.066	−.002	105.957	315.15	33392.3						
Do	20	20-62	106.172	−.066	−.002	106.104	314.67	33387.7						
A	1	1-49	20.002	+.037	−.016	20.023	3562.24	71326.7	71330.8	2.6986	1.9249	.00003	1.9249	2.4
A	1	1-50	20.010	+.037	−.016	20.031	3561.22	71334.8						
A	1	1-43	237.532	+.037	−.001	237.568	300.45	71377.3	71380.2	2.6973	1.9253	.0003	1.9250	28.2
A	1	1-44	237.133	+.037	−.001	237.169	300.97	71380.8						
A	1	1-45	237.415	+.037	−.001	237.451	300.62	71382.5						
A	20	20-53	237.405	−.076	−.001	237.328	653.16	155488	155478	1.2384	1.9254	.0003	1.9251	18.1
A	20	20-54	237.704	−.076	−.001	237.627	654.30	155479						
A	20	20-55	237.460	−.076	−.001	237.383	654.92	155467						
B	1	1-46	296.654	+.039	−.001	296.672	950.80	282076	282046	2.6986	7.6113	.0022	7.6091	2.4
B	1	1-47	296.674	+.039	−.001	296.712	950.45	282010						
B	1	1-48	296.394	+.039	−.001	296.432	951.49	282052						
B	20	20-56	296.751	−.081	−.001	296.669	2071.92	614674	614654	1.2385	7.6125	.0022	7.6103	1.5
B	20	20-57	296.679	−.081	−.001	296.597	2072.19	614605						
B	20	20-58	296.650	−.081	−.001	296.568	2072.65	614682						
C	5	5-15	302.209	−.050	−.001	302.208	1302.81	393720	393716	10.882	42.844	.017	42.827	0.2
C	5	5-16	303.062	−.050	−.001	303.011	1299.33	393711						
C	5	5-17	595.110	−.050	−.001	595.059	661.92	393881	393830	10.882	42.857	.034	42.823	.5
C	5	5-18	595.070	−.050	−.001	595.019	661.79	393778						

7.5. Calibration of Viscometers M25–1 and M25–2 with Water

Viscometer	Filling	Temperature	t	t, mean	t, adjusted for mean[a]	$\Delta h_1/h$	$\Delta h_2/h$	$\Delta h_3/h$	$\Delta h_4/h$	$(1+\Delta h/h)$	t_c	$\eta/(\rho t_c)$	Rt
		° C	sec	sec	sec						sec		
M25–1	1	20	736.33	736.46	736.46	+0.00002	0.00000	0.00000	0.00000	1.00002	736.47	1.36299×10^{-3}	15
M25–1	2	20	736.53										
M25–1	3	20	736.58										
M25–1	4	20	736.42										
M25–1	1	40	482.72	482.72	482.81	+.00002	−.00012	+.00008	+.0001	1.00008	482.85	1.3632	34
M25–1	2	60	348.17	348.17	348.14	+.00002	−.00031	+.00016	+.0002	1.00007	348.16	1.3629	66
M25–1	3	80	267.90	267.90	267.85	+.00002	−.00056	+.00026	+.0003	1.00002	267.86	1.3630	111
M25–2	1	20	674.95	674.96	674.96	+.00002	.00000	.00000	.00000	1.00002	674.97	1.48718	16
M25–2	2	20	674.95										
M25–2	3	20	674.97										
M25–2	1	40	442.43	442.43	442.44	+.00002	−.00012	+.00008	+.0001	1.00008	442.48	1.4875	37
M25–2	2	60	319.07	319.07	319.07	+.00002	−.00031	+.00016	+.0002	1.00007	319.09	1.4870	71
M25–2	3	80	245.44	245.44	245.44	+.00002	−.00056	+.00026	+.0003	1.00002	245.44	1.4875	120

[a] The observed differences in the times of flow at 20° C for the different fillings are assumed to be largely due to differences in the volume of liquid charged into the viscometers. Since the data at 40°, 60°, and 80° C were obtained with different single fillings, the observed times of flow at these temperatures were adjusted to correspond to a hypothetical filling represented by the mean of the observed times at 20° C.

7.6. Properties of Water

Temperature	γ[a]	η[b]	ρ[c]	η/ρ
° C	Dynes/cm	cp	g/cm³	cs
20	72.7	1.0020	0.99821	1.0038
40	69.6	0.6531	.99222	0.6582
60	66.2	.4665	.98321	.4745
80	62.6	.3548	.97180	.3651

[a] International Critical Tables.
[b] Hardy and Cottington [12], based on $\eta_{20}=1.005$ cp and converting to $\eta_{20}=1.002$ cp.
[c] N. E. Dorsey, Properties of ordinary water substance, table 93, in grams per milliliter and converting to grams per cubic centimeter, using 1 ml = 1.000027 cm³.

7.7. Calibration of Viscometers M104 and M105 with Oils

Viscometer	Oil	Filling	t	t, mean	$\Delta h_1/h$	$\Delta h_2/h$	$\Delta h_4/h$	$(1+\Delta h/h)$	t_c	ν/ρ	K_c	Kc, mean
			sec	sec					sec	cs		
M104	A	1	298.08	298.08	+0.00009	−0.00034	+0.00144	1.00119	298.44	2.4642	8.2572×10^{-3}	8.2569×10^{-3}
M104	A	2	298.09									
M104	B	1	1110.54	1110.57	+.00009	−.00025	+.00142	1.00126	1111.97	9.1811	8.2566	
M104	B	2	1110.60									
M105	A	1	291.30	291.28	+.00009	−.00034	+.00144	1.00119	291.63	2.4642	8.4499	8.4496
M105	A	2	291.25									
M105	B	1	1085.11	1085.26	+.00009	−.00025	+.00142	1.00126	1086.63	9.1811	8.4492	
M105	B	2	1085.40									

7.8. Results Obtained with Cannon Viscometers

Oil	Viscometer	Filling	t	t, mean	$\Delta h_1/h$	$\Delta h_2/h$	$\Delta h_3/h$	$(1+\Delta h/h)$	Drainage factor	t_c	ν, K_c	η/ρ	E
			sec	sec						sec		cs	
n-Heptane	M25-1	1	440.36	440.37	+0.00009	−0.00055	+0.00126	1.00080	1.00000	440.72	1.36299×10^{-3}	0.60070	42.0
Do	M25-1	2	440.38										
Do	M25-2	1	403.60	403.59	+.00009	−.00055	+.00126	1.00080	1.00000	403.91	1.48718	.60069	45.0
Do	M25-2	2	403.58										
A	M25-1	1	1806.05	1805.92	+.00008	−.00034	+.00144	1.00118	0.99980	1807.87	1.36299	2.4641	2.5
A	M25-1	2	1805.80										
A	M25-2	1	1655.44	1655.36	+.00008	−.00034	+.00144	1.00118	.99980	1657.15	1.48718	2.4645	2.6
A	M25-2	2	1655.28										
B	M25-1	1	6727.52	6727.41	+.00008	−.00025	+.00142	1.00125	1.00000	6735.82	1.36299	9.1809	0.2
B	M25-1	2	6727.30										
B	M25-2	1	6165.99	6166.06	+.00008	−.00025	+.00142	1.00125	1.00000	6173.77	1.48718	9.1815	.2
B	M25-2	2	6166.12										
C	M104	1	5997.22	5997.43	+.00007	−.00019	+.00139	1.00127	1.00000	6005.05	8.2509	49.583	.03
C	M104	2	5997.64										
C	M105	1	5860.62	5860.89	+.00007	−.00019	+.00139	1.00127	1.00000	5868.33	8.4496	49.585	.03
C	M105	2	5861.16										

WASHINGTON, September 16, 1953.

Journal of Research of the National Bureau of Standards Vol. 52, No. 3, March 1954 Research Paper 2480

Coaxial Radio-Frequency Connectors and Their Electrical Quality

M. C. Selby, E. C. Wolzien, and R. M. Jickling

The widely accepted manner of evaluating the quality of coaxial radio-frequency connectors was in the past limited to a single case, namely, to the condition when the load terminating the system was equal to the characteristic impedance of the line on the output end of the connector. The quality was expressed as the voltage standing-wave ratio in the input line.

To broaden this method of evaluation a "connector" is redefined, and several methods are given to find the corrections of various types of connectors with any termination. Typical results of measurements made by these methods are given for frequencies from 100 to 900 megacycles. Application of these methods are also indicated in determining the quality of transmission lines in general.

1. Introduction

The accuracy of impedance measurement depends, among other things, upon the frequency at which it is to be measured. It is generally admitted that the frequency range of 30 to about 1,000 Mc/s, which is under consideration throughout this paper, happens to be one of the more difficult ranges from the standpoint of impedance measurements. This is the transition range where components cease to act as lumped-constant elements. Dimensions and distributed constants must be considered, particularly when optimum accuracies are desired. Unfortunately, it is difficult to specify quantitatively the accuracy sought because the accuracy of an impedance measurement is generally a function of both the magnitude and phase angle of the unknown. One may however indicate its order of magnitude as 1 percent or better for "matched" conditions. In searching for reliable measurement techniques and equipment for this frequency range to meet the needs of the National Bureau of Standards, the well-known slotted-line method was found the most promising. After considerable effort, slotted lines having the highest available mechanical and electrical precision were realized. These lines, usable down to 30 Mc/s, had a uniformity of probe-voltage output of 0.25 percent or better over the entire working range at all useful frequencies, and a potential accuracy considerably higher than any other available equipment. To make use of that potential accuracy, it was necessary to minimize the errors introduced by various connectors required between unknown impedances and the uniform section of the precision slotted line. These errors, usually negligible with equipment of lower accuracy, could no longer be disregarded for full utilization of the quality of the new lines. This led to an investigation of methods of determining connector quality in general with results presented below.

The determination of errors introduced by connecting elements has been a problem for a number of years, particularly when used with measuring or controlling equipment, e. g., attenuators, terminating loads, matching indicators, power monitors, bridges, etc. In most cases these connecting elements consist of rigid coaxial structures, referred to as "connectors," with or without a short solid-dielectric cable or air-dielectric rigid transmission line. The characteristic impedances of the components of these connecting elements usually differ from each other by several percent. In addition, the connectors may have a nonuniform internal structure and discontinuities of their own. The losses are usually negligible and are assumed to be so throughout this treatment.

2. Definition of Connector and of Its Quality

The tendency has been to interpret a "connector" as the physical body of a connecting element, such as an adapter, a balun, a taper, a jack, or a plug, by itself or in combinations without regard to discontinuities located immediately at the terminating planes. Thus, some indefinitely located plane between a type N plug and jack was taken as a reference plane for all purposes, e. g., the plane where a short circuit was to be located, the plane where the unknown impedance, voltage, or current was to be measured, etc. When accurate knowledge of impedance is desired, this interpretation of a connector is not always acceptable, because for TEM propagation (considered here) impedance is basically defined and treated as the ratio of voltage to current or of electric to magnetic fields in a cross sectional plane of a uniform distributed-constant system. There are no known commercial connectors meeting the requirements of such a system; all have appreciable discontinuities affecting the field distribution in a manner difficult to compute, predict, or measure.

The term "connector" as used here includes all lossless circuit arrangements used to interconnect two transmission lines of any configuration and characteristic impedance. An example of such a

FIGURE 1. *Typical connector showing one of terminating planes.*

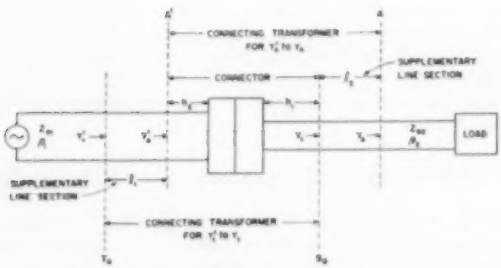

FIGURE 2. *Representation of connector and connecting transformers.*

connector is shown in figure 1. The transmission lines are assumed to have uniform distributed constants up to the connector. To complete the definition of a connector, it is necessary to fix the minimum allowable distance between its terminating planes and its adjacent discontinuities (e. g., h, fig. 2). This distance depends on the particular configuration of the transmission lines and the attenuation rate of the higher modes generated at the discontinuities. For coaxial lines, h (fig. 2) should be equal to or larger than the diameter of the outer conductor [1].[1] When used in this sense, connectors can be readily treated as four-terminal networks and their constants defined and measured.

Another accepted convention is to indicate the quality of a connector by the voltage standing-wave ratio (VSWR) introduced on a uniform transmission line feeding the connector when the latter is terminated in a load equal to the characteristic impedance of the line. This convention can only be used to estimate the maximum error in a measured VSWR caused by connector reflections. It does not furnish necessary corrections for all impedance values. The approach in this paper is to treat the connector as a component part of a transformer; the figures of merit of this transformer are two transformation corrections for the components of its terminating impedances. The problem is to establish relationships between the connector input and output impedances or admittances. Admittance relationships prove to be more convenient for computation simplicity.

Let, in figure 2, a uniform transmission line having a characteristic impedance Z_{01} be joined with another uniform line, Z_{02}, by means of a connector terminated in the planes A', at its input end, and S_0, at its output end. Also, let T_0 be the location of a voltage node when a short circuit is placed at S_0. It can be shown [2] that simple expressions interrelate admittances on opposite side of the connector, e. g., the admittances $Y_A=G_A+jB_A$ and $Y_{A'}=G_{A'}+jB_{A'}$ at planes A and A', where A and A' are effectively an integral number of half wavelengths apart. Two planes in a transmission-line system are effectively an integral number of half wavelengths apart when a voltage node placed in one of these planes (closer to the load) will cause a voltage node to appear in the other plane irrespective of what the physical distance is between them. A supplementary line section, l_2, is added to fulfill the above requirement. The relationships of these admittance components (fig. 2), as shown by Oliver [2], are given by

$$G_1'=a_1^2G_1 \tag{1}$$

and

$$B_1'=a_1^2B_1+a_1b_1', \tag{2}$$

where a_1^2 is a dimensionless constant, and a_1b_1' is an additive constant in mhos. Similarly,

$$G_A'=a_A^2G_A \tag{3}$$

and

$$B_A'=a_A^2B_A+a_Ab_A'. \tag{4}$$

If desired, one can treat the connector shown in figure 2 between A' and S_0 (minus the supplementary line section l_2) as a transformer by expressing the input admittance in terms of the output admittance. From well-known interrelations

$$g_1=\frac{g_A(1+\cot^2\beta_2l_2)}{(\cot\beta_2l_2-b_A)^2+g_A^2} \tag{5}$$

$$b_1=\frac{b_A\cot^2\beta_2l_2+(1-g_A^2-b_A^2)\cot\beta_2l_2-b_A}{(\cot\beta_2l_2-b_A)^2+g_A^2}, \tag{6}$$

where: β_2 is the phase constant and the admittance components are normalized with respect to Y_{02}.

[1] Figures in brackets indicate the literature references at the end of this paper.

The termination admittance of the connector may also be obtained, using various charts and diagrams and thus avoiding computation of eq (5) and (6). However, there is no great advantage in knowing the admittance at the plane S_0 in preference to that at any other plane. The additional computation work involved is therefore seldom justified.

The definition of a "connecting transformer" may here be introduced as follows:

> A connecting transformer is any linear bilateral passive four-terminal lossless network terminated at both ends in uniform line sections; the latter are electrically and mechanically identical to the corresponding adjacent lines of the system. When a short circuit is placed at either end of the connecting transformer, a voltage node appears at its other end.

Thus the connecting transformer consists of the connector and 1 or 2 supplementary line sections. However, there is generally no practical advantage of having more than one supplementary section; the disadvantage is, of course, the need of two (instead of one) admittance transformations when one is interested in the actual input and output admittance of the connector. A connecting transformer, as defined above, therefore consists of the connector proper and one supplementary line section at its output or at its input end. In figure 2, l_1 is the input-end supplementary line section of the connecting transformer correlating Y_1'' and Y_1 through a set of corrections a_1^2 and a_1b_1'. If the output supplementary line section l_2 is chosen, a set of corrections, a_A^2 and a_Ab_A', is required, and the correlation between Y_A'' and Y_A is established. It is convenient to use l_2 in preference to l_1 when the quality of connectors is studied. On the other hand, l_1 is used when the connector is an integral part of an admittance measuring system used to determine Y_1 with optimum accuracy. The justification for these preferences will be further clarified below when the methods of obtaining the transformation corrections are discussed. Special problems may indicate a different choice of supplementary sections and may justify the use of two sections simultaneously (i. e., one at the input, the other at the output). However, the two major groups of problems anticipated at present are impedance and connector measurements; therefore the discussion below will be limited to connecting transformers using either l_1 or l_2.

The interpretation of a^2 and ab' in the case of impedance measurements is straightforward. For connector measurements the interpretation is as follows: With a perfect connector (referring to fig. 2) normalized admittance Y_A''/Y_{01} will always be equal to the normalized Y_A/Y_{02}; otherwise the values of a^2 and ab' will indicate the errors introduced by the connector discontinuities, i. e., the relative quality of various connectors for all values of admittances. For a connector mounted on the panel of an enclosed network like an attenuator, voltage generator, etc., one may simply consider the connector as a part of the enclosed network with the reference plane at A'. Otherwise, required reference impedance-planes like S_0 and A may be assumed inside the network.

To summarize, the definitions of connector, connecting transformer, and connector quality, as applied here, are as follows: (a) A connector is a lossless linear bilateral passive four-terminal network terminated at each end in a uniform line section of a minimum length required to attenuate higher modes likely to appear at these ends. These line sections are identical electrically and mechanically to the respective lines of the interconnected system. (b) A connecting transformer is a connector as defined in (a), terminated at one end in a supplementary lossless line section. This supplementary line section is less than half a wavelength long and is identical electrically and mechanically to that at the connector end. When a short circuit is placed at either end of a connecting transformer (with r-f power fed from the opposite end), a voltage node will appear at the other end of the transformer. With perfect connectors a connecting transformer is an ideal transformer; the normalized input admittance components of this transformer are equal to its normalized output admittance components. (Normalization is with reference to input and output lines, respectively.) (c) With imperfect connectors one must apply corrections to obtain accurate termination admittances. These "transformation corrections" a^2 and ab' indicate the quality of the connectors. The simplest form of the corrections are given in eq (1) to (4). These transformation corrections hold only for the chosen combination of connector and supplementary line section.

3. Determination of Connector Quality

3.1. Analytical Background

The inadequacy of specifying the VSWR of a "matched" connector as its quality index has been pointed out above. For systems of equal characteristic impedances the effective characteristic impedance of the connector is frequently taken as the square root of the product of the measured open and shorted input impedances (i. e., $Z_0=\sqrt{Z_{OC}Z_{SC}}$). This yields, strictly speaking, an inaccurate parameter, because the approach assumes infinite and zero impedances at open- and short-circuited conditions, respectively, and uniformly distributed constants, none of which are true in practice. In addition, this approach neglects likely discontinuities at the termination planes of the connector as the latter is conventionally referred to. Therefore, the value of Z_0 so obtained cannot be used as a simple transformation factor. A reliable way to find quantitative values of the transformation corrections of connectors is the one employing the node-shift method [2, 3, 4, 5]. Frequency-variation methods can be used only to find qualitative data.

The node-shift (n-s) method is well described in the references cited and consists briefly in measuring corresponding shifts of voltage-minima at both ends of the connecting transformer. The original application of this method involved a less efficient and

less accurate handling of measurement data, requiring the determination of tangents to curves of uncertain regularity. An improvement, introduced by Oliver, largely eliminated this difficulty, because the transformation corrections are obtained from a curve that is analytically shown to be a straight line; measurement errors can be readily detected in the plot of a straight line. Techniques developed for the practical application of this method in systems employing equal or unequal characteristic impedances are described in section 3.3. Several variations in these techniques may be used, depending on conditions and requirements.

The essential analytical steps underlying this method of approach are as follows: Let a, b, c, d represent, at one frequency, linear parameters [2] of a four-terminal network equivalent to either one of the two connecting transformers shown in figure 2. As the elements of the network are assumed passive and linear, and a zero termination impedance is transformed into a zero input imedpance,

$$ad-bc=1 \tag{7}$$

$$c=0 \tag{8}$$

$$Z_1'=\frac{Z_1}{A^2+abZ_1} \tag{9}$$

$$Y_1'=a^2Y_1+ab. \tag{10}$$

In the last two expressions a and b are the parameters of the transformer between Y_1' and Y_1 (i. e., between planes T_0 and S_0).

As pointed out above, a voltage node at S_0 will cause a voltage node at T_0. The plane T_0 may be located at the input to the connecting transformer or at any other plane an integral number of half wavelengths away from it. Let the voltage node now be moved a distance s from S_0 by means of a movable short circuit. This is equivalent to varying the reactance of Z_1 by a given amount. The node at T_0 will therefore shift in turn by some distance t, not necessarily equal to s, as shown in figure 3. Here the transformer input plane is shown at K and T_0 is chosen a half wavelength away from K; this is necessary to permit measurements along a uniform line section. With the nodes in these positions,

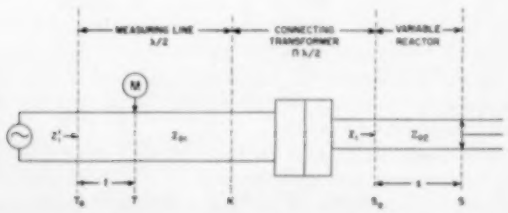

FIGURE 3. *Basic arrangement to measure quality of a connecting transformer.*

$$Z_1'=jZ_{01}\tan\beta_1 t \tag{11}$$

$$Z_1=jZ_{02}\tan\beta_2 s \tag{12}$$

where $\beta=2\pi/\lambda$ is the phase constant of the respective lines.

Using eq (9),

$$\frac{Z_{01}}{Z_{02}}\tan\beta_1 t=\frac{\tan\beta_2 s}{a^2+jabZ_{02}\tan\beta_2 s}, \tag{13}$$

since the network is lossless, b is an imaginary quantity [2] and one may substitute $-b'$ for jb. Rewriting the terms,

$$\cot\beta_1 t=\frac{Z_{01}}{Z_{02}}(a^2\cot\beta_2 s-ab'Z_{02}), \tag{14}$$

therefore,

$$\cot\beta_1 t-\cot\beta_2 s=\left(\frac{Z_{01}}{Z_{02}}a^2-1\right)\cot\beta_2 s-ab'Z_{01}. \tag{15}$$

One can thus obtain a number of cot $\beta_1 t$ values corresponding to chosen cot $\beta_2 s$ values and the plot of (cot $\beta_1 t$ − cot $\beta_2 s$) versus cot $\beta_2 s$ will be a straight line with $[(Z_{01}/Z_{02})a^2-1]$ as its slope and $(-ab'Z_{01})$ as its intercept on the (cot $\beta_1 t$ − cot $\beta_2 s$) axis. As Z_{01} and Z_{02} are assumed to be known, a^2 and ab' can be determined for use in eq (1) to (4). In addition, relationships for impedance components can be derived to show how the load impedance, $R+jX$, of a slotted line, for example, is determined from its measured value, $R'+jX'$, when the transformation corrections of its connecting transformer are known. Thus, from eq (9), again writing $-b'=jb$,

$$R+jX=\frac{a^2(R'+jX')}{1-jab'(R'+jX')} \tag{16}$$

or

$$R=\frac{a^2R'}{1+2ab'X'+(ab')^2(R'^2+X'^2)} \tag{17}$$

$$X=\frac{a^2[X'+ab'(R'^2+X'^2)]}{1+2ab'X'+(ab')^2(R'^2+X'^2)}. \tag{18}$$

It may be of interest to note at this point the interrelation between the parameters of the same connecting transformer in the forward and reversed directions. A case may arise where it is necessary to reverse the transformer end for end. For example, because of external structural irregularities, one may wish to connect the transformer into a circuit in a direction opposite to that used for the measurement of its constants. The termination impedances must then be corrected by a new set of parameters, because the system is not necessarily symmetrical. There is a simple correlation between the "forward" and

reversed" sets of corrections, obviating the necessity of additional measurements. It can be shown [6] that

$$a_f = \frac{1}{a_r} \tag{19}$$

and

$$b_f' = b_r' = b', \tag{20}$$

where the subscripts f and r refer to the forward and reversed conditions, respectively.

Let the intercept of the straight-line plot measured in the forward direction be n; then

$$a_f b' = -\frac{n}{Z_{01}}. \tag{21}$$

Let also the slope obtained in the forward direction be m; then

$$a_f^2 = \frac{Z_{02}}{Z_{01}}(m+1). \tag{22}$$

For a reversed system

$$a_r b' = \frac{b'}{a_f} = \frac{a_f b'}{a_f^2} = \frac{-n}{Z_{02}(m+1)}. \tag{23}$$

Equations (22) and (23) may be used to compute the output impedance of a connecting transformer. The impedance at the input end of the connecting transformer is assumed to be known.

3.2. Connectors in Tandem

There is frequently the need of measuring the quality of two connectors in tandem in order to obtain the quality of one of them. A typical example is as follows: Precision slotted lines of special mechanical and electrical design are frequently constructed at a considerable cost; special diameters are chosen to obtain optimum quality of the slotted line. It is therefore necessary to employ adapters, tapers, etc. to connect this line to conventional connectors of various diameters. There is a simple relationship between the transformation corrections of a connecting transformer composed of two transformers in tandem and the corrections of the individual transformers.

In figure 4 let a precision slotted line be connected through connector 1 and connector 2 to an unknown load in plane S_{02} at the end of connecting transformer 2. The supplementary line section of transformer 1 is l_1, a section of the precision slotted line. From the eq (1) to (4),

$$a_{12} b_{12}' = a_1^2 a_2 b_2' + a_1 b_1', \tag{24}$$

where subscripts 1, 2, and 12 correspond, respectively, to connecting transformers 1, 2, and 1–2, and where planes S_{01} and T_{02} coincide.

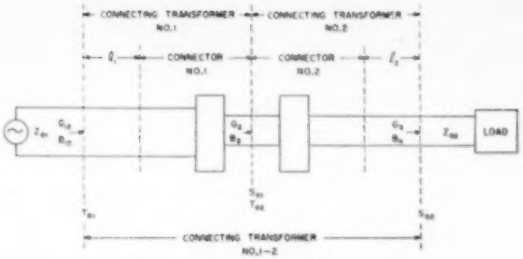

FIGURE 4. *Representation of two connecting transformers in tandem.*

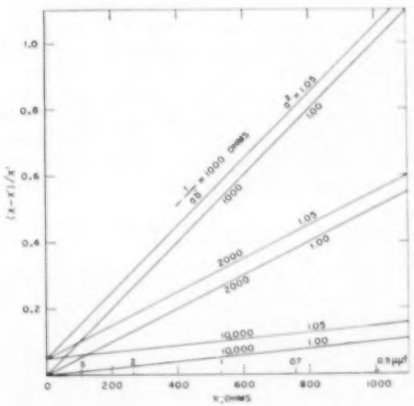

FIGURE 5. *Fractional error in measured shunt reactance versus shunt capacitive reactance terminating the connecting transformer.*

The values in micromicrofarads are the equivalent shunt capacities at 300 Mc/s. Shunt capacitive reactances equal to $(-1/ab')$ ohms are used as one of the parameters to be consistent with the values used along the axes.

It is thus seen that one can obtain the individual transformation corrections of transformer 2 from the corrections of the combined transformer 1–2. This is a great advantage, as it allows the use of slotted lines of the highest precision to accurately measure connector quality and unknown impedance, even when the latter do not match the line mechanically or electrically.

The significance of the magnitudes of the transformation corrections a^2 and ab' may be demonstrated as follows: Equation (1) indicates that the error in a measured conductance is a function of a^2, whereas eq (2) shows that the error in a measured susceptance is a function of a, b', and of the magnitude of that susceptance. From eq (2) the fractional error in this susceptance is

$$\frac{B-B'}{B} = (1-a^2) - \frac{ab'}{B} \tag{25}$$

or

$$\frac{x-x'}{x'} = -ab'x + (a^2-1), \tag{26}$$

where $B=-1/x$, $B'=-1/x'$; x and x' are the respective equivalent shunt reactances of the unknown and measured impedances at the ends of the connecting transformer.

Equation (26) thus gives the errors in the measured shunt reactances, which can be plotted versus s as straight lines with shunt capacitive reactances equivalent to $(-ab')$ mhos as slopes, and (a^2-1) as intercepts. Representative values usually encountered in practice at frequencies to 1,000 Mc/s are shown in figure 5.

3.3. Techniques and Procedures

The node-shift method of connector-quality determination may utilize one of the following reactors, depending on the problem and facilities at hand: (a) An adjustable stub, (b) fixed line sections, (c) a slotted line, or (d) a perforated line. Steps of procedure and precautions that are common to the use of all of these reactors will first be discussed; then features of each device and its associated technique will be described individually.

a. Equipment

In general, the equipment requirements are these: The known reactor, connected as shown in figure 3 at S_0 (the end of the unknown connecting transformer) must be lossless, uniform, and adjustable or variable over at least half a wavelength. The junction at S_0 must be free of discontinuities; thus, for best results, the cross-sectional dimensions and dielectric material of the reactor and the connecting transformer must be the same at this plane. In addition, this uniformity must be maintained on the input side of S_0 for an axial distance equal to at least the diameter of the outer conductor. Sometimes, as mentioned in section g, a small amount of mismatch may be tolerated without invalidating the measured data. Good mechanical alinement and contact at this plane are essential. All discontinuities should lie between S_0 and K, the latter being a plane of reference on the measuring line, effectively an integral number of half wavelengths from S_0.

b. General Procedure

The measurement procedure consists in first placing a short circuit at S_0 and locating T_0, a position on the measuring line where a voltage node occurs, one or more half wavelengths from K. Whenever possible, the first T_0 beyond K should be used so as not to introduce extra losses into the measuring system. As the short circuit is moved from S_0 to S, a distance s, the voltage node on the measuring line moves from T_0 to T, a distance t. From 5 to 10 corresponding positions of S and T are recorded. This number of points has been found desirable to identify any irregularities in the data. Values of s are chosen so that the distribution of cot $\beta_2 s$ will be fairly evenly spaced from -2 to $+2$. These limits are selected because usable data, for the rapidly changing cotangent function outside this interval, require equipment precision which is usually beyond practical achievement. When the magnitude of the s values is limited by the usable length of the reactor, lengths of s corresponding to cot $\beta_2 s$ values from 0 to $+2$ may be adequate. Each of the S and T nodes are located by determining the midpoint between two positions of equal detector response one on each side of the minimum. However, when structural defects in the slotted line produce nonuniformity in the voltage distribution along the line, errors may be caused in the determination of the nodal positions. To minimize these errors, it has been shown [7] that the optimum equal-response voltage in the determination of a nodal position should be approximately 3 db (within ± 0.5 db) above the minimum voltage when the VSWR is above 7. In addition to structural defects, the presence of losses in the measuring system may introduce errors in making accurate nodal measurements. When such is the case, one may minimize these errors by following the procedure outlined later in section g.

The difference, cot $\beta_1 l$—cot $\beta_2 s$, is then plotted versus cot $\beta_2 s$ and the resulting straight line interpreted as shown in section 3.1. The values of a^2 and ab' thus obtained are the transformation corrections of the unknown connecting transformer at the test frequency.

As the magnitudes of a^2 and ab' are functions of the relative positions of the discontinuities in the connecting transformer, and as these positions are scattered and unknown, the effect of these discontinuities may cancel at some frequencies and increase at others. Therefore, the number of frequencies at which measurements must be made in order to find the quality of a connector over a given frequency range will be determined by the extent of the frequency range and the accuracy desired. Measurements indicated that the transformation corrections for commercial connectors varied rather slowly with frequency up to 1,000 Mc/s, and that measurements at 100-Mc/s intervals in this range would be sufficient to determine the frequency characteristics of a given connector.

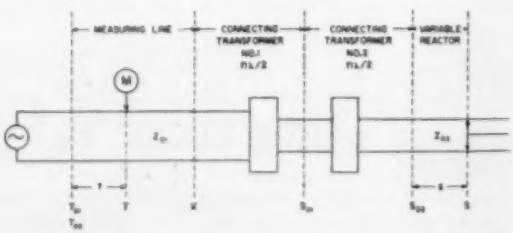

FIGURE 6. *Basic arrangement to measure quality of two connecting transformers in tandem.*

c. Connectors in Tandem

When the measuring line does not match the unknown connector in size or characteristic impedance, or both, an adapter is required between them. Then it is necessary to separate the corrections of the unknown connector from those of the adapter according to the procedure described above in section 3.2. In this situation S_{02} (see fig. 6) must be so placed that a voltage node appears at S_{01}. This condition can be met by first placing a short circuit at S_{01}, the output end of connecting transformer No. 1, and by locating a corresponding T_{01} on the measuring line. Then the short circuit is replaced by the unknown connector and adjustable reactor, and the latter is varied until a voltage node again appears at T_{01}. Thus a voltage node is also assured at S_{01}. The values of s and t are then obtained as described previously. In some cases the voltage node at S_{02} cannot be moved continuously because of the type of variable reactor being employed or because connecting transformer No. 2 has a fixed length. The procedure to place a voltage node at S_{01} under such conditions will be described in section h.

d. Curvature in Plot of Data

It was occasionally observed that the plot of measurement data substituted in eq. (15) resulted in a curve rather than a straight line. The following precautions were found to prevent such curvature. (1) The phase constants of the measuring line and the reactor must be known to an accuracy of ± 0.01 percent. This required that the corresponding frequency stability be maintained to an accuracy of at least ± 0.01 percent. (2) The positions of S_0 and T_0 should be measured, for example, to ± 0.1 mm at 300 Mc/s for lines with dielectrics having constants of 1 to 3. The presence of any appreciable discontinuity at these planes, such as a poor contact at S_0, may cause an excessive error. (3) When the voltage distribution near a node is nonsymmetrical because of losses in the measuring system, proper precautions must be taken to locate the positions of S and T correctly. These precautions are described in section g. (4) The accuracy of finding voltage-node positions may be improved by keeping the input voltage high and the probe penetration deep (for low input voltages), probe reflections being negligible near voltage nodes, by filtering out harmonics from the input voltage, and by operating probe output indicators at the most sensitive positions of the meters and circuit action. Means of minimizing errors caused by structural defects in slotted lines were indicated under section b.

e. Use of an Adjustable Stub as a Reactor

This type of reactor is the most obvious one to select for use in n-s measurements of air-dielectric elements and is quite simple to operate. A 5-ft 50-ohm stub of this type was found particularly useful in measuring ⅞-in. connectors in the VHF range.

To determine values of s, relative stub positions may be measured with the required precision by means of large vernier calipers, gage blocks, or a carefully engraved scale attached to the adjustable stub. An advantage of this type of reactor is that one stub of sufficient length can be used to obtain convenient values of s over a wide frequency range.

In the construction of the stub it is essential to use the least amount of solid support for the center conductor near the input end. Whatever support may be required should be small in mass and have the lowest possible dielectric constant. When it is possible to support the center conductor by the connector being measured, the omission of any additional support is desirable. Another critical construction feature is that the movable shorting device should locate a nearly lossless short circuit in positively defined planes. For small-sized connectors it is very difficult to build a stub long enough for use in low-frequency n-s measurements without an objectionable sag in the center conductor. An adjustable stub is unsuitable for measurements of solid-dielectric connectors, because of unavoidable discontinuities of the junction of the two dielectric media.

f. Use of Fixed-Line Sections as Reactors

The use of accurately constructed line sections for reactors simplifies n s measurements. First, a short circuit is placed at S_0; this is then replaced by shorted fixed-line sections of different lengths corresponding to selected s values. Alternatively, sections of equal length open at both ends may be connected in tandem; a short circuit is then placed at the output end of the combination. In both cases it is essential that a good mechanical contact exist at S_0 and that no discontinuities be introduced in this plane. In using combined sections, these conditions must also be maintained at the junctions. Otherwise, a curvature or excessive random scatter will result in the final plot of the data.

Although the procedure followed with this type of reactor is simple, a number of disadvantages are involved. First, the careful matching and alinement referred to above requires precision machining. Thus when n-s measurements are to be made over a wide frequency range, numerous costly precision sections are required. Second, if an adapter is required between the unknown connector and the measuring line, it may be awkward to use fixed sections as reactors (particularly at low frequencies) because of the requirement that the ends of the unknown connecting transformer be an effective half wavelength apart (see section 3.2). Third, although reactors of this type can be constructed to match any present-day air-dielectric connector, this can not easily be done for solid-dielectric components because it is difficult to determine with sufficient accuracy the phase constant of solid-dielectric sections. In coaxial lines having solid insulation the phase constant is very closely equal to $2\pi f(k)^{1/2}/(2.998\times 10^8)$ radians/meter, where k is the dielectric constant of

the insulation. Variations from 1 to 3 percent may be found in the dielectric constants of commonly used insulators, depending on the batch or manufacturer. In addition, these constants may be affected by a change in volume (i. e., density) caused during fabrication steps and by the application of excessive heat. The phase-constant accuracy is also limited by the accuracy (± 0.1 percent) to which the capacity of line sections can be measured, by effects of frequency on the dielectric constant, and by dimensional tolerances of the conductors. Thus it appears that the best prospect of obtaining the required accuracy of ± 0.01 percent in the phase constant is to measure the electrical lengths directly in the finished line sections. For example, a section of line can be resonated by varying the frequency within the range in question and observing the output of a fixed probe located at a precisely known distance approximately a half wavelength from the shorted end. Assuming that the dielectric and dimensional uniformity was maintained, this line section can then be cut into a number of short sections. This fixed probe method suggests the application of a perforated solid-dielectric line; it also suggests an accurate way to measure the dielectric constant of a coaxially fabricated material.

A type of reactor combining the features of the adjustable shorting stub and fixed-line sections might be used to alleviate some of the disadvantages mentioned above. First, an air-dielectric stub is required, in which the shorting device can be removed from the coaxial line. Coaxial sections of any desired solid insulator are then inserted in the coaxial line, and the shorting device is replaced so as to produce a short circuit at the end of the newly formed solid-dielectric coaxial line. It is necessary that each of the insulator sections be accurately machined to fit the coaxial line and to have end planes perpendicular to its axis. The lengths of these sections depend on the desired values of cot $\beta_2 s$. Advantages of this type of reactor are (a) the conductors are not broken; (b) numerous s values are readily available, because it is simpler to machine any desired number of insulators rather than to construct an equal number of individual line sections; (c) the terminating plane of the unknown connecting transformer (solid-dielectric type) can easily be placed at any approximate point in the reactor, when required; (d) any number of different dielectric materials may be used with the same air stub for various desired Z_{02} values; (e) the phase constants may be determined with an auxiliary fixed probe, as described above.

g. Use of a Slotted Line as a Variable Reactor

In employing a slotted line as a known reactor, an auxiliary line stretcher or adjustable stub is connected at the output end of the slotted line to move a voltage minimum along the slotted line where it is detected by a probe (see fig. 7). The method recommended for accurately locating this voltage node is the same

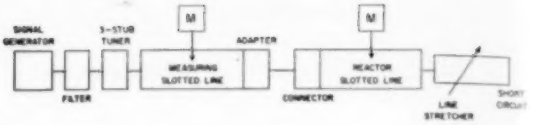

FIGURE 7. *System for node-shift measurements using a slotted line as a reactor.*

as that described in section b. It is not essential that the voltage node be moved to the exact S location previously selected; it is possible to locate the position of the voltage minimum very accurately and thus know the corresponding value of s.

At higher frequencies the presence of losses in the measuring system may make accurate measurements of S and T more difficult. As the voltage curve in the region of a minimum closely approaches a parabola, the voltage nodes may be located accurately by joining the midpoints of three horizontal chords through each selected trough of the voltage standing-wave [8]. However, this procedure is quite tedious; in most cases the following simpler method may be employed, with results of sufficient accuracy; (a) place a short circuit at S_0 and find the true T_0; (b) connect the slotted-line reactor at S_0; this will introduce losses (especially when a solid-dielectric line is used), reducing the VSWR and upsetting the symmetry of the voltage distribution in the measuring line particularly; (c) locate a node at T_0 as follows: Adjust the auxiliary variable reactor to obtain a node near T_0, using a voltage increment, ΔE_t, about 3 db above the minimum; readjust the variable reactor to move the node toward the desired location; repeat these steps until a node is obtained exactly at the true T_0; (d) then locate the corresponding minimum for S_0' (an effective half wavelength from S_0 toward the short circuit). Use a certain ΔE_s approximately 3 db above the voltage minimum. (e) Finally, locate the selected S and corresponding T positions, using the same ΔE_s and ΔE_t in each case, as was used to locate the S_0' and T_0, respectively.

Relative merits of this technique are: (a) This type of reactor is useful wherever a slotted line is available to match the connector being measured. The technique was found particularly applicable in determining the quality of ¾-in. connectors, the size in which solid-dielectric slotted lines of fairly good precision have been made. (b) Only one slotted line is needed as a reactor for n-s measurements over a wide frequency range, e. g., from 100 to 1,000 Mc/s. (c) Because of the precision with which voltage nodes can be located, the velocity of propagation, and hence the phase constant of this type of reactor, can be very accurately determined. (d) The use of this reactor is more convenient than the others for the n-s measurement of connectors in tandem, because of the ease with which S_{02} can be located whenever it must be placed in the reactor to meet the half-wavelength requirement referred to previously.

In turn, this technique possesses a few disadvantages. Measuring the s values in a slotted line is somewhat more time consuming that adjusting them, as described in the previous methods. A slotted line is considerably more expensive than reactors of the other types for use over the same frequency range. Because of the slot, it is impossible to match perfectly a slotted line to a closed line, a compromise necessarily being required either in the conductor dimensions or in the characteristic impedances. However, the use of a slotted line as a reactor is practical if the resulting discontinuity at the junction of the line and the unknown connector is kept as small as possible. For example, satisfactory data were obtained by using such a slotted line to measure the quality of adapters on precision slotted lines.

h. Use of a Perforated Line as a Variable Reactor

Although applicable to making n-s measurements of connectors in all sizes, this technique is especially recommended for use in determining the quality of large-sized connectors because of the economy made possible in the construction of the variable reactor. As an example, a 50-ohm 3⅛-in. perforated air-dielectric line, shown in figure 8, was constructed for the quality measurements of connectors and lines having that diameter and characteristic impedance. The line consisted of a 4-ft brass outer conductor with a duralumin center conductor supported at the output end by a Teflon disc ¼ in. thick. At the input end no disc was used; the center conductor was supported by the connector being measured so as to minimize the discontinuity at the junction of the connector and reactor. Stock tubing was used for the conductors. Probe holes, ⅛ in. in diameter, spaced 1 in. apart, were bored in the outer conductor. This spacing permitted the choice of convenient s values over a wide frequency range. Surrounding each hole was a milled "flat" to help center the probe. The probe was a stiff copper wire, 0.020 in. in diameter, soldered to a BNC connector, and was shielded by a short cylinder that fitted the probe hole. An external adjustable stub was used to tune the probe (see fig. 9). As with the slotted line, a short-circuited line stretcher was used at the output end to move the voltage node along the perforated line. To facilitate placing the voltage node at a preselected hole, a line stretcher that can be moved by very small increments in a positive fashion is desirable. If difficulty is experienced in this operation (as indicated by a lack of reproducibility), the following method may be used: (a) Shift the voltage node slightly to one side of the selected hole. Let the probe output voltage at this hole be V_1 and the position of a corresponding voltage node on the measuring line be T_1. (b) Move the voltage node to the other side of the selected hole so that the new probe voltage V_2 equals V_1. Let the position of the corresponding voltage node on the measuring line be T_2. (c) Then the true T for a voltage node placed at the desired hole will be midway between T_1 and T_2. This procedure assumes that the voltage curves at S and T are not distorted by excessive losses. This is not always true at T. If such is the case, the precautions discussed in section g must be observed in finding T. In all cases, when the movable short circuit is being adjusted, it is advisable to have the source impedance equal to Z_0 of the line connected

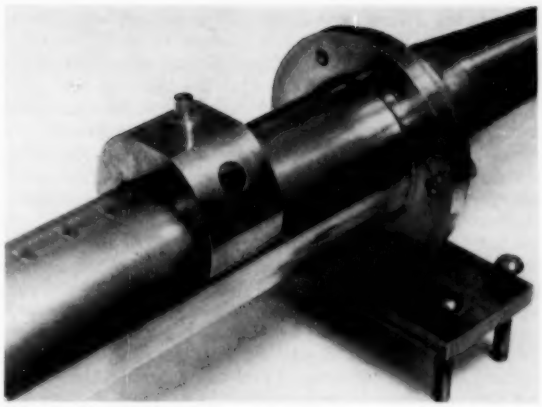

FIGURE 8. *Details of a perforated line used as a variable reactor in node-shift measurements.*

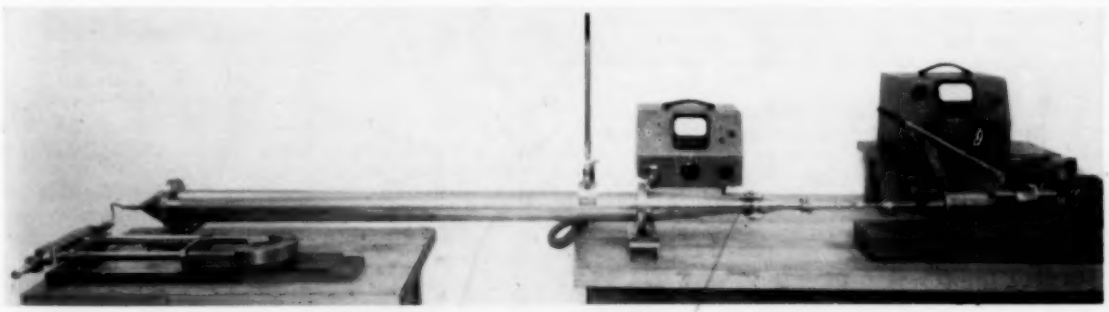

FIGURE 9. *Perforated line used as a variable reactor to measure the corrections of a transformer.*

to it; this assures a constancy of voltage amplitudes along the system.

When it is necessary to use an adapter between the unknown connector and the measuring line, the corrections of the two connectors must be separated, as previously explained. Because of the fixed probe positions of the perforated line, a special step must usually be employed here to determine the exact frequency at which the unknown connecting transformer is effectively equal to a half wavelength. A short circuit is first placed at the end of the adapter to the measuring line, and three values of T_{01} are found for three different frequencies around the estimated frequency at which the unknown connecting transformer meets the length requirement. Then the short circuit is removed, and the unknown connector and perforated line are attached, the probe of the perforated line is placed in a selected hole, and three values at T_{02} are found for three similar frequencies. With these data two curves of frequency versus T_0 are plotted. The intersection of these curves determines the desired frequency. If the effective discontinuity of the adapter is small (so that the transformation corrections remain essentially the same for small displacements of S_{01}), it is permissible to use an approximate frequency, e. g., the integral number of megacycles per second nearest the intersection of the above curves. Then the original corrections of the adapter, predetermined at a slightly different frequency, can still be used in the separation procedure. When it is necessary to know the desired frequency more precisely, the above procedure is repeated over a more narrow frequency range bracketing the frequency located above. The frequency used in this technique must be known and kept stable to 0.01 percent. The corrections of the measuring-line adapter may, of course, be remeasured at the new exact frequency if optimum accuracy is to be assured.

4. Typical Measurement Results

In all the techniques described above, a precision slotted line has been used to measure the input reactance variations of the connecting transformer corresponding to known output-reactance variations. Obviously, impedance-measuring devices other than slotted lines may be used for this purpose; e. g., bridges, Q-meters, instruments employing directional couplers, admittance comparators, etc. However, present experience indicates a need of precision in measuring input-reactance variations considerably greater than that provided by currently available commercial instruments other than slotted lines. Also, when these other impedance-measuring devices are employed for this purpose, the steps of procedure in the n-s method must be modified. A discussion of the use of such devices is reserved for another treatment of the subject.

The results of some n-s measurements of typical connecting transformers, using a precision slotted line as the measuring instrument, are compiled in table 1. The transformation corrections given do not necessarily represent average values for the particular types of commercial units listed, but rather demonstrate the typical magnitudes of these corrections. Each connecting transformer, of course, terminates in uniform line sections and, when required, includes mating connectors. For type N connectors and adapters the mating connectors are assembled from UG–21B/U plugs and UG–23B/U jacks, combined with 1½-in. uniform sections of 50-ohm Teflon-dielectric rigid line. For a particular connector the transformation corrections vary, depending on the position of the connector along the transmission-line type of transformer. The corrections for the cable connectors and adapters, Nos. 3 to 11, in table 1 represent the parameters of each transformer, with the test unit placed at the input

TABLE 1. *Transformation corrections of typical connecting transformers*

Connecting transformer		Frequency	a^2	ab'	Variable reactor
Number	Components				
		Mc/s		*Micromhos*	
1	⅜₁₆-in.-diam line; taper to 2⅜-in.-diam solid-dielectric precision slotted line.	300	1.010	−410	
		600	1.028	−260	
2	⅜₁₆-in.-diam line; taper to 1⅜-in.-diam solid-dielectric slotted line	300	0.998	−60	
		600	.991	−430	
		900	.992	−360	
3	Adapter UG–57/U [a]	300	.982	−160	⅜₁₆-in.-diam solid-dielectric slotted line. Z_0=49.9 ohms.
4	Adapter UG–57B/U [a]		1.014	110	
5	Adapter UG–29/U [a]		1.004	50	
6	Adapter UG–29A/U [a]		0.988	−130	
7	Adapter UG–27/U		1.026	0	
8	Adapter UG–27/AU [a]		0.981	−250	
9	Adapter Two GR–874–QNP [a]		.981	−20	
10	Connectors UG–21B/U, UG–23B/U		.991	−50	
11	UG–21B/U, 20 cm, RG–9/U, UG–21B/U		1.005	−680	
12	Step adapter type N to ⅞-in. diam.[b]	100	1.054	−90	⅞-in.-diam air-dielectric adjustable stub. Z_0=50.0 ohms.
13	⅞-in.-diam, 140-cm partial-air-dielectric line		1.032	−500	
14	⅞-in.-diam, 150-cm Teflon-bead line		1.005	100	
15	3⅛-in.-diam, 140-cm partial-air-dielectric line	100	0.996	130	3⅛-in.-diam air-dielectric perforated line. Z_0=50.9 ohms.
16	3⅛-in.-diam, 150-cm air-dielectric line		.999	70	

[a] UG–21B/U, UG–23B/U mating connectors were used; h=1.5 in.
[b] UG–21B/U mating connector at input end.

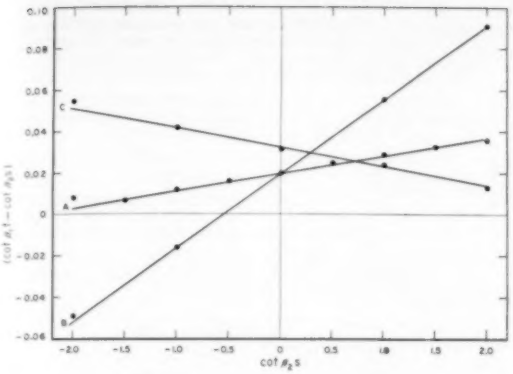

FIGURE 10. *Measurement results.*

Plots of equation (15) for connecting transformers listed in table 1: A, transformer 1; B, transformer 7 in tandem with transformer 1; and C, transformer 8 in tandem with transformer 1.

end. The magnitude of correction that can be produced by a given transformer may be estimated by considering, for example, transformer 8; $a^2=0.981$, $ab'=-250$ micromhos. Using eq (17) and (18), it can be shown that a measured impedance of $300-j10.0$ ohms at the input end of this connecting transformer corresponds to an actual load impedance of $291-j31.5$ ohms at its output end. Thus the error in the resistive component is 3 percent, and the reactive component is in error by 3 to 1.

The accuracy with which the values of a^2 and ab' can be determined depends first on the absence of curvature in the plot of eq (15) as represented in figure 10. With no observable curvature, the precision with which the straight line can be drawn depends on the scatter of the plotted points. The scatter, in turn depends on the accuracy with which the s and t values are measured. The accuracy of the transformation corrections was ± 0.5 percent or better for a^2, and $\pm$(5 percent + 0.01 micromicrofarad) for ab'.

5. Measurement of the Quality of Slotted Lines

The n-s method may advantageously be applied to determine the uniformity of a slotted line and thus indicate the order of its utility, either as a measuring line or as a variable reactor. The auxiliary equipment required in performing this quality measurement is an adjustable stub or a short-circuited line stretcher connected to the output end of the slotted line. This stub need not be of high accuracy; its purpose is only to move a voltage node along the slotted line. The procedure follows the general n-s technique. At a half wavelength from input and output ends of slotted line, voltage nodes are selected to represent, respectively, S_0 and T_0. It is desirable that the measurement frequency be high enough so that most of the line lies between S_0 and T_0. The movable short circuit is then used to place a voltage node at selected S locations, and the corresponding values of s and t are accurately measured. The data are then plotted and the values of a^2 and ab' calculated, by the usual procedure.

These resulting corrections represent the total transformation produced by all discontinuities between S_0 and T_0. Usually it is found that the magnitude of these corrections is less than would be deduced from the nonuniformity of the probe output voltage, indicated as the probe is moved along the perfectly terminated line. The choice of whether to use the n-s technique or the voltage uniformity method to determine the quality of a slotted line depends on the information desired. Variations in probe coupling do not necessarily affect the accuracy with which nodal positions can be located, but do result in probe output irregularities along the line. Hence, the n-s method (depending only on accurate nodal measurements) determines rather accurately the electrical uniformity of a slotted line, and voltage uniformity measurements (depending on line quality and probe coupling) determine the combined effect of probe penetration variations and electrical nonuniformity and establish the error limitations of complete impedance measurements. Thus, the n-s method offers means of separating the two major causes of slotted-line errors. It also follows that slotted lines, which are poor as impedance-measuring instruments, often may serve satisfactorily as variable reactors.

A way in which the uniformity of a slotted line can be qualitatively evaluated is by using it as a variable reactor in the n-s measurement of some discontinuity placed outside this line. Fixed discontinuities in the line, which change the electrical lengths of the s values, will cause curvature in the plotted results; when no curvature is obtained, the line is free from serious discontinuities.

6. Conclusions

The work described above was limited to lossless connectors. Transmission-line sections may also be considered connectors as long as their losses are negligible. A long lossless line may, of course, be looked upon as consisting of several connecting transformers in tandem; one can then obtain the transformation corrections of representative sections and calculate the transformations likely to result from the long line.

The measurements were made on connectors having ideal junctions with uniform rigid-line sections; therefore, some of the transformation corrections cited are probably better than those for connectors joined to commercial cables having braided outer conductors. One may, of course, measure a number of the latter samples and get comparative data for various types and makes of connectors, cables, and adapters, as well as for any combinations of these. The transformation corrections are obtained for discrete frequencies; it is pointed out, however, that in cases of rather small

distributed discontinuities these corrections do not vary sharply with frequency. Thus, measurements at several well-selected frequencies may be sufficient to cover a wide frequency range.

7. References

[1] J. R. Whinnery, M. W. Jamieson, and Theo. Eloise Robbins, Coaxial line discontinuities, Proc. Inst. Radio Engrs. **32**, 695–709 (Nov. 1944).

[2] M. H. Oliver, Discontinuities in concentric-line impedance measuring apparatus, Proc. Inst. Elec. Eng. **97**, part III, p. 29–38 (Jan. 1950); also discussion, p. 242 (July 1950).

[3] R. W. King, Absolute method for measuring dielectric constants of fluids at ultra-high frequencies, Rev. Sci. Instr. **8**, 201 (June 1937).

[4] Albert Weisfloch, Ein Transformationssatz über verlustlose Vierpole und seine Amvendung auf die experimentelle Untersuchung von Dezimeter und Zentimeterwellen-Schaltungen, Hochfrequenztechnik und Elektroakustik **60,** 67 (Sept. 1942).

[5] E. Feenberg, The relation between nodal position and standing wave ratio in a composite transmission system, J. Appl. Phys. **17,** 530–532. (June 1946).

[6] A. T. Starr, Electric circuits and wave filters, p. 171, 2d ed. (Pitman & Sons Ltd., London, 1948).

[7] H. E. Sorrows, W. E. Ryan, and R. C. Ellenwood, Evaluation of coaxial slotted-line impedance measurements, Proc. Inst. Radio Engrs. [2] **39,** 162–168 (Feb. 1951).

[8] F. D. Bennett, P. D. Coleman, and A. S. Meier, The design of broad-band aircraft antenna systems, Proc. Inst. Radio Engrs. p. 671–700 (Oct. 1945).

Washington, July 21, 1953.

rnal of Research of the National Bureau of Standards Vol. 52, No. 3, March 1954 Research Paper 2481

Continuous Measurement of Atmospheric Ozone by an Automatic Photoelectric Method[1]

Ralph Stair, Thomas C. Bagg, and Russell G. Johnston

An automatic photoelectric instrument and method for the continuous measurement of the ozone in the earth's atmosphere at low altitudes are described. The method is physical rather than chemical in character and is based upon the optical absorption characteristics of ozone in the Hartley and Huggins ultraviolet bands. The instrument makes use of a low-pressure mercury arc, which is situated at a distance of 1,450 feet from the recording station that employs a 1P28 photomultiplier as a detector. The light beam is modulated, at 510 cycles per second, so that the output of the photomultiplier is fed into a tuned alternating-current amplifier and amplified to the recorder level. By means of a Geneva mechanism, which changes the glass filters, the radiant energy from the lamp is separated into bands primarily at wavelengths 253.7, 365.5, and 405.0 millimicrons. From the ratios of the deflections for the different spectral regions it is possible to determine ozone concentration in the range from a few tenths of 1 part to many parts per 100 million.

1. Introduction

Although ozone is an important constituent of the atmosphere because of its protective effect in absorbing short-wave solar radiation, it is highly deleterious to rubber and related organic products. Because ozone is a highly oxidizing or catalytic agent, the presence of organic particles in the atmosphere, together with the effects of long-wave solar radiation and increased temperature at lower altitudes, results in the destruction of most of the ozone molecules below about 15 to 18 km under normal conditions of atmospheric circulation [1].[2] As a result of the loss of ozone at low altitudes and a decrease in total pressure with altitude, the partial pressure of ozone near the earth's surface is only about one-tenth that of its maximum at an altitude of about 22 km. Relative to the total number of molecules of air per unit volume, these figures become about 2 and 600 parts per 100 million, respectively.

Because ozone of significant amount is normally produced only at high altitudes in the stratosphere by short-wave ultraviolet solar radiation through a process of photochemical dissociation of the oxygen molecule, followed by recombination, any of the gas found at the earth's surface must have been transported there by some means [12]. Diffusion is slow and hence for the lower altitudes may be neglected. General large-scale air-mass movements associated with cyclonic and anticyclonic conditions, together with local air circulation resulting from thunderstorms and the like, must, therefore, be responsible for any ozone transportation at a rate sufficient to upset the static balance at the earth's surface. In fact, variations in the ozone concentration associated with air-mass movements are well known [13].

The primary purpose of this investigation has been to find a practical physical method for use in the routine measurement of the concentration of ozone in the atmosphere at low altitudes, in particular at the surface of the earth. It may be that through such studies valuable information on air-mass movement or other weather phenomena may be obtained. An instrument for this purpose should prove especially valuable in the correlation of the deterioration of rubber products with ozone changes.

Rubber, when exposed to ozone, develops a type of cracking of the surface not produced by other elements or materials normally in the atmosphere [2]. These cracks develop much more rapidly when the rubber is cured under strain [3] or when it is under stress resulting from a bending or elongation of the sample. It has been found that in outdoor exposure of rubber the amount of cracking varies seasonally and with locality. The resulting cracking is sufficiently reproducible that it may be used as a rough quantitative measure of the amount of ozone by exposing a sample of specially prepared rubber [4] to the atmosphere under the tension produced simply by bending the sample. Although the results are greatly affected by temperature [5] the method has been found useful in rough quantitative determinations of ozone.

By employing the rubber-cracking method of ozone measurement, a survey at a number of cities in 1949 showed variations from a severity factor of 360 in Los Angeles and Denver to less than 30 in New York City and Conshohocken, Pa. [6]. These tests were in general agreement with rubber-deterioration experience for the localities involved. Nor is the local ozone concentration entirely dependent upon transportation of the gas from the stratosphere. Tests made in connection with the Los Angeles smog [7] indicate the formation of excessive amounts of ozone by photochemical action associated with the oxidization of hydrocarbons by nitrogen oxides present within the area.

In recent years interest in the deteriorating effect of ozone on rubber materials has increased greatly. The development of new synthetic elastomers having

[1] This work was sponsored by the Army Ordnance Department.
[2] Figures in brackets refer to literature references at the end of this paper.

varying degrees of resistant properties to ozone also has contributed to an increased interest in this field. Although ozone is only one of several agents influencing the deterioration of rubber materials under the complex conditions of exposure to weather, it frequently proves to be the most severe [8]. Simple methods for the accurate measurement of its concentration are urgently needed.

Various chemical methods for the measurement of ozone have been suggested and set up. Most of them are elaborate, require close attention, and integrate over a relatively long interval of time. A method recently developed by Regener [1] has shortened the interval to about 30 min, as well as making all the processes of the measurement automatic. In the past, physical measurements of ozone have been considered, but no real progress has been made in this direction, although the high optical absorption of ozone between 2,500 and 2,600 A lends itself ideally to the use of a physical (optical) instrument for this purpose. The present report deals with the development of such an instrument.

2. Instruments and Methods

The method chosen for investigation, as indicated above, is physical in character and is based on the optical absorption characteristics of ozone in the ultraviolet spectrum. Although ozone has several intense absorption bands at various wavelengths within the ultraviolet, visible, and infrared regions of the spectrum, the strongest is the Hartley band centered between 2,500 and 2,600 A. The optical density of ozone (designated absorption coefficient, α, [9, 10]) as obtained by Ny Tsi-Ze and Choong Shin-Piaw is depicted as a function of wavelength in figure 1. Although the absorption band is broad, it does not extend to wavelengths longer than about 3,400 A, even for a thickness of 1 cm of ozone (normal temperature and pressure) which value is about 3 to 5 times the total in the earth's atmosphere at any time.

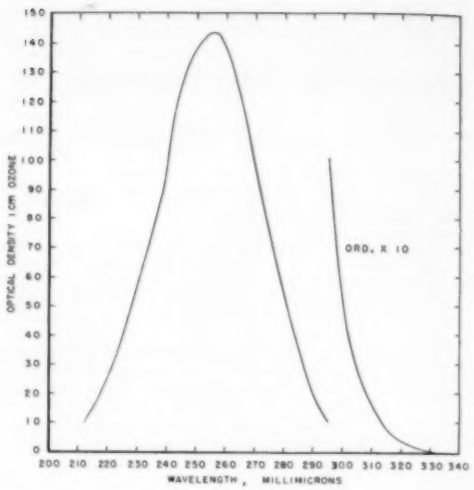

FIGURE 1. *Optical density of ozone, from the data of Ny Tsi-Ze and Choong Shin-Piaw given in references [9] and [10].*

As ozone has a maximum of absorption in the spectral region of 2,500 to 2,600 A a source having high optical emission at 2,537 A, such as a low-pressure mercury arc lamp, lends itself ideally to use in a physical setup. No other available light source has such ideal characteristics for this purpose.

TABLE 1. *Method employed in the calculation of ozone values*

This example includes a single set of data for an ozone value of 1 part per 100 million in the path distance of 1,450 feet. The spectral transmittances of this amount of ozone given in column 4 were calculated from the data of figure 1 and correspond to an equivalent layer of ozone 0.000442 cm (normal temperature and pressure) in thickness]

Center of wavelength interval	Relative spectral energy, Hg lamps	Relative response photo-multiplier 1P28	Transmittance 1 part ozone per 100 million in 1,450 ft	Product columns 2×3×4	Transmittance G9863 and wire mesh	Product columns 5×6	Transmittance G5850	Product columns 5×8	Transmittance G5860	Product columns 5×10
1	2	3	4	5	6	7	8	9	10	11
A										
2537	17.790	31.5	86.5	4.8473	18.4	0.8919	.....	.....	.....	.....
2650	.023	40.5	88.5	0.0093	22.1	.0021	.....	.....	.....	.....
2890	.005	53.7	97.8	.0026	28.9	.0008	.....	.....	.....	.....
2967	.127	55.8	99.2	.0703	29.5	.0207	3.0	0.0021	.....	.....
3024	.019	56.3	99.6	.0107	29.8	.0032	9.5	.0010	.....	.....
3132	.478	59.3	100.0	.2817	30.1	.0848	40.0	.1127	.....	.....
3342	.084	70.0	100.0	.0588	30.0	.0176	75.0	.0441	33.8	0.0199
3655	.397	92.0	100.0	.3652	28.4	.1037	88.0	.3214	59.6	.2177
4050	.496	81.0	100.0	.4018	4.2	.0169	80.0	.3214	.....	.....
4358	.913	72.3	100.0	.6601	.....	.....	56.0	.3697	.....	.....
5461	.647	32.9	100.0	.2129	.....	.....	.....	.....	.....	.....
5780	.142	24.5	100.0	.0348	.....	.....	.....	.....	.....	.....
Total	.....	.....	.....	6.9355	.....	1.1417	.....	1.1724	.....	0.2376
Percentage transmittance	.....	.....	.....	.....	.....	16.46	.....	16.86	.....	3.42
Ratio of col. 7÷col. 9 and col. 7÷col. 11	.....	.....	.....	.....	.....	.....	.....	0.973	.....	4.80

When the lamp is equipped with a glass tube that absorbs the 1,847-A emission line,[3] very little radiant energy is emitted at wavelengths below 3,650 A other than at 2,537 A. The spectral-energy distribution of such a source is given in table 1.

For convenience of modulation by a sector disk [11], a source concentrated in space is preferred. However, as no such source is commercially available, a bank of five Westinghouse Sterilamps (non-ozone type) was assembled, with a 2-in. section of each tube (see fig. 2 for a block diagram of the setup) as the source of radiation.[4] The radiant energy from the 2 in. section of these lamps is modulated by means of a rotating sector disk driven by a ½-hp, 1,800-rpm synchronous motor. The disk has 17 openings, so that the light beam is modulated at 510 c/s. One purpose of the modulated beam is to eliminate as far as possible the effect of other sources of light that might fall upon the photodetector. Other frequencies, in particular 120 c/s, were considered but were discarded in favor of the 510 cy [11].

The light source is electrically modulated at 120 c/s by the a-c line voltage. At first thought, it appeared that this would be ideal for the purpose. However, 60- and 120-cy electrical pickup and stray light modulated at the same frequencies ruled out the practical use of 120 c/s. The electrical modulation of the light source at 120 c/s has been found not to interfere with the chopped modulation at 510 c/s. Higher-frequency modulation would be preferred, except for the practical difficulties involved in the mechanical chopping of a beam of sufficient aperture to supply adequate radiant energy for the measurements.

At the detector station the modulated light beam is picked up by a 1P28 photomultiplier connected with a tuned amplifier and recorder. The special photometer unit contains a Geneva mechanism for automatically changing optical filters over the photomultiplier. A set of three Corning glass filters has been arranged on a disk, so that alternate readings are made at 2,537 A (principally), in the blue (including wavelengths 3,655, 4,050 and 4,358 A), and at 3,655 A, (see fig. 3). Each filter is placed in front of the photomultiplier for 15 sec, after which the filter disk is rapidly moved to a new position for the next filter in the series. The fourth filter position carries an opaque shutter. Hence, during each minute a complete series of measurements is completed and recorded.

By means of a timing clock the source is automatically turned on about 30 min before a similar

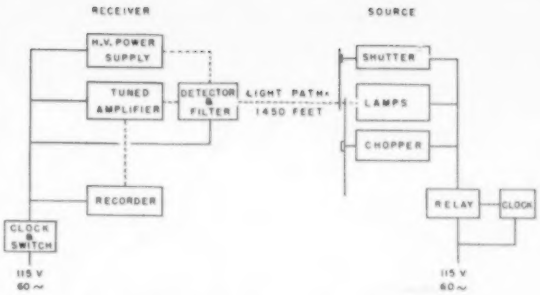

FIGURE 2. *Block diagram of ozone meter.*

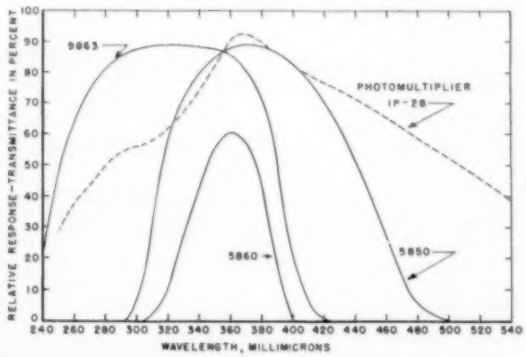

FIGURE 3. *Transmittance curves for the Corning filters and the relative spectral response of the RCA 1P28 photomultiplier.*

clock starts the receiving apparatus. Likewise, the same clocks turn off the equipment at a prearranged time each night. As all the components are controlled by timing clocks, the equipment requires no personal attention during the periods when it is in operation. Only daytime servicing and noting pertinent weather data, etc., are required.

The electric circuits for the 1P28 photomultiplier and for the tuned amplifier are displayed in figures 4 and 5. As the radiant energy transmitted through 1,450 ft from 2-in. sections of five Sterilamps is extremely low, the modulated source and the tuned-circuit amplifier were required in order to reduce the noise and to eliminate the zero drift resulting from the variable dark current in the photomultiplier. The photomultiplier was commonly operated at about 70 v per anode, which resulted in a voltage amplification of the detected signal of about 100,000. Following this, a tuned a-c amplifier (with a voltage gain of several thousand) was employed to improve the signal to noise ratio and to obtain sufficient voltage for operating a standard strip recorder.

Because the photomultiplier is highly sensitive to changes of voltage, a carefully regulated power supply is essential for precision work. The power

[3] Since ozone is created from free oxygen atoms, which are in turn created by photodissociation in the Schumann-Runge continuum, starting around 1,900 A, the source will produce a large amount of ozone if the emission line 1,847 A is not removed. Such ozone production would greatly interfere with absorption measurements. In fact a small ozone concentration near the lamp results from 2,537 A radiant energy [14]. This has negligible effects upon the measurements.

[4] No condensing lens or mirror was employed in this work. The light source was allowed to shine normally upon the detector. Although the resulting intensity was low, its constancy more than compensated for the reduced intensity because of the refractive and reflective difficulties encountered in the use of a figured reflective mirror. As the source intensity and detector sensitivity were not limiting difficulties in this work, precaution was taken to eliminate as many optical problems as possible. As a matter of fact, the size of the light source could be diminished appreciably without encountering any grave difficulties.

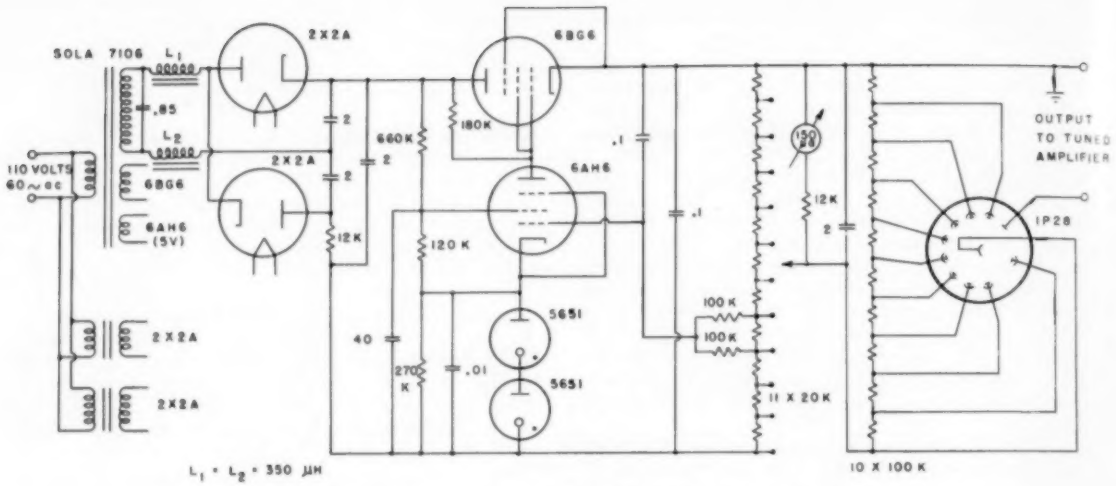

FIGURE 4. *Electronic circuit employed in the photomultiplier unit.*

Resistances in megohms and capacities in microfarads except as otherwise noted.

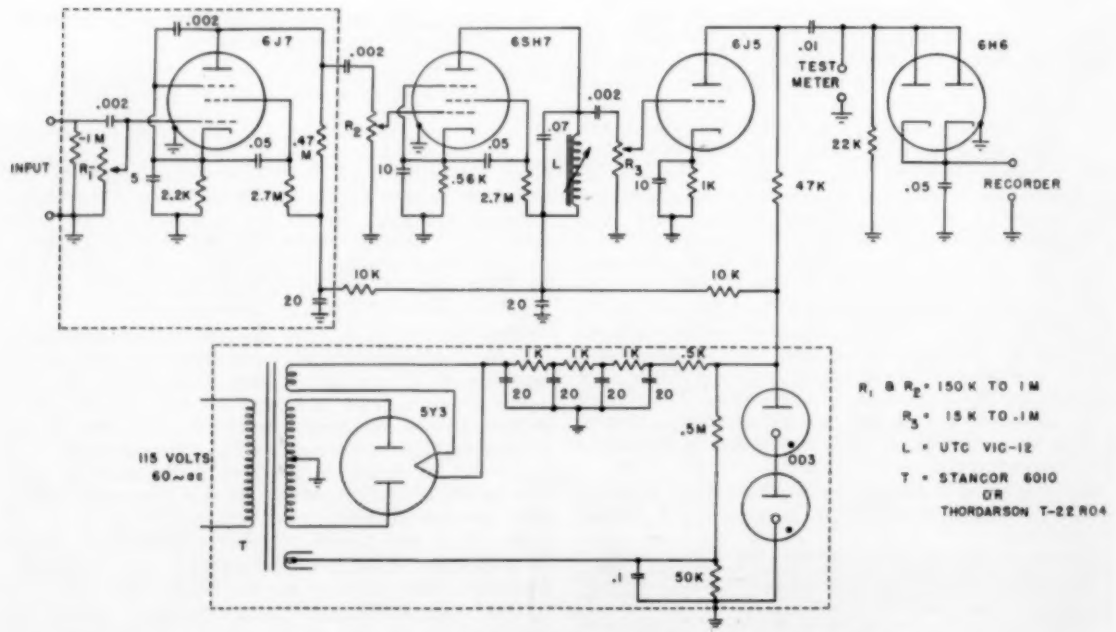

FIGURE 5. *Electronic circuit employed in the 510-cycle-per-second tuned amplifier.*

Resistance in megohms and capacities in microfarads except as otherwise noted.

pply used (see fig. 4) contains many of the circuit ements commonly employed in conventional units, keep the output voltage constant over a wide nge of input voltage. As the electric load of the plifier is relatively constant, little attention was ven to regulatory devices to cover load variations.

The tuned amplifier (see fig. 5), peaked at 510 c/s has certain characteristics that may be noted. The input stage employs a 6J7 tube for producing a relatively flat gain at a high signal-to-noise ratio. But little shaping is introduced by the coupling and feedback elements in this circuit. The second stage, employing a 6SH7 tube, contains a tuned secondary consisting of a variable inductor shunted by a fixed low-loss condenser. This combination results in a pass band of about 75 cy. The amplifier is stable at all gain settings, yet has a sufficiently narrow pass band to reduce noise and power-line frequency interference to a relatively low level.

Amplifier gain is controlled by stepped resistor banks in each of the three stages. Ample shielding of the first stage, together with plate decoupling networks, reduces noise pickup and positive feedback to a minimum.

The output of the amplifier, after rectification by a 6H6 twin diode, is fed into a commercial potentiometer-type recorder. For purposes of test and adjustment, the a-c output of the amplifier may be read on a suitable vacuum-tube voltmeter. The a-c voltage output is linear for all values below about 20 v. Recorded d-c values are slightly nonlinear as the result of contact potential within the 6H6 diode rectifier. However, this error becomes a second-order effect as ratios only are employed in the reduction of the amount of ozone. If desired, any scale errors may be eliminated through an a-c voltage calibration of the d-c recorder deflection. Usually close linearity has been obtained for all deflections above 1 v when full recorder-scale deflection was set at 10-v (alternating current) measured at the test-meter position.

The method employed in the evaluation of the amount of ozone in the 1,450-ft path between the light source and the detecting system is illustrated by a sample calculation in table 1, which gives all the steps in the determination of the filter-transmission factors corresponding to a concentration of 1 part of ozone in 100 million parts of air. Similar calculations were made for other concentrations of ozone. The results of these calculations applying to the particular photomultiplier and filters employed in the present work are illustrated by the curves of figure 6.

The work is simplified greatly by the fact that relative values only of the lamp energy and photomultiplier spectral response are required. Hence, amplifier and recorder sensitivities may be neglected, except to the extent that a reasonable deflection on the recorder chart should be obtained.

It is recognized that low-pressure mercury-arc lamps are affected in total and in relative spectral output by their operating temperatures. This is governed by the ambient temperature and especially

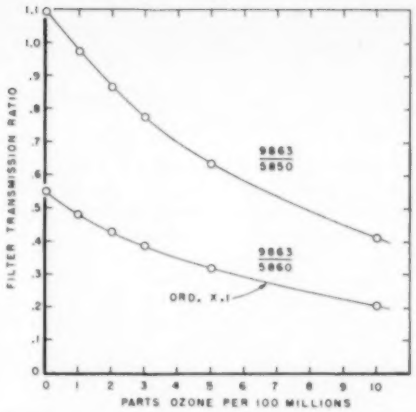

FIGURE 6. *Calibration curves for use in translating recorder records into ozone concentrations in parts per 100 million molecules of atmosphere.*

by air currents flowing past the lamp tubes. Large changes in temperature of the lamp tubes were eliminated by compactly enclosing the five lamps in a box having a small quartz-glass window through which the radiation emerged. For best results, heater units, or even temperature-control mechanisms, should be set up in the lamp box under situations of extreme temperature variation. Otherwise, the temperature may be recorded and a correction made to the calibration factor.

Selective scattering of radiation from the light by the atmosphere has been neglected in this work. Rayleigh scattering is small, and any error resulting from it is much less than that caused by other erratic changes in the atmosphere. It is assumed that any scattering by dust particles is nonselective, and therefore does not affect the transmission ratios on which the evaluation of ozone is based. In order to correct for any scattered radiation from surrounding city lights, the moon, or other sources, which might reach the photodetector, a shutter is automatically interposed in the light beam for about 1 min every 15 min.

Absorption by various impurities in the atmosphere, such as smoke or other combustion or chemical vapors associated with industry or housing, produces errors of unknown magnitude. Hence, the method cannot safely be employed where any vapors having absorption in the ultraviolet spectrum (at the wavelengths of the mercury emission lines) may be intermittenly present. Many chemical and combustion vapors are known to have high ultraviolet absorption. Chimney vapors from the burning of coal, for example, when blown into the light beam cause erratic recorder tracings.

The method is not suited to daylight operation without the installation of elaborate shielding as scattered daylight, principally in the spectral region of 3,200 to 4,000 A, will overload the 1P28 photomultiplier and make its modulated response nonlinear. When better filters are available, it may be

286398—54——3

that the response can be confined to only those wavelengths that are not in sunlight. In that case, daytime operation should be equally satisfactory.

3. Results of Ozone Measurements at Washington, D. C.

Over a period of several months during the late winter and early spring of 1953 an automatic record was kept of the ozone concentration over the grounds of the National Bureau of Standards for a period of about 3 hr during the early part of each evening. Figure 7 gives an example of sections of one of these records made during an evening on which the amount of ozone varied from time to time. On most evenings there was little or no change. Except for changes associated with incoming cold air-mass fronts, no ozone concentration exceeding a few tenths of 1 part in 100 million was normally observed. Associated with these fronts, a concentration of several parts per 100 million often appeared. Sometimes the concentration of ozone fluctuated (as shown in figs. 7 and 8) or disappeared during the evening measure-

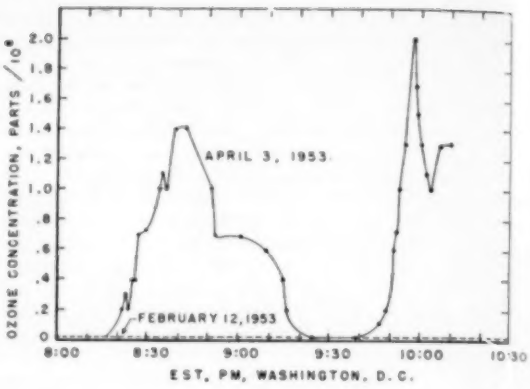

FIGURE 8. *Variations in ozone concentration for two evenings.*

February 12, 1953; mild, humid, cloudy, light northwest wind, following passage of cold front at 1:30 p. m. April 3, 1953; mild, sky clear, light south wind, preceding cold front and low moving in from northwest; possible upper air instability.

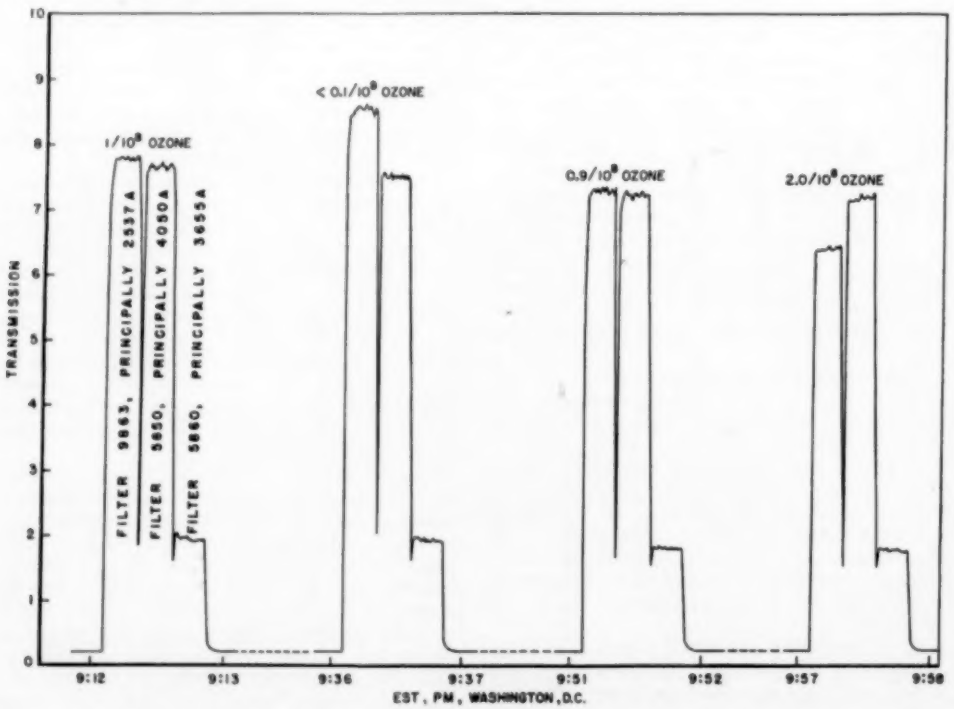

FIGURE 7. *Sections of a recorder tracing for April 3, 1953, showing fluctuations in the ozone concentration at Washington, D. C.*

The ratio of 9863 to 5850 is primarily the ratio of the transmitted intensities of 2537 A to 4050 A. Similarly, the ratio of 9863 to 5860 is primarily the ratio of the transmitted intensities of 2537 A to 3655 A.

ments. In all cases during the tests it had disappeared by the following evening.

Although the results are not conclusive, it appears that the presence of a substantial amount of ozone at Washington, D. C. is of only temporary duration. Tests with rubber samples substantiate this conclusion. No doubt the large amount of vegetation within the area is very effective in keeping ozone to a neglible value except during the short time intervals in which cold air masses are bringing it to the earth's surface within this area [15].

The high sensitivity of this equipment in the detection of ozone suggests its use in precise routine measurements at various locations in any study of the association of ozone with rubber deterioration or with possible correlations between ozone distribution and other weather phenomena.

4. References

[1] Gerald Bowen and Victor H. Regener, On the automatic chemical determination of atmospheric ozone, J. Geophys. Research **56,** No. 3, 307 (1951).

[2] James Crabtree and A. R. Kemp, Accelerated ozone weather test for rubber, Ind. Eng. Chem., Anal. Ed. **18,** 769 (1946).

[3] H. A. Winkelmann, Static exposure testing of automotive compounds, Ind. Eng. Chem. **44,** 841 (1952).

[4] C. E. Bradley and A. J. Haagen-Smit, The application of rubber in the quantitative determination of ozone, Rubber Chem. and Technol. **24,** 750 (1951).

[5] G. R. Cuthbertson and D. D. Dunnom, Cracking of rubber and GR-S in ozone, Rubber Chem. and Technol. **25,** 878 (1952)

[6] A. W. Bartel and J. W. Temple, Ozone in Los Angeles and surrounding areas, Ind. Eng. Chem. **44,** 857 (1952).

[7] A. J. Haagen-Smit, Chemistry and physiology of Los Angeles smog, Ind. Eng. Chem. **44,** 1342 (1952).

[8] D. C. Thompson, R. H. Baker, and R. W. Brownlow, Ozone resistance of neoprene vulcanizates, Ind. Eng. Chem. **44,** 850 (1952).

[9] Ny Tsi-Ze et Choong Shin-Piaw, L'absorption de la lumiére par l'ozone entre 3050 et 3400 A (region des bandes de Huggins), Compt. rend. **195,** 309 (1932).

[10] Ny Tsi-Ze et Choong Shin-Piaw, L'absorption de la lumiére par ozone entre 3050 et 2150 A., Compt. rend. **196,** 916 (1933).

[11] Ralph Stair, Photoelectric spectroradiometry and its application to the measurement of fluorescent lamps, J. Research NBS **46,** 437 (1951) RP2212.

[12] S. K. Mitra, The upper atmopshere, The Asiatic Society, Calcutta (1952); B. Haurwitz, The physical state of the upper atmosphere, Roy. Astron. Soc. Can., Toronto (1941); Richard Ansel Craig, The observations and photochemistry of atmospheric ozone and their meteorological significance. (Thesis, Mass. Inst. of Tech., 1948).

[13] G. M. B. Dobson, D. N. Harrison, and J. Lawrence, Proc. Roy. Soc. (London) [A] **122,** 456 (1929); G. M. B. Dobson, A. W. Brewer, and B. M. Cwilong, Proc. Roy. Soc. (London) [A] **185,** 144, (1946).

[14] C. F. Warburg, Z. Elektrochem. **27,** 133 (1921).

[15] Herman Bogaty, Kenneth S. Campbell, and William D. Appel, The oxidation of cellulose by ozone in small concentrations, Textile Research J. **22,** No. 2, 81 (1952); Alfred Ehmert, Gleichzeitige Messungen des Ozongehaltes bodennaher Luft an mehreren mit einem einfachen absoluten Verfahren, J. Atm. and Terr. Phys **2,** 189 (1952).

WASHINGTON, October 30, 1953.

Journal of Research of the National Bureau of Standards Vol. 52, No. 3, March 1954 Research Paper 2482

Applications of Dimensional Analysis to Spray-Nozzle Performance Data

Montgomery R. Shafer and Harry L. Bovey

Some possible applications of dimensional analysis in studies of the performance of continuous fuel-spray nozzles of the centrifugal type are presented. Equations are developed showing the relations among nozzle capacity, mean drop diameter, spray angle, nozzle size, the density, viscosity, surface tension, and pressure of the fuel. Using experimental data available at the National Bureau of Standards and in the literature, good correlation is shown in considerations of nozzle capacity, and fair correlation in those involving mean drop diameter and spray angle.

1. Introduction

In the course of research sponsored by the Bureau of Aeronautics, Department of the Navy, on various fuel-handling and metering devices for aircraft engines, one of the accessories of interest has been the spray nozzle, which is widely used for the atomization of liquid fuels in turbine-type engines. The performance of such engines is influenced by the characteristics of the nozzles, including the quantity of fuel delivered, the size of the droplets, and the angle of the spray. The latter, in turn, are known to be influenced by the configuration of the nozzle, the nozzle-pressure drop, and by certain physical properties of the fuel, including density, viscosity, and surface tension.

The well-known advantages of dimensional analysis, namely, a reduction in the number of variables, the possibility that the effect of one quantity may be studied by varying another, and the ease with which it can be shown that certain variables are unimportant, have not been utilized heretofore in published analyses of the performance of fuel nozzles. These advantages are demonstrated here by applying this method of analysis to the limited data available from research at the National Bureau of Standards and elsewhere on fixed, continuous-spray nozzles of the centrifugal type.

Relations among several dimensionless variables are developed. The particular variables suggested herein are not new, and the reader will recognize in them the Reynolds and Weber numbers and products thereof. They seem convenient for showing both the individual and combined effects of nozzle size, fuel pressure, and the properties of the fuel upon the capacity of the nozzle, upon the angle of spray, and upon the mean drop diameter.

The nozzles under consideration are of fixed configuration and deliver a continuous fuel spray. Atomization in such nozzles is produced by the conversion of potential energy of the high-pressured liquid to kinetic energy in the high-velocity liquid discharged from the nozzle orifice. Both the simplex type, having a single internal flow passage from the pressurized fuel supply, and the duplex type, having two separate fuel inlets and internal flow passages, are considered. Although only centrifugal spray nozzles are treated specifically, it is well known that the analysis holds for nozzles of other types and for restrictions through which a liquid discharges, subject only to the limitation that the device have no moving parts.

2. Nomenclature

	Dimensions (m, l, t systems)
D = a length characterizing the size of the nozzle.	(l).
d = mean drop diameter of the spray	(l).
M = mass rate of flow	(mt^{-1}).
ΔP = pressure drop through the nozzle	($ml^{-1}t^{-2}$).
ΔP_s = pressure drop through small passage of duplex nozzle.	($ml^{-1}t^{-2}$).
r_i = length ratios designating shape of nozzle.	Dimensionless.
ρ = mass density	(ml^{-3}).
σ = surface tension	(mt^{-2}).
θ = spray angle	Dimensionless.
μ = absolute viscosity	($ml^{-1}t^{-1}$).

3. Theory

A highly simplified description of the process of atomization from a simplex fuel nozzle, such as that shown schematically in figure 1, is adequate for present purposes. Pressurized liquid supplied to the nozzle inlet flows at high velocity through small tangential slots into the swirl chamber where a high angular velocity is attained. It then passes through the discharge orifice and emerges into the surrounding atmosphere in the form of a hollow, conical sheet, the apex of which is at the nozzle orifice. The liquid sheet becomes progressively thinner as it moves away from the orifice. Eventually the sheet becomes unstable, rupturing occurs, and small droplets are formed.

The effects of the liquid pressure drop, density, viscosity, and surface tension upon the rate of discharge, the mean drop size, and the angle of the spray are to be considered in this analysis. It is desired to develop relations by which experimantal data may be correlated to form characteristic curves and charts showing the relative influence of the various independent quantities upon nozzle performance.

UNIVERSITY OF MICHIGAN LIBRARIES

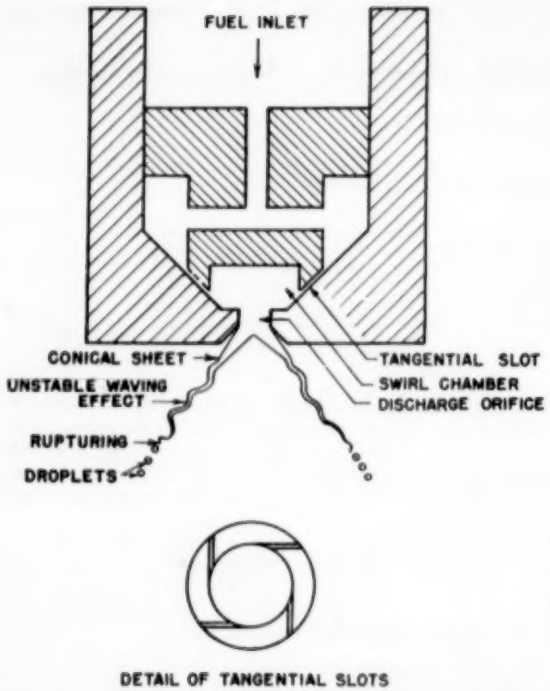

FIGURE 1. *Schematic diagram of a simplex spray nozzle.*

3.1. Flow Rate of the Simplex Nozzle

Again referring to figure 1, the flow rate of the liquid through the nozzle could be influenced by the pressure drop, i. e., the difference in pressure between the nozzle inlet and the atmosphere into which the spray discharges, by the density, viscosity, and perhaps surface tension of the liquid, and by those linear dimensions defining the configuration and the orientation of the flow passages and swirl chamber. Any one of these nozzle dimensions, such as the diameter of the orifice, may be designated as a characteristic length, D, and all others may then be expressed as dimensionless ratios ($r_1, r_2, \ldots, r_i$) of this characteristic length.

Assuming that all quantities that have an appreciable effect upon the flow rate have been enumerated their interrelation can be expressed by the general equation

$$F(M,\ \Delta P,\ \rho, \mu, \sigma, D, r_1, r_2, \ldots, r_i) = 0, \qquad (1)$$

in which F merely denotes "function of."

By applying Buckingham's pi theorem [1, 2],[1] eq (1) reduces to

$$\Pi_1 = \Phi(\Pi_2,\ \Pi_3, r_1, r_2, \ldots, r_i), \qquad (2)$$

in which each Π symbol represents a dimensionless variable or product formed through different combinations of not more than 4 of the 6 dimensional quantities in eq (1). Also, each Π is completely independent of the others, in that each contains one quantity not in either of the other two.

The three dimensionless Π products may be formed by selecting any 3 of the 6 dimensional quantities of eq (1) which are independent, and by associating these in turn with each of the remaining three dimensional quantities. Since primary interest is in the effects of viscosity and surface tension upon flow rate, it is desirable to derive each of the three Π products in such a way that one and only one will contain the quantities M, μ, and σ. This leaves ΔP, ρ, and D as the three quantities that may be involved in all three products. On this basis, the quantities can be arranged in dimensionless groups such as:

$$\Pi_1 = M/D^2\sqrt{\Delta P \rho};\quad \Pi_2 = D\sqrt{\Delta P \rho}/\mu;\quad \text{and}\quad \Pi_3 = D\Delta P/\sigma.$$

Substitution of these values in eq (2) gives

$$M/D^2\sqrt{\Delta P \rho} = \Phi(D\sqrt{\Delta P \rho}/\mu,\ D\Delta P/\sigma,\ r_1,\ r^2,\ \ldots,\ r_i). \qquad (3)$$

The function Φ is as yet unknown, and in fact it could have an infinite number of forms depending upon the shapes of the nozzles. However, if the consideration be now restricted to geometrically similar nozzles of fixed configuration but of different absolute sizes, i. e., to nozzles having the same r_i ratios, eq (3) reduces to

$$M/D^2\sqrt{\Delta P \rho} = \Phi(D\sqrt{\Delta P \rho}/\mu,\quad D\Delta P/\sigma), \qquad (4)$$

in which the form of the function Φ will differ for various nozzle configurations.

As each of the quantities appearing in eq (4) can be measured, the explicit form of the function Φ can be determined by experiment for any particular nozzle. The experimental data might be plotted in terms of $M/D^2\sqrt{\Delta P \rho}$ as a function of $D\sqrt{\Delta P \rho}/\mu$ for different values of $D\Delta P/\sigma$. If such a plot shows that, regardless of the value of the latter parameter, a single curve is defined, then it has been demonstrated that surface tension has little or no effect upon the flow rate, since σ appears in eq (4) only in the product $D\Delta P/\sigma$. Thus, to investigate the effects of changes in surface tension, it is necessary only to change the variable $D\Delta P/\sigma$. This can be accomplished by varying either σ, ΔP, or D, although it is not simple to change D by fabricating geometrically similar spray nozzles of different absolute sizes.

Herein lies one of the important advantages of dimensional analysis, in that the effect of variations in one quantity, surface tension in this illustration, may be investigated by changing some other quantity, in this case the pressure drop or the size. Another advantage of this method is seen by comparing eq (1) and (4). The former contains six independent dimensional variables, which have been combined into three independent products in eq (4). This reduction in the number of variables from 6 to 3 simplifies the presentation and application of results.

[1] Figures in brackets indicate the literature reference at the end of this paper

3.2. Flow Rates of Duplex Nozzles

As is shown in figure 2, duplex nozzles are provided with two inlets and two separate internal flow passages. The inlet pressures may or may not be equal. From the viewpoint of dimensional analysis, the duplex nozzle of fixed configuration differs from the simplex nozzle in a single important respect, namely, that the pressure drops ΔP and ΔP_s for the main and small flow passages must both be included in the consideration. Thus eq (1) for the duplex nozzle becomes

$$F(M, \Delta P, \Delta P_s, \rho, \mu, \sigma, D, r_1, r_2, \ldots, r_t)=0. \quad (5)$$

By forming the dimensionless groups as before, and by limiting the consideration to geometrically similar nozzles, there results the relation

$$M/D^2\sqrt{\Delta P\rho}=\Phi(D\sqrt{\Delta P\rho}/\mu,\ \Delta P/\Delta P_s,\ D\Delta P/\sigma). \quad (6)$$

It is known that variations in the parameter $D\Delta P/\sigma$ have no appreciable influence upon the function Φ for either the simplex or the duplex nozzles investigated. Thus $D\Delta P/\sigma$, and consequently surface tension, can be omitted from both eq (4) and (6). Equation (6) then becomes

$$M/D^2\sqrt{\Delta P\rho}=\Phi(D\sqrt{\Delta P\rho}/\mu,\ \Delta P/\Delta P_s). \quad (7)$$

In applying this relation to the experimental data, it will be found convenient to form charts of $M/D^2\sqrt{\Delta P\rho}$ versus $D\sqrt{\Delta P\rho}/\mu$ for various constant values of the pressure ratio $\Delta P/\Delta P_s$.

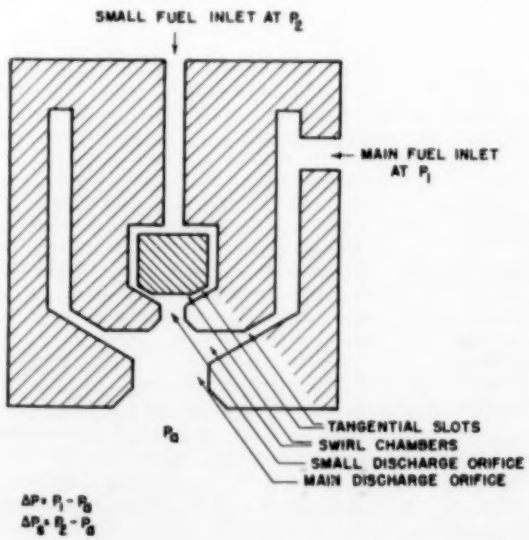

FIGURE 2. *Schematic diagram of a duplex spray nozzle.*

3.3. Mean Drop Size of the Spray

Consider next the mean diameter of the droplets formed during the rupture of the conical sheet emerging from the nozzle orifice. In an actual spray having a condensed volume, V, and consisting of N droplets of various sizes, the mean drop size, d, is taken [3] as the diameter of a sphere having a volume V/N.

Previous investigators [4, 5, 6, 7] have shown that the density, surface tension, and viscosity of the liquid, as well as the relative velocity between the liquid and the air just prior to atomization, may all influence drop size. Although the velocity of a liquid emerging from a centrifugal-type nozzle is not readily measurable, it depends upon the nozzle configuration and upon the flow rate, the latter being influenced by the pressure drop and by the density and viscosity of the liquid. The size of the drops also depends upon the shape of the spray chamber and the location of the drop-sampling apparatus within the spray. Thus, with the understanding that the procedure applies only to geometrically similar nozzles, spray chambers, and drop-determination methods, the general equation

$$F(\Delta P, \rho, \mu, \sigma, D, d)=0 \quad (8)$$

includes all the quantities that are expected to exert an appreciable influence when the spray discharges into still air.

Through the same procedure used in reducing eq (1) to eq (3), eq (8) may be reduced to the form

$$d/D=\Phi(D\Delta P/\sigma,\ D\rho\sigma/\mu^2). \quad (9)$$

Equation (9) is convenient for the present purpose, as it separates the effect of fluid viscosity. If experimental results show that the effect of viscosity is appreciable, it would be convenient to form a chart of d/D versus $D\Delta P/\sigma$ for different constant values of $D\rho\sigma/\mu^2$. For any given value of D, the latter variable is constant for a given fluid at constant temperature, and can be varied conveniently by proper selection of the test fluids.

3.4. Angle of the Spray

Similar considerations may be applied to the spray angle. For this correlation, use is again made of the data of Rupe [3], who states arbitrarily that this angle shall be symmetrical about the axis of the spray and shall include 80 percent of the total-weight flow. It seems reasonable that this dimensionless angle, θ, could be influenced by the configuration and size of the nozzle, and by the pressure drop, density, viscosity, and surface tension of the liquid. It does not seem probable that any other quantity will have a significant effect when the nozzle is discharging into stagnant air, except for the currents created by the spray itself. Thus, as before, the general equation may be written

$$F(\Delta P, \rho, \mu, \sigma, D, \theta)=0, \quad (10)$$

which reduces to

$$\theta=\Phi(D\Delta P/\sigma,\ D\rho\sigma/\mu^2). \quad (11)$$

4. Experimental Results and Discussion

The validity of the relations developed above is demonstrated if plots of the experimental values of the dimensionless parameters give curves from which the deviations of the individual points do not exceed the experimental error. Such plots provide means of correlating the experimental data, and show the influence of the various quantities upon the flow rate, mean drop size, and spray angle. In the graphs that follow, the experimental data on the flow capacity of the nozzles were obtained at the Bureau. The data on drop size and spray angle are original with Rupe [3].

4.1. Nozzle Flow-Capacity Correlation

The nozzles selected for the flow-capacity tests were types currently in use in aircraft gas turbines. These included three simplex nozzles of one make, design, and nominal size, and two duplex nozzles of different designs. All were of the fixed configuration, continuous spray, centrifugal type, and each was an unmodified production unit.

Four different liquids were used in the flow-capacity measurements. The temperature of the liquid at the nozzle, as measured in each run by a thermocouple, varied from 77° to 90° F, depending upon the operating pressure and flow rate. The pertinent physical properties of these test liquids at the average operating temperature of 81.5° F are given in table 1.

TABLE 1. *Properties of the capacity test liquids at 81.5° F*

Description	Density, ρ	Viscosity, μ	Surface tension, σ
	g/cm³	cp	Dynes/cm
Commercial grade of heptane	0.691	0.412	22.8
Light petroleum solvent	.780	.863	27.6
45% of white mineral oil plus 55% of light petroleum solvent	.813	2.38	29.2
75% of white mineral oil plus 25% of light petroleum solvent	.837	7.02	31.3

The variations of the properties of the liquids with temperature over the operating range of 75° to 90° F were also known, and the actual values corresponding to the operating temperature observed in each run were used in computing the dimensionless variables.

With a given liquid in the test system, the flow rates (M) were observed at nozzle pressure drops of 20, 40, 70, 100, 175, and 275 lb/in². These flow rates were determined for each nozzle at each of the aforementioned pressure drops before changing the liquid. This procedure requires that each nozzle be installed and removed whenever the liquid is changed. Although the simplex nozzles were torqued to approximately the same value at each insertion, it is possible that this process caused small changes in configuration, which would influence the correlation among results with different fluids.

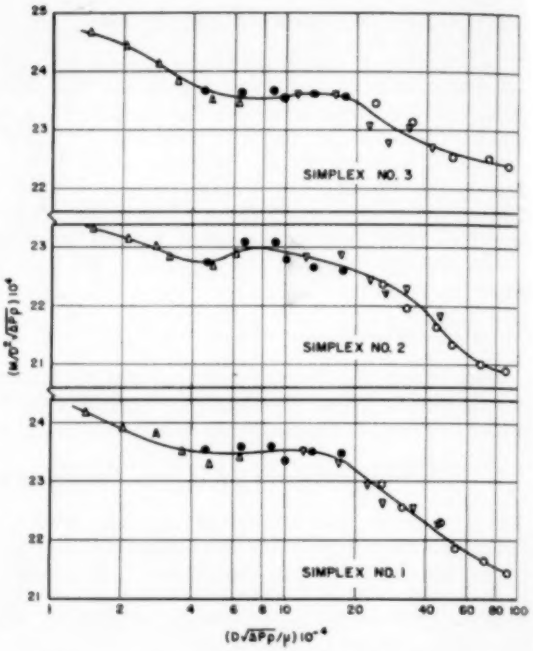

FIGURE 3. *Capacity curves for three simplex nozzles.*

The capacity of the duplex nozzles was determined in the same way as that of the simplex nozzles, except that the pressure ratio $\Delta P/\Delta P_s$ was controlled and measured. Ratios of infinity, 1.0, 0.6, and 0.0 were selected arbitrarily for these tests. The 0.6 pressure ratio had to be omitted in the case of nozzle 2, because its flow rate proved so sensitive in this region that accurate measurements could not be made.

In dealing with fuel nozzles it is common practice to express capacity in pounds per hour, pressure drop in pounds per square inch, density of the liquid in grams per cubic centimeter, its absolute viscosity in centipoises, and its surface tension in dynes per centimeter. Although these mixed units are used in this report for specifying experimental conditions and characteristics of the liquid, all measured quantities were converted to cgs units before computing the dimensionless variables presented herein. Thus the dimensionless variables are based on flow rates in grams per second, pressure drops in dynes per square centimeter, densities of the fluid in grams per cubic centimeter, its absolute viscosity in poises, and its surface tension in dynes per centimeter. The dimensionless equations are independent of the system of units employed, and the user may select the system with which he is most familiar, provided only that the same units are used in developing numerical values of the parameters and in their subsequent applications.

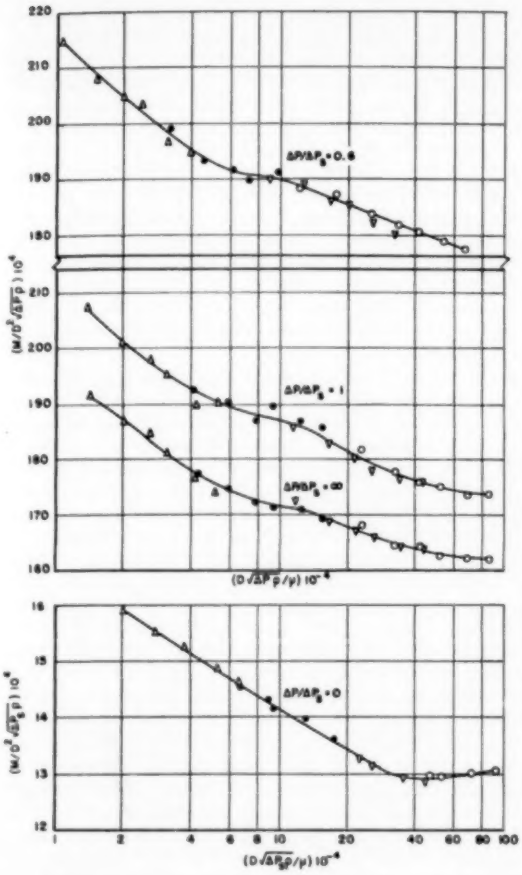

FIGURE 4. *Capacity curves for duplex nozzle 1.*

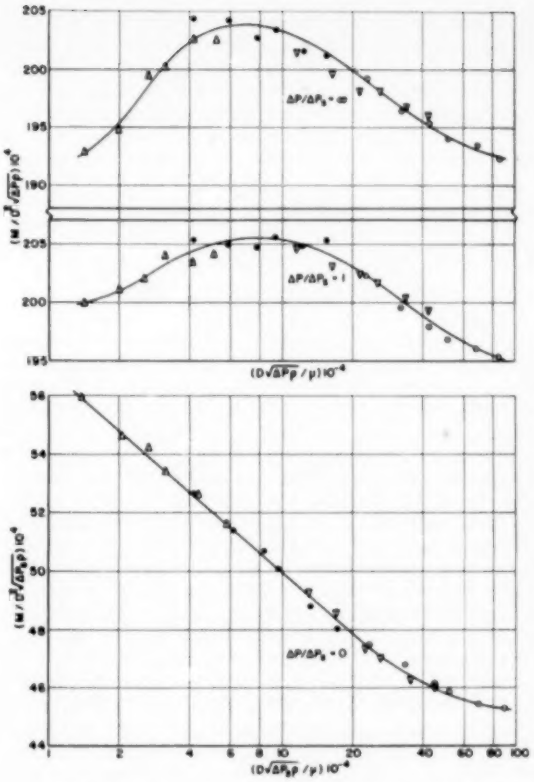

FIGURE 5. *Capacity curves for duplex nozzle 2.*

In the present state of the manufacturing art it is not practicable to make the small and intricate flow passages of production nozzles geometrically similar. It was therefore anticipated that correlation of the data for the three simplex nozzles by a single curve would not be possible. Hence a separate characteristic curve is presented for each nozzle, and since D for a given nozzle is constant, its value need not be determined. For simplicity the value of one centimeter is arbitrarily assigned to D.

With this assigned value of D, the parameters $M/D^2\sqrt{\Delta P\rho}$ and $D\sqrt{\Delta P\rho}/\mu$ can be evaluated from the experimental data for each nozzle and for each observed value of pressure drop, density and viscosity. The results for the three simplex nozzles are shown in figure 3, and those for duplex nozzles 1 and 2 are shown in figures 4 and 5, respectively. The same symbol is used in all these figures for a given test fluid. It will be seen that the results for each nozzle define a single curve or chart, from which the individual points deviate by less than ± 1 percent on the average. Such scattering is commensurate with the experimental error, thus confirming eq (4) and (7).

Referring to figures 4 and 5, the capacity curves for the duplex nozzles show that the treatment of the two inlet pressures, through the formation of the dimensionless pressure ratio $\Delta P/\Delta P_s$, is valid. Thus, through the relation expressed in eq (7), it is possible to obtain characteristic capacity curves at selected, constant values of pressure ratio for the duplex nozzles.

In general, the capacity curves show slightly increasing flow rates with increasing viscosity, for constant values of D, ΔP, and ρ. They also show a noticeable difference between nozzles that have the same nominal size and shape. After a curve of this type has been established for a given nozzle, it may be used for estimating the capacity of that nozzle to deliver other fluids.

As an illustration of the utility of such capacity curves, the possible effects of changes in surface tension upon flow rate will be considered. In performing the capacity tests, the product $D\Delta P/\sigma$ was varied between 4.5×10^4 and 83×10^4. Despite the

286398—54——4

fact that the parameter $D\Delta P/\sigma$ appears in eq (4), all values of $M/D^2\sqrt{\Delta P\rho}$ and of $D\sqrt{\Delta P\rho}/\mu$ for a given nozzle lie on a single curve. As the surface tension does not appear in the plotted parameters and as the experimental values of the latter lie on a smooth curve, regardless of the value of $D\Delta P/\sigma$, the results indicate that the flow rate is not affected significantly by the surface tension of the liquid that is flowing. This conclusion is limited to variations in σ that produce changes in $D\Delta P/\sigma$ within the range specified above.

4.2. Mean Drop-Size Correlation

Although no measurements of drop size or spray angle have been made at the Bureau, the applicability of eq (9) and (11) can be examined by referring to data obtained elsewhere. Rupe [3] presents extensive data on a few nozzles with different liquids, and his results will now be inserted in the equations. The pertinent properties of the liquids used by Rupe are listed in table 2.

Rupe's method of determining drop size involved collecting the spray droplets for a predetermined time interval in cells having non-wetting glass bottoms. These contained an immersion liquid having a lower density than that of the sprayed fluid. The droplets collected on the bottom were photographed under magnification and their images were counted with an automatic electronic scanner-counter in 14 size groups down to 5 microns. The results of interest

TABLE 2. *Properties of the drop-size and spray-angle test liquids*

Fluid No.	Components			Properties at 20° C			
	Water	Nigrosin	Additive [a]	Surface tension	Specific gravity 20°/20° C	Viscosity	$\frac{D\rho\sigma}{\mu^2}\times$ [b] 10^{-4}
	wt %	wt %	wt %	Dynes/cm		cp	
1	96.63	3.37	0.00	67.0	1.003	1.158	49.7
2	86.93	3.37	9.70	63.3	1.029	1.332	27.8
3	79.92	3.37	16.71	61.6	1.048	1.936	17.2
4	73.00	3.37	23.63	59.4	1.068	2.531	9.9
5	95.13	3.37	1.50	46.0	1.008	1.293	28.2
6	93.63	3.37	3.00	38.0	1.001	1.284	23.1
7	90.36	3.34	6.30	28.0	0.996	1.429	13.6
8	100-octane gasoline			19.0	[c] .712	[c] 0.497	[c] 54.6

[a] Additive to fluids 2, 3, and 4 was glycerol; to fluids 5, 6, and 7 was butyl alcohol.
[b] Value of D taken as 1 cm in the parameter $D\rho\sigma/\mu^2$.
[c] Specific gravity and viscosity are estimated values.

here, as presented in figures 12, 13, and 15 of reference [3], apply to a single spray nozzle with droplets collected from the same relative position in successive runs.

Rupe's figure 12 applies for fluid 1, and shows mean drop diameter as a function of pressure drop. In his figure 13 the ratio of the mean drop diameters of fluids 5, 6, and 7 to that of fluid 1 are plotted as functions of surface tension at pressure drops of 25, 30, and 100 lb/in^2. In his figure 15 the ratio of the mean drop diameters of fluids 2, 3, and 4 to that of fluid 1 are shown as functions of viscosity at pressure drops of 50, 100, and 150 lb/in^2. His method of analyzing the results required data on two groups of fluids, one (fluids 1, 5, 6, and 7) having equal viscosities but different surface tensions and one (fluids 1, 2, 3, and 4) having equal surface tensions but different viscosities. Three separate graphs were required for presenting the results, and these concealed rather than revealed possible unevaluated influences. Had he planned to treat the results by dimensional analysis, there would have been much greater leeway in the choice of test fluids and in the selection of experimental pressure drops. The results could also have been presented on a single chart.

In the present treatment the data of reference [3] have been substituted in eq (9), using the arbitrary value of 1 cm for D. The resulting values of d/D and $D\Delta P/\sigma$ are plotted in figure 6 for the seven test fluids. It will be noted that the points define a single curve, from which the deviations are usually within ± 10 percent. For values of $D\Delta P/\sigma$ between 2.8×10^4 and 10×10^4, even better correlation is obtained. Considering the difficulties encountered in collecting, photographing and counting the numerous droplets ranging in diameter from 5 to 200 microns, such correlation is surprisingly good. Nevertheless, an examination of the probable causes of the scattering is of interest, as it indicates the presence of some unevaluated influence in the experiments.

It seems improbable that the effects of viscosity are a primary cause of the scattering. Equation (9) indicates that a plot of d/D versus $D\Delta P/\sigma$ should yield a chart with each curve representing a constant value of the product $D\rho\sigma/\mu^2$. Thus all fluids having the same value of this parameter should define the same curve, even though their separate values of ρ, σ, and μ may differ considerably. Furthermore, if the plot of d/D versus $D\Delta P/\sigma$ yields a single curve for any particular range of the product $D\rho\sigma/\mu^2$, then it is known that changes in ρ or μ, which cause the product to vary within this range will not affect the d/D ratio, and consequently the drop size.

Referring to figure 6 and table 2, the points representing fluids 2, 3, and 4 all define the same curve, even though their respective values of $(D\rho\sigma/\mu^2)\times10^{-4}$ are 27.8, 17.2, and 9.9. Thus, con-

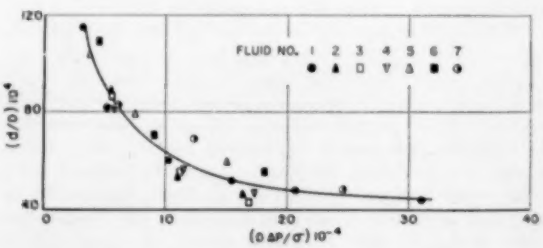

FIGURE 6. *Mean drop-size curve (Rupe's nozzle 4).*

sidering only these three fluids, it could be concluded that variations in viscosity that cause the product $(D\rho\sigma/\mu^2)\times10^{-4}$ to vary within the range 10 to 28 will not affect the drop size. Considering fluids 5, 6, and 7, for which the respective values of $(D\rho\sigma/\mu^2)\times10^{-4}$ are 28.2, 23.1, and 13.6, it appears that these fluids define a different single curve. As these two groups of fluids embrace the same range of $D\rho\sigma/\mu^2$, the separation between the curves defined by the two groups cannot be attributed to either viscosity or density effects.

Some possible explanations of the scattering in figure 6 are that some influential quantity has been omitted from the theoretical consideration; that the nozzle configuration may have changed, either from dirt or rust, during the experiments; or that properties of the test fluids at the instant of drop formation may have been different from the tabulated static values. Rupe mentions the latter possibility in connection with the surface tension of the water-alcohol mixtures. The method of collecting and counting the smaller droplets may also have been inadequate, thus resulting in appreciable errors in the total number of drops and consequently in their mean diameter.

The curve of figure 6 may be used to predict with fair accuracy the mean drop diameter from geometrically similar nozzles of different sizes, with any liquid and pressure drop, provided only that the values of $D\Delta P/\sigma$ and $D\rho\sigma/\mu^2$ are within the ranges investigated. As the ratio d/D is nearly constant at the higher values of $D\Delta P/\sigma$, the mean drop size would be expected to increase in direct proportion to the size of the nozzle. This is not true, however, in the region of lower values of $D\Delta P/\sigma$.

4.3. Spray-Angle Correlation

Spray angle data for a single nozzle at different pressure drops within the range from 5 to 100 lb/in^2 are given in figure 24 of reference [3]. These data, obtained with liquids 1, 5, 6, 7, and 8 of table 2, were presented in terms of θ as a function of ΔP, with a separate curve for each liquid.

From these data, the dimensionless variables of eq (11) were computed, with the result shown in figure 7. Each symbol represents a single test liquid, and hence also a single value of the product $D\rho\sigma/\mu^2$. As the individual points do not deviate from the curve by more than $\pm5°$, the correlation is considered reasonable. However, for $D\Delta P/\sigma$ from 3.5×10^4 and 10×10^4, fluid 1 appears to define a different curve from that of fluids 5 through 8. As in the case of the mean drop-size correlation, viscosity effects are not believed responsible, because table 2 shows that fluid 1 has a value of $D\Delta P\sigma/\mu^2$ within the range encompassed by fluids 5 through 8. Therefore, it appears that either the nozzle configuration changed or some unknown influence has been omitted from the consideration.

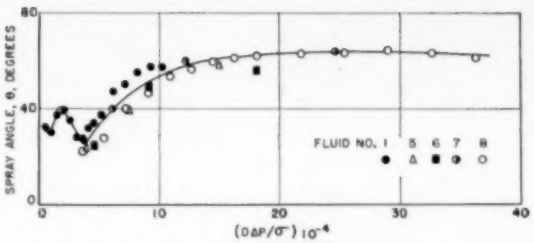

FIGURE 7. *Spray-angle curve (Rupe's nozzle 4).*

5. Conclusion

Dimensional analysis provides a useful and convenient method for correlating and presenting experimental data on the performance of fuel spray nozzles. It is shown that experimental values of flow capacity with liquids of various physical properties define a single curve for each nozzle, when plotted in terms of logical dimensionless variables. Correlations of available data on mean drop size and on spray angle are less exact than those on capacity. This lack of correlation may be ascribed, at least in part, to experimental error. However, the possibility that some important quantity has been omitted in formulating the dimensionless relations is not excluded.

The curves presented to indicate nozzle performance apply specifically only to the particular nozzles for which they were determined. They are used solely to illustrate possible applications of dimensional analysis to the study of spray nozzles for such purposes as determining effects of individual variables that cannot be changed readily and independently; developing test programs leading to a desired end result from a limited number of experiments; analyzing, correlating, and interpreting experimental data; and predicting differences in performance due to the use of liquids of different physical properties.

6. References

[1] H. L. Langhaar, Dimensional analysis and theory of models (John Wiley & Sons, Inc., 1951).

[2] E. Buckingham, On physically similar systems; illustrations of the use of dimensional equations, Phys. Rev. **4,** 345 (1914).

[3] J. H. Rupe, A technique for the investigation of spray characteristics of constant flow nozzles (Conference on Fuel Sprays, University of Michigan, March 31, 1949).

[4] R. A. Castleman, The mechanism of the atomization of liquids, BS J. Research **6,** 369–376 (1931) RP281.

[5] A. Haenlein, Disintegration of a liquid jet, NACA Tech. Mem. No. 659 (1932).

[6] R. Kühn, Atomization of liquid fuels, NACA Tech. Mem. No. 329, 330, 331 (1925).

[7] K. J. DeJuhasz, Bibliography on sprays (Published by the Texas Co., Refining Department, Technical and Research Division, New York, N. Y., August 1948). Also Supplement No. 1 (May 1949).

WASHINGTON, October 13, 1953.

Silver-Uranium System [1]

R. W. Buzzard, D. P. Fickle, and J. J. Park

The phase diagram of the system silver-uranium was constructed from data obtained by thermal analysis, metallographic examination, and X-ray diffraction. The system is characterized by a eutectic having a composition of approximately 5 weight percent of uranium occurring at 950° C, and a monotectic occurring at 1,132° C, and 0.23 weight percent of silver. The solid solubility of uranium in silver appeared to be between 0.1 and 0.4 weight percent at the eutectic temperature; no appreciable solubility of silver in uranium was noted. The temperatures of the gamma-beta and the beta-alpha transformation of uranium apparently were unaffected by silver.

1. Introduction

The purpose of this investigation was to make a survey of the silver-uranium system and to develop the constitution diagram by correlation of thermal, X-ray, and microscopic studies.

2. Previous Work

A survey of the literature showed that information on the constitution of the silver-uranium system was meager [1].[2] It has been reported that silver and uranium separated into two distinct layers on melting, with very little evidence of alloying [2] and were mutually insoluble. A eutectic was observed in the silver layer, and considerable loss of silver by evaporization was noted [2].

3. Preparation of Alloys

The base metals consisted of ~99.9 percent of uranium (Mallinckrodt Biscuit) and 999-fine silver. The alloys were prepared in beryllia crucibles in a high-frequency induction furnace under an atmosphere of purified argon [3].

It was observed from sectioned ingots prepared in the composition range of 30 weight percent of silver that silver and uranium separated into layers when molten (fig. 1). Chemical analysis of a number of ingots revealed that the silver layer consistently contained 4 to 5 weight percent of uranium. This factor was later used to advantage by taking the 4 to 5 weight percent of uranium alloy as a master alloy; other alloys were made by direct alloying. The melting characteristics of the system required that the temperature of charges consisting of primary uranium and silver be raised above the melting point of uranium in order to obtain alloying. The molten silver had a high vapor pressure and, at the melting temperature of uranium, a high loss of silver by vaporization was encountered.

Uranium was an effective deoxidizer of silver so that, as uranium oxide was rejected from the melt, this oxidation caused a loss of uranium from the silver-rich alloys on each subsequent melting or heat-treating operation. Analyses of the silver-rich alloys were made only for uranium and, as uranium oxide was included in the total uranium reported by this method, there is a possibility that sufficient uranium oxide was retained in the low-uranium alloys (<0.5 weight percent) to cause the results of the chemical analyses for uranium to be higher than the actual uranium content of the alloys. In view of the change of composition of the alloys caused by these factors during subsequent thermal studies, the reported compositions of the alloys (tables 1 and 2) were determined after examination rather than on the "as-cast" material.

TABLE 1. *Summary of thermal data obtained for silver uranium alloys*

Silver [a]	Thermal arrest				
	Liquidus	$\delta+L_\alpha \rightarrow \delta$	$\delta+L_\alpha \rightarrow \gamma+\delta$	$\gamma \rightarrow \beta$	$\beta \rightarrow \alpha$
wt-%	°C	°C	°C	°C	°C
100	961	.....	.....	.....	.....
99.99	959	958	.....	.....	.....
99.98	959	.....	.....	.....	.....
99.97	957	954	.....	.....	.....
99.95	956	954	.....	.....	.....
99.85	956	955	.....	.....	.....
98.30	959	.....	950	.....	.....
95.70	.....	.....	949	770	658
0.23	1,135	.....	952	764	661
.04	1,128	.....	956	765	654
.035	1,133	.....	942	766	650
0	1,133	.....	.....	762	653

[a] Compositions show the ratio of the component metals and do not reflect the impurities.

TABLE 2. *Summary of microscopic data obtained for silver-uranium alloys*

Uranium [a]	Number of phases observed—quenching temperatures, °C						
	As cast	600	700	800	900	930	935
wt-%							
0.01	1	1	1	1	1	1	1
.03	1	1	1	1	1	1	1
.1	1	1	1	1	1	1	1
.4	2	2	2	2	2	Fusion	Fusion.
1.7	2	2	2	2	2	.....	Do.
1.8	2	2	2	2	2	Fusion	Do.
2.1	2	2	2	2	2	do	Do.
3.0	2	2	2	2	2	do	Do.
4.0	2	2	2	2	2	do	Do.
5.0	2	2	2	2	2	do	Do.

[a] Compositions show the ratio of the component metals and do not reflect the impurities.

[1] Investigation sponsored by the Atomic Energy Commission at the National Bureau of Standards.

[2] Figures in brackets indicate the literature references at the end of this paper.

FIGURE 1. *Ingot containing 30 weight percent of silver showing the uranium (dark) and silver (light) layers.*

4. Experimental Procedures

4.1. Thermal Analysis

The thermal arrests were determined by time-temperature analysis, using a molybdenum-wound resistance furnace. The accessory apparatus included a program controller to maintain uniform heating and cooling rates and an electronic recorder to reproduce automatically the heating and cooling curves [4]. The thermal curves were obtained from specimens of approximately 50 g, which were heated and cooled at a controlled rate of 2° C/min with the furnace operating under an atmosphere of purified argon. The thermal arrests were derived from the cooling curves.

4.2. Microscopic Analysis

The specimens for microscopic examination were mounted in Bakelite, ground on a series of silicon-carbide papers, with the finishing paper of 000 grit, and finished either on a levigated alumina lap or electrolytically, using 70 v at 1½ amp, 3 to 6 immersions of 10-sec duration in an electrolyte of the following composition: 20 g of chromic acid; 30 ml of water, and 100 ml of glacial acetic acid.

In general, the structures of the silver-rich alloys were developed by swabbing with a modified chromic–sulfuric-acid solution [5] composed of 1 part of a concentrated stock solution (100-ml saturated solution of potassium dichromate in water, 2-ml saturated solution of sodium chloride in water, and 10-ml of concentrated sulfuric acid) in 9 parts of water. The silver-rich alloys developed a grayish coating and required a light polish on a alumina finishing lap after etching. The structures of the uranium alloys were developed electrolytically in a 10-percent chromic-acid solution, using 0.5 amp and 4 v at 25° C.

Specimens to be quenched were sealed under argon in high-silica glass tubes of 7-mm bore, homogenized for 8 days at 925° C, and furnace-cooled. The alloys were quenched in ice water, using the nickel-block technique, in the manner described for the titanium-uranium alloys [3].

4.3. X-ray Analysis

The specimens used for the microscopic studies were subsequently placed in an X-ray spectrometer and a chart obtained of the (Cu-Kα) X-ray diffraction lines at room temperature. By this method it was possible to identify the phases present in the alloys and correlate the X-ray and microscopic data.

5. Results

5.1. Thermal Data

The results of thermal analysis (table 1) were were obtained from the two terminal-alloy series (0 to 0.23 weight percent of silver and 0 to 5 weight percent of uranium). The alloys in the composition range 0.23 to 95 weight percent of silver separated into two layers during the thermal-analysis cycle, each layer having an analysis within the respective terminal-alloy composition range, as indicated above.

Thermal-analysis data of the silver-rich alloys (1 to 5 weight percent of uranium) showed consistent arrests in the vicinity of 950° C. Similar arrests were observed for the uranium-rich alloys; in these alloys a second arrest was observed at approximately 1,132° C. The uranium transformations were noted in all alloys and were apparently unaffected by silver.

Two alloys (30 weight percent and 50 weight percent of silver) in the composition range of the liquid miscibility gap were prepared, and time-temperature cooling curves were determined on the

whole ingot. Arrests identical to those previously recorded for the uranium-rich terminal alloys were observed. The resultant ingots showed a sharp line of demarcation between a silver-rich and an uranium-rich layer. The layers were parted and reexamined by thermal analysis. Each layer developed arrests characteristic of the respective terminal-alloy series. The miscibility gap extended over the greater portion of the system. It was not possible to obtain liquidus determinations for compositions in excess of 5 weight percent of uranium because the alloys separated into two layers during thermal analysis. This indicated that the liquidus rose sharply from the eutectic to the monotectic temperature. On the basis of these observations, it was concluded that the composition range of the miscibility gap was determined to be approximately 0.23 to 94.5 weight percent of silver at the monotectic temperatures. The vapor pressure of silver greatly influenced the determination of the thermal arrests in the uranium-rich alloys. It was evident that silver had little effect on the thermal arrests of the uranium-rich alloys, and the temperatures used in the construction of the diagram were based on the values obtained for uranium.

5.2. Microstructures of the Alloys

In the study of the microstructures of these alloys (table 2), using the number of identifiable phases present as the criterion, it was revealed that the solubility of uranium in silver lies between 0.1 and 0.4 weight percent at room temperature, and little change in this value was observed between 25° C and 950° C.

A eutectic-like structure was observed in both the uranium-rich (fig. 2A) and the silver-rich (fig. 2B) alloys. Results of the microscopic analyses showed the eutectic composition to be approximately 5 weight percent of uranium and the monotectic composition to be approximately 0.23 weight percent of silver. In the composition range 0.4 to 5.0 weight percent of uranium, some evidence of fusion was observed at the edges of the specimens quenched from 950° C and complete fusion was observed at 955° C. This confirmed the eutectic temperature of 950° C as observed by thermal analysis.

5.3. X-ray Identification

X-ray diffraction charts were obtained, using the same surfaces of the specimens as were examined microscopically; the results of the X-ray and microscopic examination were then correlated. Only uranium and silver lines were observed for the alloys examined in this system.

6. Proposed Diagram

The thermal arrests, derived from the cooling curves, were obtained from "as-cast" alloys that were rapidly cooled from the liquid condition. Chemical analysis showed these ingots to be homogeneous from top to bottom. Since both silver and uranium were lost during the thermal analysis cycle, the reported alloy compositions are those determined from the chemical analysis of samples cut from the ingot (at the thermocouple tip) after thermal analysis.

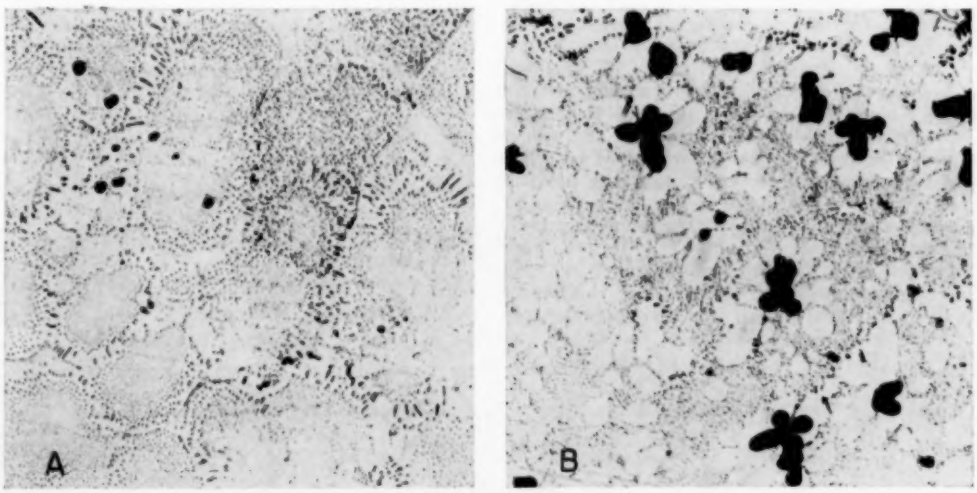

FIGURE 2. *As-cast alloys, showing characteristic eutecticlike structutes found in both the uranium-rich and the silver-rich terminal alloys.*

A, 4.5 weight percent of uranium, chromic-sulfuric etch. B, 0.07 weight percent of silver, electrolytic etch, 10-percent chromic acid. Magnification, X100.

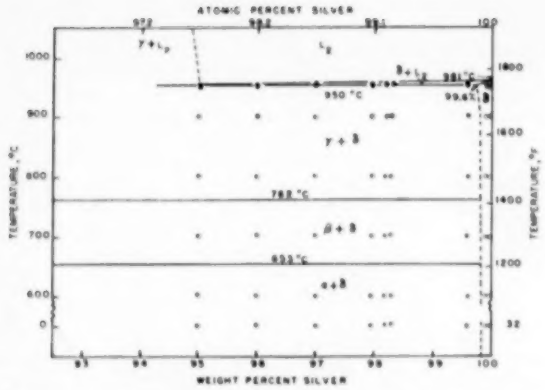

FIGURE 3. *Silver-uranium system, 94 to 100 weight percent of silver.*

Microscopic data: ○, one phase; ◐, two phase; ●, fusion.

Thermal arrests were observed at about 950°, 762°, and 653° C in both the uranium and silver-rich alloys, and in the vicinity of 1,132° C in the uranium-rich alloys. Microscopic studies revealed a eutectic-like structure in both series of alloys. It was indicated that a monotectic occurred in the system at approximately 0.23 weight percent of silver and at the melting point of uranium; it was not possible to differentiate between the melting point of uranium and the monotectic temperature. In the silver-rich terminal alloys, fusion was noted at about 950° C in the composition range 0.4 to 5.0 weight percent of uranium (table 2), indicating a eutectic occurring at 950° C and approximately 5 weight percent of uranium. The microscopic studies of the quenched alloys used in the determination of the silver-uranium solvus were made on specimens that were heat treated prior to chemical analysis. It was well established that the solubility of uranium in silver is less than 0.4 weight percent at the eutectic temperature of 950° C (fig. 3). In evaluating the studies of the alloys in the composition range of less than 0.4 weight percent of uranium, it must be borne in mind that the uranium-oxide content of the alloy appears as uranium in the chemical analysis, and it is quite possible that the solubility may be even lower than reported. No intermediate phases or intermetallic compounds were observed in the system as a result of X-ray, thermal, or microscopic analysis.

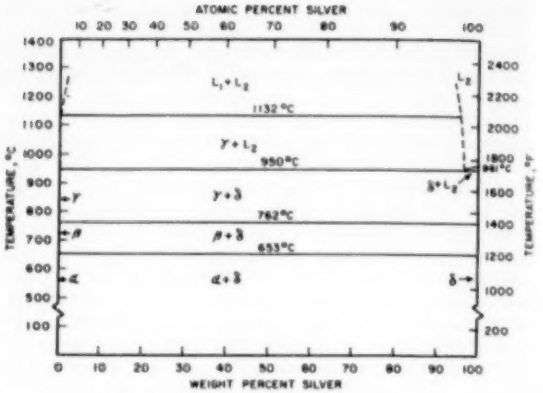

FIGURE 4. *Silver-uranium system.*

7. Summary

The silver-uranium system (fig. 4) was constructed from data obtained by thermal, microscopic and X-ray analyses.

The important features of the system include: (a) A monotectic at 0.23 weight percent of silver and 1,132° C with a liquid miscibility gap extending from 0.23 weight percent to approximately 94.5 weight percent of silver. (b) A eutectic at approximately 5 weight percent of uranium and 950° C. (c) The solubility of uranium in silver appeared to be between 0.1 and 0.4 weight percent at the eutectic temperature while no appreciable solubility of silver in uranium was noted. (d) The gamma-beta and the beta-alpha transformations of uranium were apparently unaffected by silver.

The authors express their appreciation to Martha S. Richmond for the chemical analysis.

8. References

[1] R. W. Buzzard and H. E. Cleaves, J. Met. and Ceram. (TID65) **1,** 43 (1948).
[2] Battelle Memorial Inst., Report CT 2483 (Dec. 1, 1944).
[3] R. W. Buzzard, R. B. Liss, and D. P. Fickle, J. Research NBS **50,** 209–214 (1953) RP2412.
[4] R. W. Buzzard, J. Research NBS **50,** 63–67 (1953) RP2389.
[5] Am. Soc. Metals Handbook, p. 1110 (1948).

WASHINGTON, November 4, 1953.

Journal of Research of the National Bureau of Standards Vol. 52, No. 3, March 1954 Research Paper 2484

Nonnegative Trigonometric Polynomials and Certain Rational Characteristic Functions

Eugene Lukacs [1] and Otto Szász [2]

Let $0<b_1<b_2< \ldots <b_n$ be n integers and $0<d_1<d_2< \ldots <d_m$ be $m (m \leq n)$ real numbers (not necessarily integers). Denote by $g(\theta)$ the Vandermonde determinant formed from the $b_1^2, b_2^2, \ldots, b_n^2$ with the first row replaced by $1-\lambda_j \cos b_j\theta$, where $\lambda_j = \prod_{k=1}^{m}(1-b_j^2/d_k^2)$ for $j=1, 2, \ldots, n$. The question whether $g(\theta)$ is nonnegative for all values of θ is closely connected with the problem whether certain rational functions are characteristic functions. Four configurations of the $b_1, \ldots, b_n$, and $d_1, \ldots, d_m$ are studied, which lead to nonnegative trigonometric polynomials.

1. Introduction

In this paper we study several nonnegative trigonometric polynomials that are connected with the question whether certain rational functions are Fourier transforms of distribution functions (characteristic functions).

We consider in the following a rational function $\phi(t)$ whose poles and zeros have the same imaginary part a and assume further that all poles and all zeros have the order one. Let $-ia$, iv_j, $-i\overline{v}_j (j=1,2, \ldots, n)$ be the poles and $-i\overline{w}_k$, $-iw_k (k=1,2, \ldots, m)$, $m \leq n$, be the zeros of $\phi(t)$, where $v_j=a+ib_j$, $w_k=a+id_k$, and $a>0$, $0<b_1<b_2< \ldots <b_n$, $0<d_1<d_2< \ldots <d_m$. Such a function $\phi(t)$ fulfills the necessary conditions that a rational function must satisfy in order to be the Fourier transform of a distribution function. These conditions were given in two earlier papers [1, 2].[3]

In the following we denote by

$$V_k = \begin{vmatrix} b_1^{2k}, & b_2^{2k}, & \ldots, & b_n^{2k} \\ b_1^2, & b_2^2, & \ldots, & b_n^2 \\ \cdot & \cdot & \ldots, & \cdot \\ \cdot & \cdot & \ldots, & \cdot \\ \cdot & \cdot & \ldots, & \cdot \\ b_1^{2(n-1)}, & b_2^{2(n-1)}, & \ldots, & b_n^{2(n-1)} \end{vmatrix} \tag{1}$$

the generalized Vandermonde determinant formed from the numbers $b_1^2, \ldots, b_n^2$ with the exponents $k, 1, 2, \ldots, (n-1)$. We write further Δ_j for the minor of the element in the first row and jth column of this determinant, so that $V_k = \sum_{j=1}^{n}(-1)^{j-1}b_j^{2k}\Delta_j$.

In order to decide whether the function $\phi(t)$ is a characteristic function, we decompose it into partial fractions and apply the Fourier inversion formula. We see then after some computation that $\phi(t)$ is the Fourier transform of a certain function $f(x)$, i. e., $\phi(t) = \int_{-\infty}^{\infty} e^{itx} f(x)dx$, where $f(x)$ is given by

$$f(x) = \begin{cases} 0, & \text{if } x<0 \\ Ce^{-ax}\left\{V_0 - \sum_{j=1}^{n}(-1)^{j-1}\Delta_j\lambda_j \cos b_j x\right\}, & \text{if } x>0 \end{cases} \tag{2}$$

[1] National Bureau of Standards.
[2] University of Cincinnati. Deceased September 19, 1952.
[3] Figures in brackets indicate the literature references at the end of this paper.

with

$$C=\frac{a\prod_{j=1}^{n}(a^2+b_j^2)\prod_{k=1}^{m}d_k^2}{V_0\prod_{k=1}^{m}(a^2+d_k^2)\prod_{j=1}^{n}b_j^2}$$

$$\lambda_j=\prod_{k=1}^{m}\left(1-\frac{b_j^2}{d_k^2}\right)\quad(j=1,2,\ldots n). \tag{2a}$$

If we introduce the polynomial

$$H(z)=c_0(z-d_1^2)(z-d_2^2)\ \ldots\ (z-d_m^2)=\sum_{k=0}^{m}c_k z^{m-k}, \tag{3}$$

where

$$c_0=(-1)^m\left\{\prod_{k=1}^{m}d_k^2\right\}^{-1}\text{ and }c_m=1, \tag{3a}$$

we can write

$$\lambda_j=H(b_j^2),\quad j=1,2,\ldots,n. \tag{4}$$

The function $f(x)$ as determined by (2) is real, after some computation it is seen that $\int_0^\infty f(x)dx=1$. If $f(x)$ is nonnegative, it is the frequency function of an absolutely continuous probability distribution. We obtain therefore the following condition:

CONDITION I. *The rational function $\phi(t)$ is a characteristic function if, and only if,*

$$g(\theta)=\begin{vmatrix}(1-\lambda_1\cos b_1\theta), & (1-\lambda_2\cos b_2\theta), & \ldots, & (1-\lambda_n\cos b_n\theta)\\ b_1^2, & b_2^2, & \ldots, & b_n^2\\ \cdot & \cdot & \ldots, & \cdot\\ \cdot & \cdot & \ldots, & \cdot\\ \cdot & \cdot & \ldots, & \cdot\\ b_1^{2(n-1)}, & b_2^{2(n-1)}, & \ldots, & b_n^{2(n-1)}\end{vmatrix}\geq 0 \tag{5}$$

for all θ.

If we consider a rational function without zeros, that is, if we assume that $\phi_0(t)$ is the reciprocal of a polynomial whose roots are $-ia$, $-iv_j$, $-i\bar{v}_j$ $(j=1,2,\ldots,n)$, then we derive by a similar reasoning the following statement:

CONDITION II. *The function $\phi_0(t)$ is a characteristic function if, and only if,*

$$g_0(\theta)=\begin{vmatrix}1-\cos b_1\theta, & 1-\cos b_2\theta, & \ldots, & 1-\cos b_n\theta\\ b_1^2, & b_2^2, & \ldots, & b_n^2\\ \cdot & \cdot & \ldots, & \cdot\\ \cdot & \cdot & \ldots, & \cdot\\ \cdot & \cdot & \ldots, & \cdot\\ b_1^{2(n-1)}, & b_2^{2(n-1)}, & \ldots, & b_n^{2(n-1)}\end{vmatrix}\geq 0 \tag{6}$$

for all θ.

This condition is analogous to (5), in fact, (6) may be obtained from (5) by putting $\lambda_j=1$ for $j=1,2,\ldots,n$. We agree, therefore, to put $\lambda_j=1$ whenever $m=0$.

In this paper we consider the determinant (5) only for integer values of the b_j and show that it represents for certain configurations of the b_j and d_k a nonnegative trigonometric polynomial. In this manner we can construct certain rational characteristic functions.

2. Some Lemmas

For the discussion of the nonnegativity of $g(\theta)$ we need the following lemmas:

LEMMA 1. *If $b_1, b_2, \ldots, b_n$ are integers, the determinant (5) can be factored so that*

$$g(\theta)=(1-\cos\theta)^{n-m}A(\cos\theta), \tag{7}$$

where $A(x)$ is a polynomial in x of degree b_n-n+m.

LEMMA 2. *If $b_1, b_2, \ldots, b_n$ are odd integers, and if $n>m$, we have*

$$g'(\theta)=\sin\theta(1-\cos^2\theta)^{n-m-1}B(\cos\theta), \tag{8}$$

where $B(x)$ is a polynomial of degree $b_n-2n+2m+1$.

LEMMA 3. *Let*

$$P_s(x)=\int_x^1 (1-t^2)^{n-1}t^{2s}\,dt \qquad \text{for } s=0,\ 1, \tag{9}$$

and

$$Q(x,\zeta)=P_1(x)-\zeta^2P_0(x). \tag{10}$$

The polynomial $Q(x,\zeta)$ is nonnegative in the interval $-1\leq x\leq 1$ if, and only if,

$$\zeta\leq z_n. \tag{11}$$

Here z_n is the root of the equation

$$R(z)\equiv Q(-z,z)\equiv\int_{-z}^{1}(1-t^2)^{n-1}(t^2-z^2)\,dt=0, \tag{12}$$

which falls into the interval (0,1).

Moreover, let $w_n=\sqrt{n+\frac{1}{2}}\,z_n$.

Then $\lim_{n\to\infty} w_n=\rho$ *exists and is the root of the equation*

$$F(\rho)=\sqrt{\pi}\,(\tfrac{1}{2}-\rho^2)-2\rho^2\int_0^1(1-t^2)e^{-\rho^2t^2}dt=0 \tag{13}$$

which is located in the interval $(0,\sqrt{\frac{1}{2}})$.

The proofs of the lemmas 1 and 2 are completely analogous to the proofs given for the corresponding lemmas in an earlier paper [3], in which nonnegative trigonometric polynomials of the form (6) were studied. Lemma 3 is identical with lemma 3 of [3]; we omit therefore the proofs of the three lemmas and refer instead to [3].

The function $g(\theta)$ as defined by (5) and (2a) depends on the parameters $b_1, \ldots, b_n$, $d_1, \ldots, d_m$. It is sometimes convenient to indicate this fact by writing $g(\theta)=g(\theta|b_1, \ldots, b_n;d_1, \ldots, d_m)$. Similarly, we shall write occasionally $V_0=V_0(b_1, \ldots, b_n)$ for the Vandermonde determinant formed from the numbers $b_1^2, \ldots, b_n^2$.

It is possible to obtain some of the results of our previous paper as particular cases of results obtained in the present paper. For this purpose we need the following lemma.

LEMMA 4. *Let $g(\theta|b_1, \ldots, b_n;d_1, \ldots, d_m)$ be the function defined by (5) and (2a). If we put $d_\sigma=b_\rho$, we obtain*

$$\frac{g(\theta|b_1, \ldots, b_n; d_1, \ldots, d_{\sigma-1}, b_\rho, d_{\sigma+1}, \ldots, d_m)}{V_0(b_1, \ldots, b_n)}$$

$$=\frac{g(\theta|b_1, \ldots, b_{\rho-1}, b_{\rho+1}, \ldots, b_n; d_1, \ldots, d_{\sigma-1}, d_{\sigma+1}, \ldots, d_m)}{V_0(b_1, \ldots, b_{\rho-1}, b_{\rho+1}, \ldots, b_n)}, \tag{14}$$

that is, the substitution $d_\nu = b_\mu$ transforms the function

$$\frac{g(\theta | b_1, \ldots, b_n; d_1, \ldots, d_m)}{V_0(b_1, \ldots, b_n)}$$

into a similar function that does not contain any more the parameters d_ν and b_μ.

It is possible to give an elementary proof of (14) by a straightforward computation. The validity of (14) becomes apparent, however, if we remember that the rational function $\phi(t)$ is the Fourier transform of $Ce^{-\alpha x} g(x | b_1, \ldots, b_n; \ d_1, \ldots, d_m)$.

3. Nonnegative Trigonometric Polynomials

In the following we assume that the $b_1, b_2, \ldots, b_n$ are positive integers, while the $d_1, \ldots, d_m$ may be any positive real numbers. The function $g(\theta)$, defined by (5) is then a trigonometric polynomial. According to condition (I) the function $\phi(t)$ is a characteristic function if, and only if, $g(\theta)$ is nonnegative. The purpose of this paper is to consider configurations that lead to nonnegative trigonometric polynomials. For this discussion it is convenient to introduce occasionally a new variable:

$$x = \cos \theta, \tag{15}$$

and to use the notation

$$P(x) = g(\arccos x). \tag{16}$$

Since we assume from now on that the b_j's are integers, the substitution (15) transforms $\cos b_j \theta$ into $T_{b_j}(x)$, where $T_{b_j}(x)$ is the b_jth Tchebycheff polynomial of the first kind. Therefore, we see from (5) that under the conditions of lemma 1,

$$P(x) = \sum_{j=1}^{n} (-1)^{j-1} \Delta_j [1 - \lambda_j T_{b_j}(x)] = (1-x)^{n-m} A(x). \tag{17}$$

In a similar manner, we have under the conditions of lemma 2,

$$P'(x) = \sum_{j=1}^{n} (-1)^j \Delta_j \lambda_j T'_{b_j}(x) = -(1-x^2)^{n-m-1} B(x). \tag{18}$$

When we make this substitution we shall use the fact that the trigonometric polynomial $g(\theta)$ is nonnegative for all θ if, and only if, the polynomial $P(x) \geq 0$ for $|x| \leq 1$. From (17) we obtain immediately

CONDITION (III). *The trigonometric polynomial $g(\theta)$ is nonnegative if, and only if, the polynomial $A(x)$, introduced by lemma 1, is nonnegative for $|x| \leq 1$.*

We use condition (III) and the lemmas obtained in section 2 to derive conditions for certain trigonometric polynomials. The results are contained in the subsequent statements.

STATEMENT 1. *If the b_j are the first n consecutive integers, i. e., $b_j = j$ for $j = 1, 2, \ldots, n$, and if $m = 1$, the trigonometric polynomial $g(\theta)$ is nonnegative if, and only if, $2d_1^2 \geq n$.*

In this case we have $\lambda_j \equiv 1 - j^2/d_1^2$, $j = 1, 2, \ldots, n$ and obtain from (17)

$$P(x) = \sum_{j=1}^{n} (-1)^{j-1} \Delta_j \left[1 - \left(1 - \frac{j^2}{d_1^2} \right) T_j(x) \right] = (1-x)^{n-1} (a + bx).$$

From this equation it is possible to determine the coefficients a and b. After some elementary computations we obtain

$$P(x) = 2^{n-1} \Delta_n \frac{[n(n-1) + d_1^2]}{d_1^2} (1-x)^{n-1} \left\{ 1 + \frac{n^2 - d_1^2}{n(n-1) + d_1^2} x \right\}.$$

Clearly, $P(x) \geq 0$ for $|x| \leq 1$ if, and only if, $|n^2 - d_1^2| \leq n(n-1) + d_1^2$. This inequality can be written as $-n^2 + n - d_1^2 \leq n^2 - d_1^2 \leq n^2 - n + d_1^2$. Since n is a positive integer, this condition reduces to $2d_1^2 \geq n$.

COROLLARY TO STATEMENT 1. If the b_j are the first n consecutive even integers, i. e., if $b_j = 2j$ for $j = 1, 2, \ldots, n$, and if $m = 1$, then the trigonometric polynomials $g(\theta)$ is nonnegative if, and only if, $d_1^2 \geq 2n$. The corollary follows almost immediately from statement 1.

STATEMENT 2. *If the b_j are the first n consecutive integers, i. e., if $b_j = j$ for $j = 1, 2, \ldots, n$, and if $m = 2$, the trigonometric polynomial $g(\theta)$ is nonnegative, if, and only if, a certain polynomial $Q(x)$ is nonnegative for $|x| \leq 1$. Here*

$$Q(x) = L(n, d_1, d_2)x^2 + M(n, d_1, d_2)x + N(n, d_1, d_2), \tag{19}$$

where

$$\left.\begin{aligned} L(n, d_1, d_2) &= n^4 - n^2(d_1^2 + d_2^2) + d_1^2 d_2^2, \\ M(n, d_1, d_2) &= 2n^4 - 6n^3 + 4n^2 - n + n(d_1^2 + d_2^2) - 2d_1^2 d_2^2, \\ N(n, d_1, d_2) &= n^4 - 6n^3 + 7n^2 - 2n + (n^2 - n)(d_1^2 + d_2^2) + d_1^2 d_2^2. \end{aligned}\right\} \tag{20}$$

PROOF. From (2a) we see that

$$\lambda_j = \left(1 - \frac{j^2}{d_1^2}\right)\left(1 - \frac{j^2}{d_2^2}\right)$$

for $j = 1, 2, \ldots n$, and obtain from (17)

$$P(x) = \sum_{j=1}^{n} (-1)^{j-1} \Delta_j \left\{1 - \left(1 - \frac{j^2}{d_1^2}\right)\left(1 - \frac{j^2}{d_2^2}\right) T_j(x)\right\} = (1-x)^{n-2}(ax^2 + bx + c).$$

From this equation it is possible to determine the coefficients a, b, and c. After some elementary computation, one obtains

$$P(x) = \frac{2^{n-1}\Delta_n}{d_1^2 d_2^2} (1-x)^{n-2} Q(x).$$

A particular case can be discussed easily. If $d_1 = (n+1)$ and $d_2 = (n+2)$, we obtain from (20) $L = 4(n+1)(2n+1)$, $M = -4(2n+1)(2n^2+n+2)$, $N = 4n^4 + 4n^3 + 19n^2 + 5n + 4$. It is then easy to show that $Q(x)$ is positive in $-1 \leq x \leq +1$ so that $P(x)$ is nonnegative for the values $k_j = j (j = 1, 2, \ldots, n)$ and $m = 2$, $d_1 = (n+1)$, $d_2 = (n+2)$. This means in probabilistic language that the rational function with $2n+1$ poles $-i(a \pm ij) (j = 1, \ldots, n)$ and $-ia$ and the four zeros $-i(a \pm id_1)$, $-i(a \pm id_2)$ is a characteristic function.

STATEMENT 3. *If the b_j are the first n consecutive odd integers, i. e., if $b_j = 2j - 1$ for $j = 1, 2, \ldots, n$, and if $m = 1$ while $n > 1$[4], then the trigonometric polynomial $g(\theta)$ is nonnegative if either one of the following two conditions is satisfied*

(i) $\quad d \geq \sqrt{2n-1}$,

(ii) $\quad d < \sqrt{2n-1}$,

but

$$\sqrt{\frac{(2n-1) - d^2}{(2n-1)^2 - d^2}} \leq z_{n-1},$$

[4] The case $n = m = 1$ is covered by statement 1, and can therefore be excluded here.

where z_{n-1} is the root of the equation

$$\int_{-z}^{1}(1-t^2)^{n-2}(t^2-z^2)dt=0,$$

which falls into the interval $(0, 1)$.

If neither (i) *nor* (ii) *is satisfied, then the function $g(\theta)$ assumes also negative values.*

COROLLARY TO STATEMENT 3. *If for large n and $d<2n-1$*

$$\sqrt{\frac{(n+\tfrac{1}{2})\,[(2n-1)-d^2]}{(2n-1)^2-d^2}}\leq\rho=0.5939157\ldots,$$

then $g(\theta)$ is nonnegative.

In formulating this statement, we wrote for d_1 simply d. From (2*a*) we see that

$$\lambda_j=1-\frac{(2j-1)^2}{d^2}\text{ for }j=1,\ 2,\ \ldots,\ n.$$

According to lemma 2, as expressed by (18), we have

$$P'(x)=\frac{1}{d^2}\sum_{j=1}^{n}(-1)^j[d^2-(2j-1)^2]\Delta_j T'_{2j-1}(x)=-(1-x^2)^{n-2}B(x),$$

where $B(x)$ is a polynomial of the second degree. From this equation it is possible to determine $B(x)$, we obtain

$$B(x)=\gamma\left\{\left[1-\frac{2n-1}{d^2}\right]-\left[1-\frac{(2n-1)^2}{d^2}\right]x^2\right\},\tag{21}$$

where

$$\gamma=2^{2n-2}(2n-1)\Delta_n>0.$$

From (21) we see that

$$\left.\begin{aligned}&B(-1)=B(1)=\frac{2(2n-1)\,(n-1)}{d^2}\gamma>0\\&B(0)=\left[1-\frac{2n-1}{d^2}\right]\gamma>0\\&B'(x)=-2\gamma\left[1-\frac{(2n-1)^2}{d^2}\right]x;\quad B''(x)=-2\gamma\left[1-\frac{(2n-1)^2}{d^2}\right]\end{aligned}\right\}.\tag{22}$$

We first assume $d\geq 2n-1$, then $B'(x)\leq 0$ for $0\leq x\leq 1$. Since $B(1)>0$, we have $B(x)>0$ in the interval $(0,1)$, from $B(-x)=B(x)$ it is seen that $B(x)>0$ for $|x|\leq 1$. Next we suppose $(2n-1)>d\geq\sqrt{2n-1}$, then $B(x)$ has a minimum at the point $x=0$, so that $B(x)\geq B(0)>0$. Summarizing, we see that $B(x)\geq 0$ for $|x|\leq 1$, provided $d\geq\sqrt{2n-1}$. But this means that $P'(x)\leq 0$ in $|x|\leq 1$. From (17) it is seen that $P(1)=0$ if $n>m$, so that $P(x)>0$ in $|x|\leq 1$, and therefore $g(\theta)\geq 0$ for all θ, so that condition (i) is proved.

We next consider the case $d<\sqrt{2n-1}$. We write

$$B(x)=\left[\frac{(2n-1)^2}{d^2}-1\right]\gamma\left\{x^2-\frac{(2n-1)-d^2}{(2n-1)^2-d^2}\right\}.$$

If we denote by

$$\gamma'=\left[\frac{(2n-1)^2}{d^2}-1\right]\gamma>0$$

and by

$$\zeta^2=\frac{(2n-1)-d^2}{(2n-1)^2-d^2}>0,$$

then we have

$$B(x)=\gamma'(x^2-\zeta^2) \quad \text{and} \quad P'(x)=-\gamma'(1-x^2)^{n-2}(x^2-\zeta^2).$$

Therefore,

$$P(x)=\gamma'\int_x^1(1-t^2)^{n-2}(t^2-\gamma^2)dt.$$

Condition (ii) and the corollary to statement 3 follow then immediately from lemma 3; a brief table of the z_n is contained [3].

We proceed to discuss a more complicated case by assuming that the rational function $\phi(t)$ has two zeros (i. e., $m=2$) and that it has the first n consecutive odd integers as poles, so that $b_j=2j-1$ for $j=1,2,\ldots,n$.

We obtain then from (18)

$$P'(x)=-\gamma(1-x^2)^{n-3}[A+Cx^2+Dx^4], \tag{23}$$

where

$$\left.\begin{aligned}\gamma&=2^{2n-6}(2n-1)\Delta_n\\ D&=16\lambda_n\\ C&=4[(2n-9)\lambda_n-(2n-1)\lambda_{n-1}]\\ A&=(2n^2-13n+22)\lambda_n-(2n-1)(2n-7)\lambda_{n-1}+(n-1)(2n-1)\lambda_{n-2}\end{aligned}\right\}. \tag{23a}$$

We write [5]

$$a=\frac{C}{4\lambda_n}, \quad b=-\frac{A}{4\lambda_n}, \tag{24}$$

so that

$$P'(x)=-4\gamma\lambda_n(1-x^2)^{n-3}(4x^4+ax^2-b). \tag{25}$$

For $n>m=2$ we have $P(1)=0$, and therefore [6]

$$P(x)=4\gamma\lambda_n\int_x^1(1-t^2)^{n-3}(4t^4+at^2-b)dt \qquad \text{for } n\geq 3. \tag{26}$$

The nonnegativity of the polynomial $P(x)$ depends on the nature of the roots of the polynomial $B(x)=4x^4+ax^2-b$. This introduces the need to distinguish a number of cases, for this purpose we write $h(\tau)=4\tau^2+a\tau-b=4(\tau-\tau_1)(\tau-\tau_2)$, where

$$\left.\begin{aligned}\tau_1&=(-a-\sqrt{a^2+16b})/8\\ \tau_2&=(-a+\sqrt{a^2+16b})/8\\ B(x)&=h(x^2)\end{aligned}\right\}. \tag{27}$$

In the following we denote by

$$R_i(z)=\int_-^1(1-t^2)^{n-3}t^{2(i-1)}(t^2-z^2)dt \text{ for } i=1,2.$$

We are now in a position to formulate statement 4.

[5] We assume here $\lambda_n\neq 0$. We need not consider the case $\lambda_n=0$, since this reduces by lemma 4 to the case covered by statement 3.

[6] If $n=m$, lemma 2 is not valid, and moreover, $P(1)>0$. The case $n=m=2$ would therefore require a separate discussion.

STATEMENT 4. *If the b_j are the first n consecutive odd integers, that is, if $b_j=2j-1$ for $j=1, 2, \ldots, n$, and if $n>m=2$, then the trigonometric polynomial $g(\theta)$ is nonnegative if, and only if, one of the following nine, mutually exclusive, conditions is satisfied*

(i) $\lambda_s>0$, $a\geq 0$, *and* $b\leq 0$

(ii) $\lambda_s>0$, $a<0$, *and* $a^2+16b\leq 0$

(iii) $\lambda_s>0$, $a\geq 0$, $0<b<a+4$, *and* $R_2(\sqrt{\tau_2})-\tau_1 R_1(\sqrt{\tau_2})\geq 0$

(iv) $\lambda_s>0$, $0>a>-4$, $4+a>b>-a^2/16$, *and* $R_2(\sqrt{\tau_2})-\tau_1 R_1(\sqrt{\tau_2})\geq 0$; *if* $b<0$, *we have the additional condition* $R_2(-\sqrt{\tau_1})-\tau_2 R_1(-\sqrt{\tau_1})\geq 0$

(v) $\lambda_s>0\geq a+8>a+4\geq b>-a^2/16$

(vi) $\lambda_s>0$, $-4\geq a>-8$, $0\geq a+4\geq b>-a^2/16$, *and also* $R_2(\sqrt{\tau_2})-\tau_1 R_1(\sqrt{\tau_2})\geq 0$; *if* $b\neq 0$, *we have the additional condition* $R_2(-\sqrt{\tau_1})-\tau_2 R_1(-\sqrt{\tau_1})\geq 0$

(vii) $\lambda_s<0$, $a\geq 0$, *and* $b\geq a+4$

(viii) $\lambda_s<0$, $a<0$, *and* $b\geq \max[0, a+4]$

(ix) $\lambda_s<0$, $a+4\leq b<0$, *and* $R_2(\sqrt{\tau_1})-\tau_2 R_1(\sqrt{\tau_1})\leq 0$.

The proof of this statement is rather tedious. It is, however, similar to the proof of statement 3 of the present paper and of statement (F) of [3] and is therefore omitted.

We conclude this section by using lemma 4 to show that the earlier results may be obtained as particular cases of the statements of the present paper. We consider as an example statement 1 and write $n=s+1$ and put $d_1=k$, where k is an integer. From lemma 4 we see that $g(\theta|1, \ldots, s+1;k)$ and $g_0(\theta|1, \ldots, k-1, k+1, \ldots, s+1)$ are simultaneously nonnegative so that statement 1 reduces to statement C of [3].

4. References

[1] E. Lukacs and O. Szász, Certain Fourier transforms of distributions, Can. J. Math. **3**, 140–144 (1951).

[2] E. Lukacs and O. Szász, Analytic characteristic functions, Pac. J. Math. **II**, 615–625 (December 1952).

[3] E. Lukacs and O. Szász, Some nonnegative trigonometric polynomials connected with a problem in probability, J. Research NBS **48**, 139–146 (1952) RP2297.

WASHINGTON, December 19, 1952.

Journal of Research of the National Bureau of Standards Vol. 52, No. 3, March 1954 Research Paper 2485

Flame-Emission Spectrum of Water Vapor in the 1.9-Micron Region [1, 2]

W. S. Benedict,[3] Arnold M. Bass, and Earle K. Plyler

The emission of hydrogen-oxygen and acetylene-oxygen flames has been studied by using a 15,000-lines-per-inch grating spectrometer with a lead-sulfide photoconductive detector. The water-vapor band, which in room-temperature absorption extends from about 1.80 to 1.96 microns, is broadened in emission to 1.7 to 2.2 microns. Nearly 1,000 lines have been measured, and a rotational analysis has been given for many of them. Many lines of the (011–000) band agree with those found in laboratory and atmospheric absoprtion, and many additional lines from higher energy levels may be identified. The principal series $J_{-J} \longleftrightarrow (J+1)_{-(J+1)}$ may be followed out to $J=23$ in both P and R branches. Corresponding lines in the upper-state bands (021–010) and (031–020) have also been identified. A smaller number of lines may be assigned to the (041–030), (051–040), (012–001), 022–011), (032–021), (111–100), and (121–110) bands.

1. Introduction

When hydrogen, hydrocarbons, or other hydrogen-containing compounds burn in air or oxygen, considerable energy is radiated in the infrared region. With spectrometers of low dispersion, three principal regions of strong emission were noted [1][4] near 2.7, 1.9, and 1.4 microns. These correspond to regions of strong atmospheric absorption, due to water vapor [2, 3] and the emission must also be attributed to the H_2O molecule. Studies of the emission with resolving power sufficient to separate lines due to individual rotational transitions in these rotation-vibration bands have not previously been reported. Due to the great increase in resolving power in the near infrared region resulting from the use of photoconductive detectors, it is now possible to obtain spectra showing very much more detail, and to pursue the analysis to a point where the major part of the emission may be understood. In addition to the fundamental interest in determining the higher energy levels of the H_2O molecule from spectra and in interpreting a rather complex spectrum, the present studies are also of practical importance in providing the data from which relative intensities within the H_2O emission spectrum may be used to determine whether the H_2O molecule appears in combustion processes in nonequilibrium distributions [4] and to determine the equilibrium "temperature" of that molecule in flames.

In this paper we present the results of measurements in the region 1.7 to 2.2 μ (5,900 to 4,600 cm^{-1}). When acetylene-oxygen and hydrogen-oxygen flames were observed with a 15,000-lines-per-inch grating spectrometer in this region, the intensity was sufficient so that slits subtending a spectral interval as narrow as 0.2 cm^{-1} could be used. This region (referred to for brevity as the 1.9-μ region) is the most suitable for beginning the analysis of the vibration-rotation flame spectrum, for a number of reasons. The sensitivity of the lead-sulfide detector and the efficiency of the spectrometer are high; at the same time, the intensity of the emission is high without involving emissivities so great that self-absorption effects cause distortion of the relative intensities. (There is some distortion of the intensities due to absorption of the lower-energy lines by the water-vapor molecules at room temperature in the spectrometer path, but this is confined to scattered frequencies in the center of the band, from 5,100 to 5,500 cm^{-1} [5].) The vibrational transitions involved in this region are few and do not show strong perturbations. The principal band, the only strong one in room-temperature absorption, is the transition $(v_1'v_2'v_3'-v_1''v_2''v_3'')=(011–000)$. "Upper-state" bands, e. g., (021–010), (031–020), etc., also are excited at the high temperatures of the flame; these also involve states whose energies are well known from absorption studies and cause relatively little confusion. The "convergence" resulting from the difference in rotational constants between the upper and lower states of all these transitions is such that the bands are well spread out, with no regions where many lines crowd together.

Other regions in the emission spectrum of H_2O have also been studied, but will not be reported in detail here. The 2.7-μ region, in which the principal band is the ν_2 fundamental, is extremely intense, with the result that both self-absorption and atmospheric absorption cause difficulties. Moreover, the 15,000 lines-per-inch grating with lead-sulfide detector loses sensitivity rapidly at wavelengths beyond 2.6 μ. Hence only the short-wavelength portion of this band (R branch) appears to advantage on our tracings. The 1.4-μ region is quite strong, so that resolution only slightly inferior to that achieved in the 1.9 μ region was attained, but there are a number of vibrational transitions in the region, and convergence is such that the R branches are extremely crowded (forming a characteristic head near 7,500 cm^{-1}), while the P branches fall in the region of strong OH emission [6]. At wavelengths shorter than 1.33 μ, the H_2O emission becomes progressively weaker. The present observations extend to 1 μ, but

[1] Supported in part by the Office of Naval Research.
[2] Presented at the Symposium on Molecular Structure and Spectroscopy, Columbus, Ohio, June 1951.
[3] Present address, The Johns Hopkins University, Baltimore, Md.
[4] Figures in brackets indicate literature references at the end of this paper.

slits as wide as 1 cm^{-1} were required to develop the bands centering around 1.1 μ, so that little detail in the rotational structure could be separated. In the photographic infrared and red [7] good resolution has been attained, especially in the region 7,100 to 8,800 A; rotational analysis of this interval is in progress, but the structure is more complicated than in the 1.9-μ region because the vibrational levels are more numerous and show perturbations. In addition to the emission measurements, studies have recently be made [8] of the absorption of heated H_2O in the long-wavelength region greater than 4 μ. The observations in the spectral regions other than 1.9 μ were useful in confirming many of the rotation-vibration assignments made in the present paper.

2. Experimental Procedure

The spectrometer and the general arrangement for observing flame spectra have been described elsewhere [6]. In the present work, hydrogen-oxygen and acetylene-oxygen flames were observed, both just above the tip of the inner cone, and at greater heights in the outer cone. Various fuel-oxygen ratios in the neighborhood of stoichiometric were fed to the welding-torch burner. These varied conditions caused little change in the relative intensities of the emission in the 1.9-μ region, a fact which indicates that practically all of the emission is due to the H_2O molecule, and that the energy distribution for that molecule is not very sensitive to the burning conditions. This is to be expected, inasmuch as H_2O is the major component of the burnt gas. Its emission, in regions other than those of active combustion (and with the type of burner used most of the radiation entering the spectrometer must come from such regions), would be predominantly thermal, characteristic of the weighted average temperature of the molecules in the line-of-sight of the spectrometer. With the fuel-oxygen ratios used, the maximum (adiabatic) temperatures attained did not vary greatly, and were in the neighborhood of 3,000° K for both hydrogen and acetylene as fuels. The hydrogen-oxygen emission was somewhat the stronger, the larger proportion of H_2O in the burnt gas presumably overcoming the slightly higher temperatures in the acetylene-oxygen flame.

Four of the hydrogen-oxygen tracings, showing optimum resolution, were selected for the measurement of wavelength. Wavelength standards were obtained by superimposing on the emission spectra lines of either neon or krypton from gaseous discharges, focused through the flame. A smooth dispersion curve was fitted to the standard lines, and the H_2O lines were measured with reference to this. Prominent lines were measured on all four tracings, and were usually concordant to ± 0.2 cm^{-1}. Weaker lines were measured on one or two tracings, using the strong H_2O lines in the neighborhood as secondary standards. In the center of the band, the strong absorption lines due to atmospheric water vapor could be used as checks on the emission measurements. Moreover, many weak lines that are observed in the absorption of large columns of water vapor [5, 9] appear strongly in emission in these tracings because of the much higher temperature in the flame. The measured positions of these lines are in good agreement with the absorption data. Because of the internal and external consistency of the measurements, it is believed that the frequencies of strong unblended lines are correct to within ± 0.1 cm^{-1}, and of the weaker or blended lines to ± 0.25 cm^{-1}. Wavelengths in air were converted to wave numbers and corrected to vacuum in the usual manner.

3. Results

A complete listing of the lines between 4,600 and 5,900 cm^{-1} has been prepared. Selected portions of this listing, corresponding to the regions of the P, Q, and R branches as illustrated in figures 1 to 3, are presented in table 1. The first column gives the intensity, as observed on a typical H_2-O_2 tracing, in arbitrary units of recorder deflection above the background of unresolved emission in the neighborhood. The intensities are uncorrected for instrumental sensitivity and hence can be given only rough quantitative significance; the sensitivity, however, does not vary greatly over the frequency interval studied. Lines whose intensity and position are very strongly affected by atmospheric absorption are marked with an asterisk (*). It should be mentioned that the peak deflection of the most intense lines is of the order of one-tenth of that for a black body at the flame temperature. Making allowance for the fact that the slit width exceeds the line width, it is estimated that the maximum emissivity at the center of strong lines does not exceed 0.2 to 0.4. This would appear to be experimentally confirmed by the fact that the peak deflection was very nearly doubled when a mirror reflected the flame upon itself, thus doubling the effective path of hot gas in the line of sight of the spectrometer. The second column of the table gives the position, in cm^{-1}. The remaining columns of the table list rotational assignments for the observed absorption.

The measured region contains over 1,000 lines. These include all lines with a measured intensity of 10 or greater (the strongest observed line, 4,999.99 cm^{-1}, having an intensity of 90), together with some weaker lines down to $I=3$ at the wings of the band. The noise level of the instrument and flame instability corresponded to $I<2$, so that all lines, which have been observed on several tracings, are considered definite peaks in the emission. Many weaker lines of probable but not certain reality might have been added, and there is also a background of unresolved emission, whose intensity, in the stronger portions of the band, may reach 5 to 10 units. Some of the strongest atmospheric-absorption lines, arising from the lowest energy levels of the ground state, appear as dips in this background. There is little question but that if still higher resolving power could be used, many more "lines" would appear in this region. However, as will be discussed presently,

TABLE 1. *Emission lines in the region 1.9 μ due to H_2O*

Observed		Identification	Calculated		Observed		Identification	Calculated	
Intensity	Wave number ν_{vac}	$J'_{\tau'}-J''_{\tau''}$	Wave number ν_{vac}	Intensity (~2,877° K)	Intensity	Wave number ν_{vac}	$J'_{\tau'}-J''_{\tau''}$	Wave number ν_{vac}	Intensity (~2,877° K)
	cm^{-1}		cm^{-1}			cm^{-1}		cm^{-1}	
35	4910.80	b $16_{14,-13}-17_{15,-14}$	-------	13	30	63.83	f $8_{-8}-9_{-9}$	63.69	3
		g $8_{-8}-9_{-9}$	4910.6	3	37	65.39	a $16_{12,-11}-17_{13,-12}$	65.4	13
45	12.07	a $18_{16,-15}-19_{17,-16}$	12.0	12			d $9_{-9,-8}-10_{10,-9}$	-------	10
20	13.07				37	65.74	a $14_{-4}-15_{-5}$	65.8	9
25	14.62	j $12_{-12,-11}-13_{13,-12}$	14.22	6			g 5_0-6_1	65.8	2
22	15.83	j $12_{-10,-9}-13_{11,-10}$	15.8	5	18	66.60	e $12_{-12,-11}-13_{13,-12}$	66.8	6
16	16.49	h $9_{-9,-8}-10_{10,-9}$	-------	6	25	67.00	a $15_{-6}-16_{-7}$	66.9	9
18	17.13				14	68.37	e $12_{-10,-9}-13_{11,-10}$	68.5	5
18	17.87				35	68.98			
15	18.74	e $14_{-14,-13}-15_{15,-14}$	18.8	6	35	69.15	a $16_{-10}-17_{-11}$	69.2	9
20	19.28				35	69.46			
20	20.25	g $6_{-2}-7_{-3}$	19.98	1	17	70.53	g $5_{-4}-6_{-5}$	70.37	2
		f $10_{-10,-9}-11_{11,-10}$	20.3	4	30	71.47	b $12_{-6}-13_{-7}$	71.4	11
14	21.31				60	73.16	e $11_{-11,-10}-12_{12,-11}$	-------	15
10	22.14						f 6_0-7_{-1}	73.07	2
45	23.17						g $4_{-2}-5_{-3}$	73.46	2
50	24.05	d $11_{-11,-10}-12_{12,-11}$	-------	10	45	74.40	a $14_{-6}-15_{-7}$	-------	9
		a $18_{14,-13}-19_{15,-14}$	24.2	10			b $13_{-8}-14_{-9}$	74.4	11
40	24.68	a $17_{17,-16}-18_{18,-17}$	24.7	16	50	75.66	a $15_{15,-14}-16_{16,-15}$	75.6	19
19	25.35	k $9_{-9,-8}-10_{10,-9}$	25.35	4	55	76.72	b $13_{13,-12}-14_{14,-13}$	76.7	20
17	25.72				50	78.46	b $13_{11,-10}-14_{12,-11}$	78.4	17
12	26.51				14	80.12	j $9_{-9,-8}-10_{10,-9}$	80.13	6
56	27.77	b $15_{15,-14}-16_{16,-15}$	27.7	17	19	80.98			
50	27.99				30	81.70			
50	28.11	c $13_{13,-12}-14_{14,-13}$	-------	14	30	82.07	a $15_{13,-12}-16_{14,-13}$	82.5	16
20	28.92				25	82.90			
20	29.17				28	83.48	a $14_{-2}-15_{-3}$	83.3	9
15	30.55				40	84.05	a $15_{11,-10}-16_{12,-11}$	84.1	13
40	31.16	g $7_{-7,-6}-8_{-8,-7}$	31.20	3	25	85.36	d $8_{-8}-9_{-9}$	85.36	7
36	33.29	b $15_{13,-12}-16_{14,-13}$	-------	14			a $15_{-8}-16_{-9}$	85.5	9
34	33.48				16	86.14			
26	33.94	b $15_{11,-10}-16_{12,-11}$	-------	12	16	86.50	d $8_{-7}-9_{-8}$	86.57	2
17	34.82				15	87.34			
48	35.67	a $17_{15,-14}-18_{16,-15}$	35.6	13	16	88.22			
		g $6_{-4}-7_{-5}$	35.67	2	35	89.18	e $11_{-9,-8}-12_{10,-9}$	89.2	6
28	36.28				25	90.00	e $11_{-11,-10}-12_{12,-11}$	89.98	7
30	26.65	j $11_{-11,-10}-12_{12,-11}$	36.62	6			g $4_{-4}-5_{-5}$	90.10	2
30	37.27				35	91.58	b $12_{-8}-13_{-9}$	91.5	11
20	38.29				10	92.72	f $6_{-4}-7_{-5}$	93.08	2
30	39.70				35	94.06			
25	42.49	f $9_{-9,-8}-10_{10,-9}$	42.20	4	35	95.23			
30	43.42				16	96.04	e $10_{-10,-9}-11_{11,-10}$	95.81	15
30	43.75	e $13_{13,-12}-14_{14,-13}$	43.75	6			f 6_2-7_1		
35	44.76	a $17_{13,-12}-18_{14,-13}$	44.7	11	20	96.67			
		d $10_{-10,-9}-11_{11,-10}$	-------	10	25	97.44	a $14_{-8}-15_{-9}$	97.67	9
20	45.71	k $8_{-7}-9_{-8}$	45.7	3	17	98.54	a 15_0-16_{-1}	-------	5
14	46.56	e $13_{-11,-10}-14_{12,-11}$	46.8	5	90	99.99	b $12_{-10}-13_{-11}$	99.79	14
12	47.02						b $12_{-12,-11}-13_{13,-12}$	99.94	21
20	48.66						a $14_{-14,-13}-15_{15,-14}$	5000.10	21
35	49.08				26	5001.07	a $14_{-7}-15_{-8}$	5000.92	3
35	49.27						c $8_{-8}-9_{-9}$	01.04	9
45	50.46	a $16_{16,-15}-17_{17,-16}$	50.4	18	17	01.55	j $8_{-7}-9_{-8}$	-------	5
55	51.28	c $12_{-12,-11}-13_{13,-12}$	-------	14	12	02.91	d $6_{-6}-7_{-5}$	02.96	6
45	51.77	b $14_{-14,-13}-15_{15,-14}$	51.8	19	25	03.49	a $14_{-10,-9}-15_{11,-10}$	03.60	16
		g $6_{-6}-7_{-7}$	51.8	2	35	05.18	d $7_{-7}-8_{-8}$	05.16	2
20	53.19				40	05.60	a $14_{-12,-11}-15_{13,-12}$	05.40	18
20	53.60				30	06.60	d $7_{-6}-8_{-7}$	06.86	7
28	54.35	b $14_{-10,-9}-15_{11,-10}$	-------	11	7	08.43	g 3_0-4_{-1}	08.11	1
20	55.72	b $14_{-12,-11}-15_{12,-12}$	55.93	16	8	08.58			
30	57.43				9	08.77			
33	58.84	j $10_{-10,-9}-11_{11,-10}$	58.55	6	7	09.50	e $10_{-8}-11_{-9}$	09.3	1
		a $16_{14,-13}-11_{11,-10}$	58.8	15	5	10.08			
33	59.91				27	11.03			
17	60.95				21	11.53	a 14_0-15_{-1}	11.53	6
42	61.54						b $11_{-4}-12_{-5}$	11.62	11
32	62.03				23	11.83	b $10_{-4}-11_{-5}$	11.82	13
9	63.10								

TABLE 1. *Emission lines in the region 1.9 μ due to H_2O*—Continued

Observed		Identification		Calculated		Observed		Identification		Calculated	
Intensity	Wave number Vac		$J'_{\tau'} - J''_{\tau''}$	Wave number Vac	Intensity (~2,877° K)	Intensity	Wave number Vac		$J'_{\tau'} - J''_{\tau''}$	Wave number Vac	Intensity (~2,877° K)
	cm^{-1}			cm^{-1}			cm^{-1}			cm^{-1}	
21	12.39	e	$10_{10,\ -9} - 11_{11,\ -10}$	12.39	6	85	5049.65	a	$12_{12,-11} - 13_{13,-12}$	49.54	23
		a	$15_{2,\ 3} - 16_{1,\ 2}$		6			c	$7_{-2} - 8_{-3}$	49.65	9
23	13.21	a	$13_{-7} - 14_{-8}$	13.11	4			c	$8_{-1} - 9_{-2}$	49.79	1
15	14.11							a	$12_{10,-9} - 13_{11,-10}$	49.90	20
20	14.79	b	$11_{-6} - 12_{-7}$	14.77	13						
		a	$13_{-4} - 14_{-5}$	14.86	9						
35	16.86	c	$9_{-9,\ -8} - 10_{-10,\ -9}$	16.78	15	*10	5280.59				
		b	$10_{-2} - 11_{-3}$	16.92	11	15	81.09	c	$9_{3,2} - 9_{2,3}$		8
14	17.94	f	$5_0 - 6_{-1}$	17.78	2	15	81.64				
		g	$2_0 - 3_1$	18.09	1	25	82.21				
17	18.75	f	$5_{-2} - 6_{-3}$	18.71	2	25	82.44	c	$8_{4,3} - 8_{3,4}$		10
14	19.65	a	$15_{4,5} - 16_{3,4}$		5	30	84.06	c	$7_{4,5} - 7_{5,4}$		13
		a	$17_{-14} - 17_{-13}$	19.5	1	*32	85.22	d	$6_{-6} - 5_{-5}$	5284.91	5
31	20.54	a	$12_{-4} - 13_{-5}$	20.32	12			k	$9_{-9} - 8_{-8}$	84.96	3
		a	$13_{-2} - 14_{-3}$	20.32	9			d	$4_0 - 3_1$	85.12	3
		b	$11_{-8} - 12_{-9}$	20.68	14			c	$3_{-2} - 2_{-1}$	85.31	5
43	20.90	a	$13_{-6} - 14_{-7}$	20.90	12	30	86.25	c	$6_{5,\ 5} - 6_{5,\ 6}$	85.87	16
		a	$12_{-2} - 13_{-3}$	21.19	12			b	$2_2 - 2_1$	85.91	8
44	23.07	b	$11_{-11,\ -10} - 12_{-12,\ -11}$	23.01	22	22	86.81	a	$11_{-4} - 11_{-3}$	86.76	2
20	23.70	a	$14_2 - 15_1$		6	17	87.29	c	$7_{5,\ 4} - 7_{4,\ 5}$		5
27	24.21	a	$13_{-9} - 14_{-10}$	24.27	4	17	87.74	c	$6_{5,\ 5} - 6_{5,\ 6}$	87.74	7
		a	$13_{-8} - 14_{-9}$	24.44	12	20	88.44	c	$3_{-3} - 2_{-2}$	88.25	2
		d	$6_{-6} - 7_{-7}$	24.55	6			b	$5_0 - 5_1$	88.37	6
25	25.12					16	89.19	c	$2_{-2} - 1_{-1}$	89.38	2
45	25.47	a	$13_{-13,\ -12} - 14_{-14,\ -13}$	25.46	22	17	90.14	a	$1_0 - 2_{-1}$	90.28	4
30	26.40	b	$10_{-6} - 11_{-7}$	26.5	13	25	91.29	f	$8_{-6} - 7_{-7}$	91.24	3
40	27.36	f	$5_{-4} - 6_{-5}$	27.19	2			f	$6_{-4} - 5_{-3}$	91.29	2
		a	$13_{-11,\ -10} - 14_{-12,\ -11}$	27.2	19	30	93.07	c	$8_{5,\ 5} - 8_{5,\ 6}$		13
		d	$6_{-5} - 7_{-6}$	27.25	1	47	94.32	b	$3_2 - 3_3$	93.93	12
		g	$2_{-2} - 3_{-3}$	27.52	1			b	$3_3 - 3_2$	94.07	4
20	29.26	c	$9_{-7} - 10_{-8}$	29.20	4			b	$4_2 - 4_1$	94.43	9
25	29.73	f	$5_2 - 6_1$	29.88	1	41	94.87	c	$7_{7,\ 6} - 7_{6,\ 7}$		16
		f	$4_{-2} - 5_{-3}$	30.05	2	13	95.73	b	$2_0 - 2_{-1}$	95.68	2
20	31.50	a	$11_{-3} - 12_{-4}$	31.53	4	15	96.50	b	$5_1 - 5_0$	96.51	2
10	33.47					15	97.26	b	$4_0 - 4_{-1}$	97.31	4
13	34.65					13	97.97	d	$4_2 - 3_3$	97.61	1
16	34.99	c	$9_{-9,\ -8} - 10_{-10,\ -9}$	35.01	7			e	$9_{3,\ 4} - 9_{1,\ 5}$		5
10	35.53					14	98.52	e	$2_0 - 1_1$	98.41	1
15	35.97							e	$8_{5,\ 5} - 8_{5,\ 6}$		6
20	36.70	a	$13_1 - 14_0$		2	32	99.28	d	$5_{-2} - 4_{-1}$	99.22	5
		a	$14_{3,4} - 15_{2,3}$		6			e	$7_{7,\ 6} - 7_{6,\ 7}$	99.26	7
32	37.91	b	$10_0 - 11_{-1}$		10			d	$7_{-6} - 6_{-5}$	99.44	6
		c	$8_{-8,\ -7} - 9_{-9,\ -8}$	37.88	14			b	$7_0 - 7_1$	99.64	7
		a	$13_0 - 14_{-1}$	38.06	6	*19	5300.23	a	$3_{-2} - 3_{-1}$	99.77	2
20	40.13							k	$10_{-10,\ -9} - 9_{-9,\ -8}$	5300.0	4
28	40.61	f	$4_2 - 5_1$	40.48	1			d	$7_{-7} - 6_{-6}$	00.25	2
		b	$10_{-8} - 11_{-9}$	40.69	15	23	02.05	b	$6_0 - 6_{-1}$	02.15	5
		a	$12_{-3} - 13_{-4}$	40.88	4	52	04.48	b	$6_2 - 6_1$	04.17	13
		a	$12_{-5} - 13_{-6}$	40.90	4			f	$6_{-2} - 5_{-1}$	04.32	2
8	41.71	b	$10_{-7} - 11_{-8}$	41.55	5			b	$5_{3,2} - 5_{2,3}$	04.58	15
10	42.03							b	$7_1 - 7_0$	04.84	2
21	43.26	d	$5_{-5} - 6_{-6}$	42.82	5			c	$3_{-1} - 2_0$	04.84	2
35	43.77	a	$12_0 - 13_{-1}$	43.39	9	55	05.57	f	$9_{-9,\ -8} - 8_{-9,\ -7}$	05.60	4
		a	$12_{-8} - 13_{-9}$	43.70	12			c	$3_{-2} - 2_1$	05.62	2
		d	$4_{-2} - 5_{-3}$	43.71	5			b	$4_{4,\ 3} - 4_{3,\ 4}$	05.68	20
27	44.28	d	$5_{-2} - 6_{-3}$	44.08	5	20	06.30	c	$4_{-4} - 3_{-3}$	06.27	6
		a	$12_{-7} - 13_{-6}$	45.17	4	*16	08.29	b	$8_0 - 8_{-1}$	08.53	5
		a	$14_{5,6} - 15_{4,5}$	44.59	5	7	08.98	c	$3_1 - 4_0$	08.95	2
45	45.79	b	$10_{-10,\ -9} - 11_{-11,\ -10}$	45.64	22	15	09.66	e	$9_{7,\ 6} - 9_{6,\ 7}$		6
		f	$4_{-4} - 5_{-5}$	46.05	2			a	$10_{-2} - 10_{-3}$	09.77	1
		a	$11_{-5} - 12_{-6}$	46.06	4	16	10.80	e	$8_{9,\ 7} - 8_{7,\ 8}$		7
21	46.66	e	$8_{-3} - 9_{-4}$	46.42	4	9	11.70	f	$6_2 - 5_3$	11.73	1
15	47.45	e	$7_{-3} - 8_{-4}$	47.41	4			b	$3_{-1} - 3_{-2}$	11.81	2
		d	$5_{-4} - 6_{-5}$	47.51	6	9	12.15				
		a	$12_{-1} - 13_{-2}$	47.55	3	32	13.46	a	$13_{-4} - 13_{-3}$	12.82	1
12	48.72	a	$13_{2,3} - 14_{1,2}$	49.2	8			b	$8_1 - 8_2$	13.25	3

TABLE 1. *Emission lines in the region 1.9 μ due to H_2O*—Continued

Observed		Identification		Calculated	
Intensity	Wave number Vac		$J'_{\tau'}-J''_{\tau''}$	Wave number Vac	Intensity (~2,877° K)
	cm^{-1}			cm^{-1}	
25	14.25	a	$7_{-2}-7_{-1}$	14.20	4
		b	8_2-8_1	14.25	8
		k	$11_{-11,\,-10}-10_{-10,\,-9}$	14.3	4
25	14.96	b	$5_{-1}-5_{-2}$	14.68	3
30	15.17	d	$8_{-2}-7_{-6}$	15.06	2
		b	7_2-7_3	15.28	10
30	15.60	d	$8_{-8}-7_{-7}$	15.96	6
*22	16.58	b	$6_{4,\,3}-6_{3,\,4}$	16.20	18
43	17.82	b	$5_{5,\,4}-5_{4,\,5}$	17.33	23
19	18.38				
14	19.28				
26	20.03	b	$2_{-1}-1_0$	20.01	1
		e	3_0-2_1	20.41	1
40	20.90	c	$5_{-4}-4_{-3}$	20.55	8
		d	5_0-4_1	20.69	3
18	22.04				
42	22.70	d	$6_{-4}-5_{-3}$	22.60	5
		b	$2_{-2}-1_{-1}$	22.63	5
		e	$5_{-5}-4_{-4}$	22.67	3
		f	$7_{-2}-6_{-1}$	22.79	2
30	25.20	b	$9_{3,\,2}-9_{2,\,3}$	25.20	11
		e	$4_{-4}-3_{-3}$	25.30	3
*20	26.81	a	$12_{-3}-12_{-2}$	26.44	1
		c	$4_{-1}-3_0$	26.47	2
		b	$8_{4,\,3}-8_{3,\,4}$	26.81	15
		j	$8_{-7}-7_{-6}$	27.23	5
30	28.24	b	$8_{-2}-8_{-3}$	28.10	2
		k	$12_{-12,\,-11}-11_{-11,\,-10}$	28.1	4
		b	$7_{3,\,4}-7_{4,\,3}$	28.36	18
		a	$6_{-1}-6_0$	28.61	2
50	29.31	b	$6_{6,\,5}-6_{5,\,6}$	29.25	24
		e	$4_{-2}-3_{-1}$	29.48	6
17	31.40	f	$11_{-11,\,-10}-10_{-10,\,-9}$	31.09	4
*10	32.71	d	$9_{-9}-8_{-8}$		2
		b	2_0-1_1	32.27	4
		b	$4_{-2}-4_{-3}$	32.77	1
18	33.10				
30	34.00	b	$6_{-2}-6_{-3}$	33.71	2
14	34.82				
*32	35.98	e	4_0-3_1	35.58	6
		a	2_1-2_2	26.14	3
38	37.36	b	$10_{4,\,3}-10_{3,\,4}$		12
		d	5_2-4_3	36.96	2
		c	$6_{-5}-5_{-4}$	37.08	3
		a	5_0-5_1	37.68	7
30	39.84	b	$8_{6,\,5}-8_{5,\,6}$		18
		a	$8_{-1}-8_0$	39.34	2
		b	$3_{-2}-2_{-1}$	39.55	7
		k	$13_{-13,\,-12}-12_{-12,\,-11}$	39.6	4
		e	$5_{-4}-4_{-3}$	39.70	3
		f	7_0-6_1	39.71	1
35	40.83	b	$7_{7,\,6}-7_{6,\,7}$		24
		a	$11_{-2}-11_{-1}$	40.78	4
17	41.99	e	$5_{-5}-4_{-4}$	41.60	1
		j	$9_{-9,\,-8}-8_{-8,\,-7}$	41.97	5
		b	$3_{-3}-2_{-2}$	42.33	2
		a	4_1-4_2	42.41	3
10	42.95				
10	43.18	f	$12_{-12,\,-11}-11_{-11,\,-10}$	43.37	3
*10	43.47	a	3_1-3_0	43.39	2
*14	44.07	c	4_2-3_3	43.99	3
12	46.09	e	$4_{-2}-3_{-1}$	46.44	3
15	46.78	d	6_0-5_1	46.54	4
		a	7_0-7_1	46.64	8
		f	$7_{2,\,3}-6_{3,\,4}$	46.86	1
14	47.66	a	5_1-5_0	47.26	2
*20	48.34	c	$5_{-2}-4_{-1}$	48.12	6
		a	2_0-2_{-1}	48.68	2
		a	$13_{-2}-13_{-1}$	48.71	3

Observed		Identification		Calculated	
Intensity	Wave number Vac		$J'_{\tau'}-J''_{\tau''}$	Wave number Vac	Intensity (~2,877° K)
	cm^{-1}			cm^{-1}	
10	49.78	b	$10_{3,\,6}-10_{6,\,5}$	49.78	14
14	50.36	a	$10_{-1}-10_0$	50.34	2
		b	$9_{6,\,7}-9_{7,\,6}$	50.47	18
15	51.06	a	6_1-6_2	50.81	2
17	51.24	b	$8_{7,\,8}-8_{8,\,7}$		22
12	51.81	k	$14_{-14,\,-13}-13_{-13,\,-12}$	51.8	3
*8	52.46	e	4_0-3_1	52.27	2
		c	$5_{-3}-4_{-2}$	52.30	2
		a	6_2-6_1	52.57	10
		a	4_0-4_1	52.60	4
		c	$7_{-6}-6_{-5}$	52.68	9
		a	5_2-5_3	52.69	13
15	53.23	e	$7_{-7}-6_{-6}$	53.00	3
		a	5_3-5_2	53.04	4
		a	6_0-6_{-1}	53.34	5
*14	53.60	a	$4_{4,\,3}-4_{3,\,4}$	53.86	23
*5	54.53	e	4_2-3_3	54.30	1
		f	$8_{-2}-7_{-1}$	54.41	2
25	55.90	b	3_0-2_1	55.64	4
		a	9_0-9_1	55.81	7
		j	$10_{-10,\,-9}-9_{-9,\,-8}$	55.90	6
		e	$6_{-6,\,-5}-5_{-5,\,-4}$	56.56	5
20	56.68	b	$4_{-3}-3_{-2}$	57.02	3
21	57.13	a	8_0-8_{-1}	57.17	6
25	57.92	b	$3_{-1}-2_0$	57.82	2
		a	$12_{-1}-12_0$	58.11	2
18	59.44	a	8_1-8_2	59.34	3
42	60.19	b	3_1-2_2	59.88	1
		b	$4_{-4}-3_{-3}$	60.02	9
		a	9_1-9_0	60.34	2
40	61.11	a	8_2-8_1	60.88	9
		a	10_0-10_{-1}	61.22	5
34	61.68	e	$5_{-2}-4_{-1}$	61.66	3
		a	$7_{3,\,2}-7_{2,\,3}$	61.73	15
*25	63.04	a	$6_{4,\,3}-6_{3,\,4}$	63.06	20
		a	$7_{-1}-7_{-2}$	63.13	1
*19	63.80	a	$5_{5,\,4}-5_{4,\,5}$	64.16	25
19	64.85	a	11_0-11_1	64.54	6
		a	$9_{-1}-9_{-2}$	65.16	1
34	66.13	a	12_0-12_{-1}	65.86	5
		a	$11_{-1}-11_{-2}$	65.97	1
		c	5_0-4_1	66.20	5
20	67.04	e	$5_{-3}-4_{-2}$	67.26	1
45	68.14	a	11_1-11_0	67.74	2
		a	10_1-10_2	68.00	3
		c	$6_{-3}-5_{-2}$	68.07	2
		c	$8_{-8}-7_{-7}$	68.08	10
		c	5_1-4_2	68.24	2
25	69.25	a	10_2-10_1	69.12	8
		j	$11_{-11,\,-10}-10_{-10,\,-9}$	69.28	6
27	70.59	a	$9_{3,\,2}-9_{2,\,3}$	70.39	13
30	71.50	e	$7_{-7,\,-6}-6_{-6,\,-5}$	71.42	6
		a	$14_{-2}-14_{-3}$	71.48	2
62	72.38	a	$8_{4,\,3}-8_{3,\,4}$	72.43	17
31	73.23	c	$6_{-4}-5_{-3}$	73.17	8
32	73.83	a	$7_{5,\,4}-7_{4,\,5}$	73.71	21
		a	13_0-13_1	73.81	4
*34	74.74	b	$5_{-4}-4_{-3}$	74.45	11
		a	13_1-13_0	74.88	2
33	75.08	a	$6_{6,\,5}-6_{5,\,6}$	75.02	26
		a	12_2-12_{-2}	75.08	3
33	75.78				
*33	76.41	b	$5_{-5}-4_{-4}$	76.10	4
40	78.05	a	12_2-12_1	77.39	6
		a	$10_{-2}-10_{-3}$	78.13	3
60	78.74	a	$11_{3,\,2}-11_{2,\,3}$	78.53	10
		e	$5_{-1}-4_0$	78.53	3
28	79.44				
18	80.08	e	$6_{-3}-5_{-2}$	79.87	3

TABLE 1. *Emission lines in the region 1.9 μ due to H_2O*—Continued

Observed		Identification		Calculated		Observed		Identification		Calculated	
Intensity	Wave number Vac		$J'_{\tau'}-J''_{\tau''}$	Wave number Vac	Intensity (~2,877° K)	Intensity	Wave number Vac		$J'_{\tau'}-J''_{\tau''}$	Wave number Vac	Intensity (~2,877° K)
	cm^{-1}			cm^{-1}			cm^{-1}			cm^{-1}	
50	80. 98	a	$10_{4,\ 3}-10_{3,\ 4}$	80. 89	13	17	17. 55				
		c	$5_{2,\ 3}-4_{3,\ 4}$	81. 17	5	40	18. 37	b	$6_{-3}-5_{-2}$	18. 11	4
48	81. 83							a	$13_{5,\ 9}-13_{9,\ 8}$	18. 42	10
65	82. 02	j	$12_{-12,\ -11}-11_{-11,\ -10}$	82. 07	6	18	20. 07	c	$6_{5,\ 4}-5_{4,\ 5}$	19. 99	3
		a	15_0-15_1	82. 1	5			a	$12_{9,\ 10}-12_{10,\ 9}$	20. 02	13
		b	$4_{-2}-3_{-1}$	82. 10	9	65	21. 56	b	$8_{-7}-7_{-6}$	21. 12	5
52	82. 67	a	$9_{5,\ 4}-9_{4,\ 5}$	82. 57	17			b	$8_{-8}-7_{-7}$	21. 44	14
		c	$9_{-9}8_{-8}$	83. 08	6			c	$7_{-3}-6_{-2}$	21. 78	4
68	84. 27	b	$8_{-4}-8_{-5}$	84. 04	1			a	$11_{11,\ 10}-11_{10,\ 11}$	21. 82	17
		a	$8_{8,\ 5}-8_{5,\ 6}$	84. 57	21	56	23. 02				
*35	85. 62	a	14_2-14_1	85. 5	4	40	24. 03	b	$6_{-4}-5_{-3}$	23. 98	11
		a	$7_{7,\ 6}-7_{6,\ 7}$	85. 63	26	17	24. 80	j	$12_{-10,\ -9}-11_{-9,\ -8}$	24. 8	4
		a	2_0-1_1	85. 79	4	22	26. 14	c	$11_{-11,\ -10}-10_{-10,\ -9}$	26. 2	6
		a	13_2-13_3		6	11	26. 85	b	$5_{2,\ 3}-4_{3,\ 4}$	26. 81	5
		c	$8_{-7}-7_{-6}$	85. 98	4	20	27. 96	a	$6_{-4}-6_{-5}$	27. 48	1
35	87. 41	c	$7_{-4}-6_{-2}$	87. 47	8			c	7_0-6_1	28. 28	6
35	88. 41	a	$8_{-2}-8_{-3}$	88. 13	3	*15	29. 40	a	$12_{-4}-12_{-3}$	29. 62	2
		a	$12_{4,\ 3}-12_{3,\ 4}$	88. 35	10	5	30. 79				
12	89. 29	c	$6_{-1}-7_{-2}$	89. 26	3	5	31. 38				
40	90. 74	b	4_1-3_2	90. 67	1	25	32. 30	c	$9_{-7}-8_{-6}$	32. 36	4
		b	$6_{-5}-5_{-4}$	90. 75	4			a	$10_{-4}-10_{-5}$	32. 43	2
		a	$11_{5,\ 4}-11_{4,\ 5}$	90. 76	12	7	33. 41	a	$8_{-4}-8_{-5}$	33. 09	1
48	91. 87	b	4_2-3_3	91. 61	4			a	$4_{-1}-3_0$	33. 41	3
		b	$6_{-6}-5_{-5}$	91. 78	13	7	34. 02				
		c	$7_{-5}-6_{-4}$	91. 78	3	*30	35. 56	b	$9_{-8}-8_{-7}$	35. 21	15
27	92. 78	a	$10_{6,\ 5}-10_{5,\ 6}$	92. 70	16			b	$9_{-9}-8_{-8}$	35. 34	5
45	94. 34	c	$6_{-2}-5_{-1}$	94. 08	7			j	$13_{-11,\ -10}-12_{-10,\ -9}$	35. 8	
		a	$9_{7,\ 6}-9_{6,\ 7}$	94. 18	20	50	37. 14	c	$8_{-4}-7_{-3}$		8
		c	6_0-5_1	94. 29	6			b	$6_{-1}-5_0$	36. 75	3
		j	$13_{-13,\ -12}-12_{-12,\ -11}$	94. 32	6			b	$7_{-4}-6_{-3}$	37. 02	12
50	95. 70	a	$8_{8,\ 7}-8_{7,\ 8}$	95. 65	25	17	37. 79				
*38	96. 28	a	$3_{-3}-2_{-2}$	96. 52	3	8	39. 16	e	$12_{-12,\ -11}-11_{-11,\ -10}$	38. 9	5
15	97. 19	c	$10_{-10,\ -9}-9_{-9,\ -8}$	97. 11	14	8	39. 59				
10	97. 80	a	$13_{5,\ 4}-13_{4,\ 5}$	97. 83	9	*7	40. 24				
38	98. 76	b	$5_{-2}-4_{-1}$	98. 46	9	25	41. 46	b	$6_{-2}-5_{-1}$	41. 15	11
25	99. 71	a	$12_{6,\ 5}-12_{5,\ 6}$	99. 40	11			b	$7_{-5}-6_{-4}$	41. 29	4
		e	$9_{-9,\ -8}-8_{-8,\ -7}$	99. 68	6	30	43. 31	b	6_0-5_1	43. 23	9
30	5401. 58	c	$7_{-5}-6_{-4}$	5401. 56	4	7	44. 29				
		a	$11_{7,\ 6}-11_{6,\ 7}$	01. 83	14	*5	45. 39	a	$6_{-3}-5_{-4}$	45. 09	5
30	03. 20	a	$10_{8,\ 7}-10_{7,\ 8}$	03. 10	18			a	$6_{-6}-5_{-5}$	45. 73	14
50	04. 60	b	$5_{-3}-4_{-2}$	04. 23	3	20	46. 96	c	7_2-6_3	47. 04	2
		a	$9_{9,\ 8}-9_{8,\ 9}$	04. 81	24	30	47. 47	c	$10_{-8}-9_{-7}$	47. 7	2
14	05. 42	j	$14_{-14,\ -13}-13_{-13,\ -12}$	05. 3	5	6	48. 88				
		c	$6_{1,\ 2}-7_{0,\ 1}$	05. 47	8	*11	49. 63	b	$10_{-9}-9_{-8}$	49. 23	5
50	06. 55	a	$14_{8,\ 6}-14_{6,\ 8}$		8			a	$5_{-2}-4_{-1}$	49. 32	10
		b	$7_{-6}-6_{-5}$	06. 34	14			b	$10_{-10}-9_{-9}$	49. 36	15
50	07. 05	b	$7_{-7}-6_{-6}$	06. 74	5	13	49. 92	b	6_1-5_2	49. 97	2
*35	08. 98	a	$13_{7,\ 6}-13_{6,\ 7}$	08. 1	10	16	5450. 79	b	6_2-5_3	5450. 73	6
		c	$8_{-8}-7_{-8}$	09. 17	9						
		a	3_0-2_1	09. 31	5						
26	09. 79	c	$11_{-11,\ -10}-10_{-10,\ -9}$		14	60	5509. 44	b	$15_{-15,\ -14}-14_{-14,\ -13}$	5509. 49	16
		c	$7_{-7}-8_{-8}$	09. 65	9			a	$6_{3,\ 4}-5_{4,\ 3}$	09. 65	5
		c	6_0-5_1	09. 70	1			b	8_2-7_3	09. 71	9
*23	10. 32	a	$12_{9,\ 7}-12_{7,\ 9}$	10. 34	12	5	11. 14				
15	11. 89	a	$11_{9,\ 8}-11_{8,\ 9}$	11. 93	15	15	11. 89				
		e	6_2-5_3	11. 96	2	15	12. 92				
28	12. 23					25	14. 09				
*17	13. 06	a	$10_{10,\ 9}-10_{9,\ 10}$	12. 99	20	55	16. 73	a	$11_{-11,\ -10}-10_{-10,\ -9}$	16. 83	22
		e	$10_{-10,\ -9}-9_{-9,\ -8}$	13. 06	6	40	17. 19	b	$9_{-9}-8_{-8}$	17. 30	10
20	15. 22	j	$11_{-9}-10_{-8}$	13. 45	3	35	17. 97	b	$12_{-10}-11_{-9}$	18. 17	13
		a	$15_{8,\ 7}-15_{7,\ 6}$	15. 37	7			a	$7_{-1}-6_0$	18. 24	4
17	16. 12	b	$5_{-1}-4_0$	15. 88	3	8	19. 11				
		j	$15_{-15,\ -14}-14_{-14,\ -13}$	15. 9	5	47	20. 26	b	$16_{-16,\ -15}-15_{-15,\ -14}$	19. 93	15
27	17. 05	b	5_1-4_2	16. 83	2	28	21. 38	a	7_0-6_1	21. 11	9
		a	$14_{7,\ 8}-14_{8,\ 7}$	17. 09	8	40	21. 74	a	$9_{-4}-8_{-5}$	21. 96	15

TABLE 1. *Emission lines in the region 1.9 μ due to H_2O*—Continued

Observed		Identification	Calculated		Observed		Identification	Calculated	
Intensity	Wave number Vac	$J'_{\tau'}-J''_{\tau''}$	Wave number Vac	Intensity (~2,877° K)	Intensity	Wave number Vac	$J'_{\tau'}-J''_{\tau''}$	Wave number Vac	Intensity (~2,877° K)
	cm⁻¹		cm⁻¹			cm⁻¹		cm⁻¹	
43	23. 20	b $8_{3,4}-7_{4,3}$	22. 66	3	15	80. 15	a 9_1-8_2	79. 50	3
		b $10_{-6}-9_{-5}$	23. 1	12	44	80. 59	a $8_{3,6}-7_{4,7}$	80. 32	3
		a $9_{-7}-8_{-6}$	23. 23	5			a $13_{-11,-10}-12_{-10,-9}$	80. 58	18
		a 7_1-6_2	23. 50	3	46	82. 07	b $14_{-10,-9}-13_{-9,-8}$		14
15	25. 25						a $11_{-6}-10_{-5}$	82. 27	13
20	26. 12				47	82. 94	b $12_{-6}-11_{-5}$	82. 9	10
25	27. 89	a $8_{-3}-7_{-2}$	27. 91	4			a $17_{-17,-16}-16_{-16,-15}$	82. 90	15
30	28. 73				43	84. 87	b $17_{-15,-14}-16_{-14,-13}$		12
47	29. 05	a $12_{-12,-11}-11_{-11,-10}$	29. 23	22			a $11_{-7}-10_{-6}$	85. 17	4
40	30. 30	b $17_{-17,-16}-16_{-16,-15}$	30. 30	14			a $10_{-3}-9_{-2}$	85. 23	4
60	32. 04	b $13_{-10,-9}-12_{-9,-8}$	32. 08	16	8	86. 24			
24	32. 67	b 9_0-8_1	32. 77	8	15	88. 20			
		a $7_{2,3}-6_{3,4}$	32. 82	8	26	90. 06	a $9_{2,3}-8_{3,4}$	90. 31	9
19	33. 23				15	91. 15			
30	34. 50	b $11_{-6}-10_{-5}$		12	40	92. 03	a $18_{-18,-17}-17_{-17,-16}$	91. 90	14
20	35. 95	a $8_{-4}-7_{-3}$	36. 32	14	43	93. 97			
17	37. 20	a $10_{-7}-9_{-6}$	37. 60	5	46	94. 30	a $14_{-12,-11}-13_{-11,-10}$	94. 50	17
39	38. 03	a $10_{-5}-9_{-7}$	38. 19	15	57	95. 42	a $10_{-4}-9_{-3}$	95. 64	13
30	38. 65				30	96. 18			
40	39. 99	b $18_{-19,-17}-17_{-17,-16}$		13	30	96. 98	a $15_{-11,-10}-14_{-10,-9}$		12
69	41. 18	a $13_{-13,-12}-12_{-12,-11}$	41. 20	21	25	98. 19	a $12_{-7}-11_{-6}$	98. 17	4
9	42. 28						b $18_{-16,-15}-17_{-15,-14}$		10
15	43. 70	a $8_{-1}-7_0$	43. 46	3	34	99. 04	a $10_{-2}-9_{-1}$	99. 10	11
31	44. 86	b $14_{-12,-11}-13_{-11,-10}$	44. 65	15	43	99. 77	a $12_{-8}-11_{-7}$	99. 85	12
		a $7_{4,5}-6_{5,6}$	44. 95	4			a $10_{-1}-9_0$	5600. 00	3
		b $9_{2,3}-8_{3,4}$	45. 02	8	35	5600. 65	a $19_{-19,-18}-18_{-18,-17}$	00. 70	12
27	46. 09				34	02. 55	a $9_{4,5}-8_{5,6}$	02. 73	6
42	47. 10	a $9_{-4}-8_{-3}$	47. 23	13	37	03. 44	a 10_0-9_1	03. 12	10
20	48. 26	b $10_{-4}-9_{-3}$	48. 29	11	30	04. 50	a $11_{-4}-10_{-3}$	04. 44	11
25	48. 96	a 8_0-7_1	48. 72	10	12	06. 25			
		b $19_{-19,-18}-18_{-18,-17}$		11	46	07. 85	a $15_{-13,-12}-14_{-12,-11}$	07. 30	15
46	50. 44	b $10_{-2}-9_{-1}$	50. 38	10	53	08. 83	a $20_{-20,-19}-19_{-19,-18}$	08. 80	10
59	51. 82	a $14_{-14,-13}-13_{-13,-12}$	51. 74	20	22	10. 69	b $16_{-12,-11}-15_{-11,-10}$		10
		a $8_{-2}-7_{-1}$	51. 91	12	18	12. 26	a 10_1-9_2	12. 28	3
48	52. 45	a $11_{-9,-8}-10_{-8,-7}$	52. 74	19	22	12. 60	a 10_2-9_3	12. 78	8
48	53. 67	a $9_{-5}-8_{-4}$	54. 04	5	34	13. 51	a $13_{-8}-12_{-7}$	13. 34	12
		b $12_{-8}-11_{-7}$	54. 4	11	48	14. 47	a $11_{-5}-10_{-4}$	14. 45	4
14	55. 13				29	14. 99	a $13_{-9}-12_{-8}$	14. 89	4
26	55. 88	a 8_1-7_2	55. 64	3			a $9_{6,7}-8_{7,8}$	15. 08	3
30	56. 13	a 8_2-7_3	56. 18	10	26	16. 52	a $21_{-21,-20}-20_{-20,-19}$	16. 45	9
		b 10_0-9_1	56. 35	9	40	18. 89	a $16_{-14,-13}-15_{-13,-12}$	18. 9	14
69	58. 04	b $20_{-20,-19}-19_{-19,-18}$		9	23	19. 40			
		b $11_{-4}-10_{-3}$	57. 9	10	28	20. 94	a $11_{-2}-10_{-1}$	20. 76	10
		b $15_{-13,-12}-14_{-12,-11}$	58. 1	14	22	21. 43	a $11_{-3}-10_{-2}$	20. 99	4
9	59. 40				19	23. 37	a $22_{-22,-21}-21_{-21,-20}$		8
25	59. 98						a $12_{-5}-11_{-4}$	22. 78	4
12	61. 22				28	24. 95	a $10_{2,4}-9_{4,5}$	24. 68	7
10	62. 41				23	26. 21			
55	62. 96	a $15_{-13,-14}-14_{-14,-13}$	62. 99	18	10	27. 42	a $11_{-1}-10_0$	27. 25	3
30	64. 83	a $9_{-2}-8_{-1}$	64. 97	11	17	28. 35	a $14_{-9}-13_{-8}$	28. 22	4
		a $10_{-3}-9_{-4}$	65. 03	4	40	29. 11	a $14_{-10}-13_{-9}$	29. 21	11
80	66. 68	b $13_{-8}-12_{-7}$	66. 6	11	14	30. 29	a $23_{-23,-22}-22_{-22,-21}$		7
		a $12_{-10,-9}-11_{-9,-8}$	67. 24	19	65	30. 59	a $12_{-6}-11_{-5}$	30. 58	11
32	67. 63	a $8_{3,4}-7_{4,5}$	67. 63	3			a $17_{-15,-14}-16_{-14,-13}$	30. 6	13
14	69. 49				15	32. 51			
46	70. 07	a $10_{-6}-9_{-5}$	70. 03	13	20	33. 23			
26	71. 62	b $16_{-14,-13}-15_{-13,-12}$		12	31	33. 98	a 11_0-10_1	33. 76	8
61	73. 30	a $16_{-16,-15}-15_{-15,-14}$	73. 32	17	10	34. 92	a 11_1-10_2	35. 03	3
25	74. 61	a $9_{-1}-8_0$	74. 31	4					
		a $9_{-3}-8_{-2}$	74. 47	4	15	35. 71			
32	74. 96				15	36. 07	a $24_{-24,-23}-23_{-23,-22}$		5
20	75. 54				10	37. 18	a $10_{5,6}-9_{6,7}$	37. 26	5
20	76. 58				15	39. 08			
37	77. 88	a 9_0-8_1	78. 08	9	31	40. 03			
20	78. 85				18	41. 21	a $12_{-3}-11_{-2}$	41. 30	3

TABLE 1. *Emission lines in the region 1.9 μ due to H_2O*—Continued

Observed		Identification	Calculated		Observed		Identification	Calculated	
Intensity	Wave number Vac	$J'_{\tau'} - J''_{\tau''}$	Wave number Vac	Intensity (~2,877° K)	Intensity	Wave number Vac	$J'_{\tau'} - J''_{\tau''}$	Wave number Vac	Intensity (~2,877° K)
	cm⁻¹		cm⁻¹			cm⁻¹		cm⁻¹	
50	42.02	a $13_{-6} - 12_{-5}$	41.56	10	5	61.52			
		a $18_{-16,\ -15} - 17_{-15,\ -14}$	42.0	11	6	62.89	a $14_{-8} - 13_{-7}$	62.92	10
45	44.65	a $15_{-11,\ -10} - 14_{-10,\ -9}$	44.37	13	17	63.63	a $20_{-18,\ -17} - 19_{-17,\ -16}$	-------	8
27	45.77	a $11_{2,\ 2} - 10_{3,\ 4}$	46.20	8	9	64.75			
25	46.86	a $13_{-7} - 12_{-6}$	46.91	4	20	65.60			
10	47.03				32	66.68			
22	49.30	a $10_{7,\ 8} - 9_{8,\ 9}$	49.13	2	27	67.45			
31	51.68	a $12_{-2} - 11_{-1}$	51.39	10	10	68.35	a $12_{1,\ 2} - 11_{2,\ 3}$	68.43	9
23	53.30	a $19_{-17,\ -16} - 18_{-16,\ -15}$	-------	10	27	71.34	a $11_{8,\ 7} - 10_{7,\ 8}$	70.97	4
		a $12_{-1} - 11_0$	52.94	3			a $13_{-2} - 12_{-1}$	71.18	8
16	54.16				20	73.29			
42	54.80	a $12_{-4} - 11_{-5}$	55.25	11	16	74.04	a $21_{-19,\ -18} - 20_{-18,\ -17}$	-------	6
30	55.50	a $12_0 - 11_1$	55.54	8	34	74.82	a $17_{-13,\ -12} - 16_{-12,\ -11}$	74.0	11
27	56.78	a $13_{-4} - 12_{-5}$	56.71	9	10	78.01			
10	58.02				25	79.80	a $15_{-8} - 14_{-7}$	79.70	9
22	58.91	a $11_{4,\ 5} - 10_{5,\ 6}$	58.67	6			a $12_{3,\ 4} - 11_{4,\ 5}$	79.83	7
43	59.75	a $14_{-7} - 13_{-6}$	59.92	3	12	83.76	a $11_{5,\ 6} - 10_{5,\ 10}$	82.9	2
		a $16_{-12,\ -11} - 15_{-11,\ -10}$	60.16	12			a $22_{-20,\ -19} - 21_{-19,\ -18}$	-------	5
5	60.80								

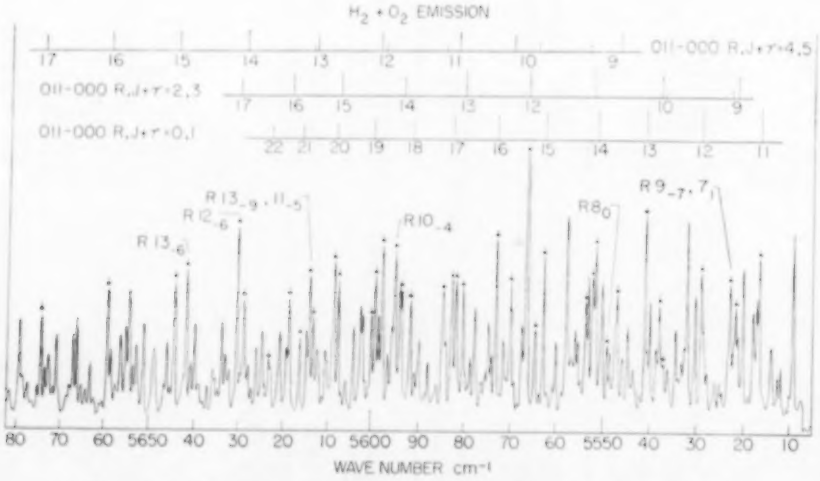

FIGURE 1. *Emission spectrum of* H_2O *in the region 5,510 to 5,680 cm⁻¹.*

the analysis has accounted for most of the expected transition intensity, and it is believed that a major fraction of the measured lines are single lines whose position and intensity will not be appreciably altered under higher resolution.

Tracings of the observed emission, in three regions which best illustrate the nature of the spectrum and its analysis, are presented in figures 1 to 3. These are tracings of the spectrum to which have been added wave-number scales and various identifying marks pointing out some of the strongest series. The spectra show the degree of resolution, and discrimination between strong and weak lines, that has been achieved. Figure 1 covers the region 5,055 to 4,908 cm^{-1}, which includes the strongest lines in the P branch of the (011–000) and upper-state bands. It is a region where atmospheric absorption is negligible. Figure 2, covering the region 5,450 to 5,280 cm^{-1}, shows how lines of the Q branch, which would normally be strong, are reduced in intensity by the atmospheric absorption. The strongest dips in the base line are also due to atmospheric absorption, as may be verified by comparison with the spectra in Nelson's report [5]. In

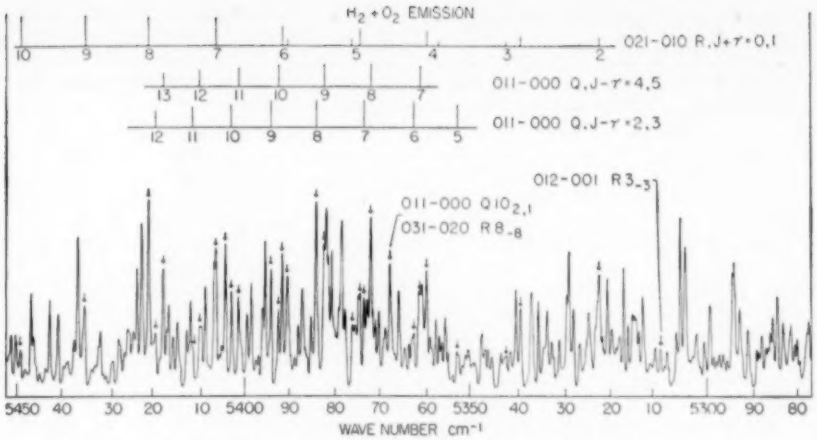

FIGURE 2. *Emission spectrum of* H_2O *in the region 5,280 to 5,450* cm^{-1}.

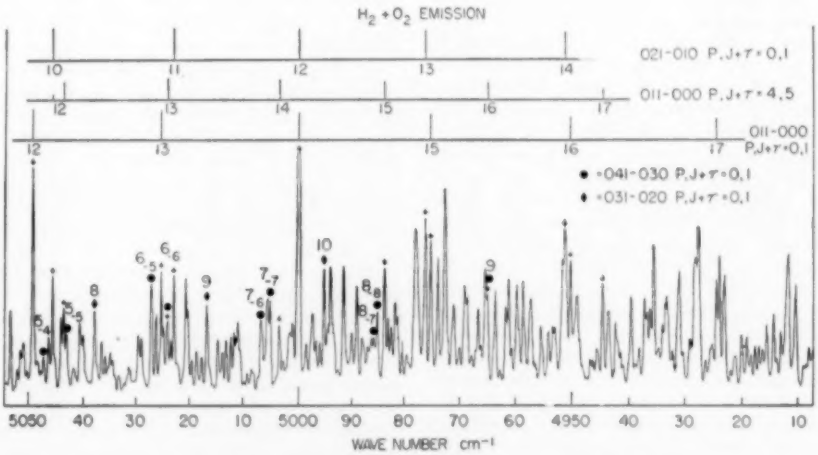

FIGURE 3. *Emission spectrum of* H_2O *in the region 4,910 to 5,050* cm^{-1}.

figure 3, covering the region 5,680 to 5,510 cm^{-1}, lines of the *R* branches of the (011–000) band appear essentially free from atmospheric absorption. These three figures include the region of strongest emission; at frequencies greater than 5,680 cm^{-1} and less than 4,910 cm^{-1} the intensity falls off gradually. In the intermediate region 5,280 to 5,055 cm^{-1} the emission is weak, since it lies near the band origins, and is further reduced by atmospheric absorption.

4. Discussion

The absorption spectrum of H_2O, both in the region of 1.9 μ now under consideration, and throughout the rotation-vibration spectrum extending from the microwave region (0.74 cm^{-1}) to the green visible (18,500 cm^{-1}), is well understood and quite completely analyzed. The water-vapor molecule is an asymmetric-top rotator with effective reciprocal moments of inertia, which in the ground vibrational state have the values $A=27.877$ cm^{-1}, $B=14.512$ cm^{-1}, $C=9.285$ cm^{-1}, leading to an asymmetry parameter $k=-0.4377$. It has three fundamental frequencies of vibration, two preserving the molecular symmetry $\nu_1=3{,}657.05$ cm^{-1}, and $\nu_2=1{,}594.59$ cm^{-1}, and the third in which the motion of the H atoms is antisymmetric to the symmetry axis, $\nu_3=3{,}755.79$ cm^{-1}. In the absorption spectrum, transitions occur from the ground vibrational level to these three fundamentals, and to a very large

number of the possible overtones and combinations of them; in all, 43 bands have been observed. Many of these, however, are quite weak; in particular, transitions to levels in which v_3 is even are very much less intense than those in which v_3 is odd. For example, in the 1.9-μ region, there are the two bands (011–000), whose origin is at 5,331.19 cm^{-1}, and (110–000), whose origin is at 5,235.0 cm^{-1}; the latter is only about one thirtieth as strong as the former, and hence plays a very minor role in the absorption and cannot be detected in emission.[5]

In each band with Δv_3=odd, the rotational structure is similar (except for differences resulting from the different values of A'–A'', B'–B'', and C'–C'' involved); namely, there are four strong branches, the relative intensity of whose lines may be calculated according to the methods of Cross, Hainer, and King [10]. The R_{01} and $P_{0\bar{1}}$ branches extend, respectively, to higher and lower frequencies from the origin, and each consists of one line for each rotational level J'_τ ($-J \leqq \tau \leqq J$). The Q_{01} and Q_{10} branches fall near the origin (in the 1.9-μ band, where A'–A'' is positive, they lie mostly at frequencies higher than the origin), and together contribute one line for each J'_τ. (Q_{01} for $J-\tau$ even; Q_{10} for $J-\tau$ odd). The intensity of an emission line is given by the formula $I=\nu^4 T_v\ g\ e^{-E'/kT}$, (in absorption, the formula is the same, except that ν^4 becomes ν, and E' becomes E''). L is the line strength, a number such that for each J'_τ, $\Sigma L=2J'+1$; for $\tau \sim -J$, $L \sim J$ for R_{01} and $P_{0\bar{1}}$, and $L \sim 0$ for the Q lines; for $\tau \sim +J$, $L \sim 0$ for R and P, and $\sim 2J$ for Q, with a gradual transition between these limits for intermediate τ. Since E' increases rapidly with τ for a given J, the intensity of the R and P lines falls off rapidly as $J+\tau$ increases. Since the Boltzmann factor and L oppose each other for Q lines, there are several lines of nearly equal intensity for each J, those with $J-\tau$ low. Another term in the intensity formula is the nuclear spin factor g, which is 3 for τ odd, 1 for τ even; hence the former lines are predominant. The final factor in the intensity is the vibrational transition probability T_v, which in first approximation should be constant for all lines of a band, but which in some bands of H_2O (but not 011–000) shows anomalies favoring one branch over another.

The absorption spectrum in the 1.9-μ region is fully in accord with the above formula. It has been possible to identify all the lines down to those of quite low intensity, comprising the strong series R_{01}, $P_{0\bar{1}}$, Q_{01}, and Q_{10} for $E'' \leqq 2{,}000$ cm^{-1}. In addition, there have been observed lines of the series $R_{2\bar{1}}$, $P_{\bar{2}1}$, and $Q_{1\bar{2}}$, and $Q_{2\bar{1}}$ (these have much lower L but can be observed in the terrestrial atmosphere, since the first two series lie at the extreme wings of the band) and, as was mentioned above, lines of the 110–000 band, which follow different selection rules, but which are all weak because they have a different and much lower T_v.

[5] An exception to this statement holds for a few rotational levels of 110, which accidentally lie close in energy to levels of 011 of equal J and like total symmetry; transitions to these are strengthened by perturbation induced by Coriolis forces.

It is to be expected, and it has been found, that the emission spectrum differs from the absorption spectrum only as a result of the much higher value of temperature in the Boltzmann factor term of the intensity formula.

The levels of higher energy that are sufficiently populated in the flame to emit with considerable intensity manifest themselves in two different ways. First, rotational levels of higher J'_τ will be populated, the fact that L increases along with J further augmenting the intensity of lines from such levels. Hence, the (011–000) band will show many new lines, especially in the long-wavelength (P branch) and short-wavelength (R branch) wings of the band. Second, higher vibrational levels, particularly the lowest ones involving v_2, will be populated; since T_v, for transitions with $\Delta v_2=1$, increases proportionally with v'_2, the intensity of all rotational transitions in such bands as (021–010), (031–020), etc., will be appreciable relative to (011–000) at flame temperatures. These new "upper-state" bands will form sequences of decreasing intensity at longer wavelengths and hence will be more prominent in the P branches than in the R, where many of their lines will fall in the region of atmospheric absorption.

A rough quantitative calculation of the expected relative intensities at flame temperatures has been made as a guide in the analysis of the new emission lines. For this purpose T was chosen at 2,877° K (kT=2,000 E'). L values were obtained for $J \leqq 12$ from the tables of Cross, Hainer, and King [10], interpolated to $k=-0.437$. For $J>12$, L was estimated by extrapolation of those tables, making use of the facts that the relative total intensities of the several branches are smooth functions of J, that the distribution of intensity within each branch at any J as a function of τ/J is roughly the same, and that the sum rules given in [10] must be obeyed. The resulting L values may be in error by as much as 10 percent at J=20, but should be adequate for showing the trends of intensity. The energies for the Boltzmann factor were in part those observed (see table 4), and in part were estimated for unobserved levels by extrapolation. The resulting relative intensities, for lines of the $P_{0\bar{1}}$ branch, are presented in table 2. The intensity factors, $gLe^{-E/kT}$, are given in a rectangular array, with J' vertical and $(J+\tau)$ horizontal. There are a number of cases, for high $J+\tau$, and for low $J+\tau$ at high J, where lines of odd and even τ fall in unresolvable pairs; these are combined in table 2, and may be recognized, inasmuch as the 3:1 intensity alternation due to the nuclear-spin factor is absent. Similar calculations of intensities in the R_{01}, Q_{10}, and Q_{01} branches (of which the two latter also coalesce at high $J+\tau$) have also been made. The calculated intensities, as listed for identified lines in the last column of table 2, are these rotational intensity factors for the case of the 011–000 band (band a). For other vibrational transitions, an additional vibrational intensity factor must be included.

TABLE 2. *Relative intensities of type A P-branch emission lines of* H_2O *at 2,877°K*

J'	$J'+f$																					
	0	1	2	3	4	5	6	7	8	9	10	11	12	13	14	15	16	17	18	19-20	21-22	23-24	25-26
0	1																						
1	6	1	4																				
2	2	3	8	3	5	2																	
3	11	3	10	3	8	2	5																
4	4	13	4	11	4	8	3	6		A													
5	15	5	14	4	13	3	11	2	7		5												
6	5	16	5	14	5	12	4	10	3		8		4										
7	17	6	15	5	15	5	14	4	11	3	9		8		4 B								
8	6	18	5	16	5	14	5	12	4	10	3		10		6		3						
9		25	16	5	15	5	14	4	13	4	11		11		8		5		3 C				
10		25	5	16	5	14	5	13	4	11	4	9	3		9		7		4	2			
11		24	16	5	14	5	13	4	13	4	11	3	9		10		8		5	3	2		
12		23		20	4	13	4	12	4	11	4	9	3		10		8		6	4	3	1	
13		22		19	12	4	11	4	11	3	10	3	9	2	7		8		6	5	3	2	1
14		21		18	4	12	3	10	3	9	3	8	3	7	2		8		6	5	3	2	1
15		19		16		14		9	3	8		3	8	2	7	2	6		7	6	5	3	3	2
16		18		15		13		3	8	2		7	2	6	2	6	2	5	2	5	4	3	3	2
17		16		13		11		7	2	6		2	6	2	6	1	5	1	4	5	4	3	2	2
18		14		12		10		2	6	2		5	2	4	1	4	1	3	1	4	3	3	2	1
19		13		10		9		7		5		2	5	1	4	1	3	1	3	1 3	3	2	2	
20		11		9		7		6		2		4	1	4	1	3	1	3	1	3 1	3	2		
21		9		7		6		5		3		1	3	1	3	1	3	1						
22		8		6		5		4		1		3	1	3										
23		7		5		4		3																
24		6		4		3																		
25		5		4																				
26		4		3																				
27		3		2																				
28		3																						

A, 287°; B, 1,438°; C, 2,877° K.

In table 2 a solid line has been drawn to delimit the range of J_τ values yielding $P_{\overline{011}}$ intensities up to 10 percent of that of the maximum. It is not to be expected that lines weaker than this could be identified under the experimental conditions. A large proportion of the lines within this limit have been found, the exceptions being principally among the levels of intermediate τ for which the energy does not vary with J and τ in as regular a manner as when $\tau \sim -J$ or $\tau \sim +J$. The two other lines in table 2 at lower J similarly delimit the 10 percent of maximum-intensity range for two lower temperatures, 1,438° and 287° K, and illustrate how the increase in temperature results in the appearance of many new rotational transitions.

The relative rotational intensities within the various upper state bands will be nearly the same as for 011–000, small differences arising from the different energies relative to the $J=0$ level. However, these may be ignored for the rough calculations made here. Table 3 gives the band origins and the relative intensities of the stronger expected bands, $I_{2877}=T_\nu e^{-(E_\nu-E_{011})/kT}$, where T_ν is the vibrational transition probability and $(E_\nu-E_{011})$ is the energy difference between the $J=0$ level of the upper state in the transition and $J=0$ of (011). The vibrational energy levels involved, with a few exceptions, have been observed in absorption, and the corresponding values of $\nu_0=E'_\nu-E''_\nu$ are given to 0.1 cm^{-1}; unobserved levels are calculable from the vibrational energy formula [3], and should be accurate to a few wave numbers. T_ν and I are expressed relative to 1.00 for 011–000; the former is proportional to $v'_2v'_3$, a result that is theoretically exact to first approximation, assuming that the combination transition (which is foridden if the dipole moment may be expanded in purely linear terms in harmonic normal coordinates) is due to cubic and quadratic anharmonic terms in the molecular potential function and to quadratic terms in the dipole expansion [11].

Each band in table 3 is designated in brief by a letter symbol. The calculated intensities are the products of rotational intensity factors like those in table 2 and the vibrational factors of table 3. A few of the higher bands in table 3 involve Darling-Dennison [12] resonance pairs ($v_{1+2}v_2v_3$ with $v_1v_2v_{3+2}$). For these the intensities are taken proportional to the fraction of $2v_3$ in the perturbed wave function, a rather questionable assumption because the intensity relation in cases of resonance are complicated by phase factors [13]. Table 3 contains 11 bands with $I>0.12$. Table 1 shows that numerous assignments

have been made to the seven of these for which both upper and lower energy states had been observed in absorption; that the strongest lines of the P and R series have been identified for two bands, 022–011(j) and 032–021(k), of which the lower state energies had previously been known; and that a few assignments have tentatively been made for the strongest remaining band, 051–040(h), of which both the upper and lower state are newly observed. No assignments have been made for band i.

TABLE 3.—*Vibrational band origins and relative intensities at 2,877° K*

Band designation	v_1'	v_2'	v_3'	v_1''	v_2''	v_3''	ν_0	T_v	$I_{2.877°}$	Number of identified lines
							cm^{-1}			
a	0	1	1	0	0	0	5331.2	1.00	1.00	424
b	0	2	1	0	1	0	5277.0	2.00	0.90	234
c	0	3	1	0	2	0	5221.8	3.00	.62	113
d	0	4	1	0	3	0	5166.9	4.00	.39	64
h	0	5	1	0	4	0	5112	5.00	.23	5
i	0	6	1	0	5	0	5067	6.00	.12	.....
e	0	1	2	0	0	1	5244.3	1.78	.28	98
j	0	2	2	0	1	1	5192	3.55	.25	20
k	0	3	2	0	2	1	5139	5.31	.16	14
f	1	1	1	1	0	0	5149.9	1.00	.16	39
g	1	2	1	1	1	0	5093.7	2.00	.15	32

The identification of a line is considered sufficiently convincing for inclusion in table 1 when both the frequency and intensity checks are satisfactory. For a satisfactory frequency check, the line position must be within 0.4 cm^{-1} of the calculated position. This calculated position is derived by taking the difference between the two energy states involved in the transition. The quantum numbers of these states are given in the central column of table 1. The corresponding energies are listed in table 4 for the two upper states of greatest importance in the 1.9-μ region, namely, 011 and 021. The lower-state energies of 000, 010, 020, 100, and 001 have been given in recent publications [8, 14, 15]. Other upper- and lower-state energy levels, particularly for the low J values, were derived from atmospheric-absorption data and will be published elsewhere. New levels of the upper states 012, 022, and 032 derived from the present data are given in table 5. Agreement of an observed and calculated frequency implies that the frequency difference between two or more emission lines is in accord with the corresponding difference in two or more (often as many as 50) absorption lines. It does not mean that the energy levels can be calculated to an accuracy of 0.4 cm^{-1} from molecular constants because the centrifugal-stretching and perturbation effects are so large as to make these calculations prohibitively difficult. However, the energy levels do agree roughly with what is to be expected, as may be seen from a comparison in table 6 of the rotational energy levels for $J=12$ of the 000 and 011 states, calculated on the rigid rotator approximation. For 000 the constants used were $A=27.877$, $B=14.512$, $C=9.285$ cm^{-1}; for 011, $A=29.54$, $B=14.59$, $C=9.014$. The calculated energies are compared with the observed rotational energies $E'-E_{J=0}$; the differences Δ are chiefly due to centrifugal stretchings. They are consistently greater by about 40 percent for 011, but follow a very similar pattern for the two vibrational states. The only rotational level of 011 that shows an anomalous Δ is 12_{-4}. The large discrepancy here can readily be attributed to perturbation by 12_{-3} of 110, whose unperturbed energy should lie within 10 cm^{-1} of the unperturbed energy of 12_{-4} of 011, because the calculated rotational-energy difference is +94.3 cm^{-1} and the vibrational difference −96.2 cm^{-1}. Similar calculations from inertial constants have been made for other J values, and likewise confirm the assignments.

TABLE 4. *Energy levels (cm^{-1}) of 011 and 021 vibration states*

J_c	$v_1v_2v_3$		J_c	$v_1v_2v_3$	
	011	021		011	021
0_0	5331.19	6871.65	6_2	6251.73	.....
			6_0	6251.77	7869.16
1_{-1}	5354.78	6895.06	$6_{0,0}$	6420.17	8063.49
1_0	5369.76	6913.55			
1_1	5375.41	6919.44	7_{-7}	5907.70	7448.47
			7_{-6}	5907.91	7449.07
2_{-2}	5400.68	6941.04	7_{-5}	6035.08	7587.68
2_{-1}	5411.42	6954.95	7_{-4}	6041.11	7598.33
2_0	5428.16	6972.75	7_{-3}	6118.75	7676.30
2_1	5472.29	7027.31	7_{-2}	6156.56	7730.09
2_2	5473.62	7028.42	7_{-1}	6179.78	.....
			7_0	6277.87	7871.75
3_{-3}	5466.58	7007.26	7_1	6281.20	7874.5
3_{-2}	5473.13	7016.62	7_2	6421.44	8039.88
3_{-1}	5506.32	7051.44	7_3	6421.58	.....
3_0	5544.22	7098.15	$7_{4,5}$	6580.10	8233.79
3_1	5549.67	7105.32	$7_{6,7}$	6780.48	8450.85
3_2	5629.97	7201.64			
3_3	5630.13	7201.81	8_{-8}	6061.98	7602.12
			8_{-7}	6061.98	7602.39
4_{-4}	5550.65	7091.94	8_{-6}	6212.07	7767.32
4_{-3}	5552.98	7096.65	8_{-5}	6215.15	7773.22
4_{-2}	5608.29	7154.40	8_{-4}	6318.73	7879.29
4_{-1}	5639.69	7191.22	8_{-3}	6344.56	.....
4_0	5652.98	7205.25	8_{-2}	6394.27	7968.54
4_1	5726.27	7298.27	8_{-1}	6471.22	.....
4_2	5727.51	7299.32	8_0	6479.95	8073.28
4_3	5842.02	7435.28	8_1	6615.32	.....
4_4	5842.02	7435.28	8_2	6616.07	8234.01
			$8_{3,4}$	6784.02	8428.09
5_{-5}	5652.10	7193.45	$8_{5,6}$	6975.17	8646.42
5_{-4}	5653.55	7196.08	$8_{7,8}$	7184.74	8882.29
5_{-3}	5731.93	7279.65			
5_{-2}	5749.70	7306.40	9_{-9}	6234.07	7772.95
5_{-1}	5783.36	7338.92	9_{-8}	6234.07	7773.05
5_0	5846.47	7418.89	9_{-7}	6406.20	.....
5_1	5851.26	7422.95	9_{-6}	6407.60	7966.97
5_2	5963.03	7556.36	9_{-5}	6537.13	.....
5_3	5963.16	7556.46	9_{-4}	6553.37	8128.39
$5_{4,5}$	6106.26	7723.57	9_{-3}	6624.67	.....
			9_{-2}	6667.75	8282.05
6_{-6}	5771.09	7312.48	9_{-1}	6706.19	.....
6_{-5}	5771.68	7313.55	9_0	6833.27	8452.35
6_{-4}	5874.72	7424.78	9_1	6835.48	.....
6_{-3}	5885.70	7442.35	9_2	7001.8	8646.30
6_{-2}	5939.32	7495.02	9_3	7002.0	.....
6_{-1}	5980.15	7563.19	$9_{4,5}$	7193.3	.....
6_0	6002.31	7573.75	$9_{6,7}$	7404.2	9103.05
6_1	6108.51	7701.80	$9_{8,9}$	7639.4	.....
6_2	6109.33	7702.56			

TABLE 4. *Energy levels (cm^{-1}) of 011 and 021 vibration states*—Continued

J_r	$v_1v_2^0v_3^1$		J_r	$v_1v_2^0v_3^1$	
	011	021		011	021
$10_{-10,-9}$	6423.82	7961.73	$12_{9,10}$	8940.5	.....
10_{-8}	6617.35	8176.59	$12_{11,12}$	9208.7	.....
10_{-7}	6618.11	8178.21			
10_{-6}	6772.07	8341.5	$13_{-12,-12}$	7099.27	8832.4
10_{-5}	6781.45	.....	$13_{-11,-10}$	7355.4	8918.5
10_{-4}	6878.66	8453.04	13_{-9}	7575.27	9159.3
10_{-3}	6926.26	.....	13_{-8}	7575.94	.....
10_{-2}	6959.66	8540.67	13_{-7}	7753.61	.....
10_{-1}	7075.14	.....	13_{-6}	7766.40	.....
10_0	7080.58	8668.11	13_{-5}	.....	.....
10_1	7243.72	.....	13_{-4}	7942.36	.....
10_2	7244.36	.....	13_{-3}	.....	.....
$10_{3,4}$	7435.4	.....	13_{-2}	8105.32	.....
$10_{5,6}$	7647.3	9347.6	13_{-1}	.....	.....
$10_{7,8}$	7874.7	.....	$13_{0,1}$	8302.26	.....
$10_{9,10}$	8115.1	.....	$13_{2,3}$	.....	.....
			$13_{4,5}$	8746.0	.....
$11_{-11,-10}$	6631.42	8167.78	$13_{6,7}$	8992	.....
11_{-9}	6846.07	.....			
11_{-8}	6846.42	8407.21	$14_{-14,-13}$	7358.68	8889.6
11_{-7}	7023.36	.....	$14_{-12,-11}$	7637.0	9198.9
11_{-6}	7028.50	8607.68	14_{-10}	7876.21	.....
11_{-5}	7152.76	.....	14_{-9}	7876.46	.....
11_{-4}	7185.97	8782.75	14_{-8}	8078.87	.....
11_{-3}	7237.48	.....	14_{-7}	8085.12	.....
11_{-2}	7340.12	.....			
11_{-1}	7352.05	.....	$15_{-15,-14}$	7636.8	9165.2
11_0	7509.0	.....	$15_{-13,-12}$	7935.5	.....
11_1	7510.8	.....	$15_{-11,-10}$	8195.6	.....
$11_{2,3}$	7700.8	.....	15_{-9}	.....	.....
$11_{4,5}$	7913.2	.....	15_{-8}	8425.2	.....
$11_{6,7}$	8142.6	.....			
$11_{8,9}$	8385.0	.....	$16_{-16,-15}$	7931.9	9457.8
$11_{10,11}$	8638.4	.....	$16_{-14,-13}$	8250.4	.....
			$16_{-12,-11}$	8532.9	.....
$12_{-12,-11}$	6856.48	8391.4			
$12_{-10,-9}$	7092.4	8654.07	$17_{-17,-16}$	8244.1	9767.8
12_{-8}	7280.7	8869.4	$17_{-15,-14}$	8583.7	.....
12_{-7}	7283.4	.....	$17_{-13,-12}$	8885.5	.....
12_{-6}	7444.05	9024.1			
12_{-5}	7466.10	.....	$18_{-18,-17}$	8573.4	.....
12_{-4}	7554.46	.....	$18_{-16,-15}$	8933.7	.....
12_{-3}	7627.38	.....	$18_{-14,-13}$	9255.2	.....
12_{-2}	7650.73	.....			
12_{-1}	7795.95	.....	$19_{-19,-18}$	8920.1	.....
12_0	7800.0	.....	$19_{-17,-16}$	9305.6	.....
$12_{1,2}$	7999.7	.....			
$12_{3,4}$	8202.3	.....	$20_{-20,-19}$	9283.5	.....
$12_{5,6}$	8432.6	.....			
$12_{7,8}$	8677.5	.....	$21_{-21,-20}$	9664.5	.....

TABLE 5. *Energy levels (cm^{-1}) of 012, 022, and 032 vibration states*

J_r	$v_1v_2^0v_3^1$			J_r	$v_1v_2^0v_3^1$		
	012	022	032		012	022	032
0_0	9000.10	.....	.....	7_{-4}	.....	.....	.....
				7_{-3}	9772.48	.....	.....
1_{-1}	9023.51	.....	.....	7_{-2}	.....	.....	.....
1_0	9037.20	.....	.....	7_{-1}	9833.65	.....	.....
1_1	9042.79	.....	.....	7_0	9924.9	.....	.....
				7_1	9928.99	.....	.....
2_{-2}	9068.74	.....	.....	7_2	10060.76	.....	.....
2_{-1}	9078.29	.....	.....	7_3	10061.15	.....	.....
2_0	9095.16	.....	.....	$7_{4,5}$	10211.83	.....	.....
2_1	9135.82	.....	.....	$7_{6,7}$	10395.5	.....	.....
2_2	9137.21	.....	.....				
				$8_{-8,-7}$	9718.90	11235.2	12718.8
3_{-3}	9133.58	.....	.....	8_{-6}	.....	.....	.....
3_{-2}	9138.98	.....	.....	8_{-5}	9864.09	.....	.....
3_{-1}	9172.47	.....	.....	8_{-4}	.....	.....	.....
3_0	9205.99	.....	.....	8_{-3}	9995.6	.....	.....
3_1	9212.47	.....	.....	8_{-2}	.....	.....	.....
3_2	9287.18	.....	.....	8_{-1}	10116.86	.....	.....
3_3	9287.42	.....	.....	8_0	.....	.....	.....
				8_1	10254.39	.....	.....
4_{-4}	9216.10	.....	.....	8_2	.....	.....	.....
4_{-3}	9218.82	.....	.....	$8_{3,4}$	.....	.....	.....
4_{-2}	9273.19	.....	.....	$8_{5,6}$	10588.4	.....	.....
4_{-1}	9288.19	.....	.....				
4_0	9315.1	.....	.....	$9_{-9,-8}$	9887.9	11403.9	12887.1
4_1	9383.09	.....	.....	9_{-7}	10056.69	.....	.....
4_2	9384.57	.....	.....	9_{-6}	.....	.....	.....
$4_{3,4}$	9490.92	.....	.....	9_{-5}	.....	.....	.....
				9_{-4}	.....	.....	.....
5_{-5}	9316.14	.....	.....	9_{-3}	.....	.....	.....
5_{-4}	9316.97	.....	.....	9_{-2}	.....	.....	.....
5_{-3}	9394.95	.....	.....	9_{-1}	.....	.....	.....
5_{-2}	9411.60	.....	.....	9_0	.....	.....	.....
5_{-1}	9444.69	.....	.....	9_1	.....	.....	.....
5_0	9502.64	.....	.....	$9_{2,3}$	.....	.....	.....
5_1	9508.18	.....	.....	$9_{4,5}$	10805.5	.....	.....
5_2	9611.48	.....	.....	$9_{6,7}$	11004.1	.....	.....
5_3	9611.79	.....	.....				
$5_{4,5}$	9745.59	.....	.....	$10_{-10,-9}$	10074.61	11590.1	13073.0
				10_{-8}	10264.9	.....	.....
6_{-6}	9432.52	.....	.....				
6_{-5}	9433.51	.....	.....	$11_{-11,-10}$	10279.1	11793.1	13276.0
6_{-4}	9533.18	.....	.....	$11_{-9,-8}$	10490.7	.....	.....
6_{-3}	9545.32	.....	.....				
6_{-2}	9608.2	.....	.....	$12_{-12,-11}$	10501.2	12013.5	13495.9
6_{-1}	9645.23	.....	.....	$12_{-10,-9}$	10732.9	12271.0	.....
6_0	9657.66	.....	.....				
6_1	9756.20	.....	.....	$13_{-13,-12}$	10740.9	12250.8	13731.1
6_2	9757.53	.....	.....	$13_{-11,-10}$	10992.2	12528.2	.....
$6_{3,4}$	9891.22	.....	.....				
$6_{5,6}$	10047.54	.....	.....	$14_{-14,-13}$	10998.3	12504.6	13984.2
				$15_{-15,-14}$	11268.8	12774.6	.....
7_{-7}	9566.91	.....	.....				
7_{-6}	.....	.....	.....				
7_{-5}	9692.27	.....	.....	$16_{-16,-15}$	11558.2	.....	.....

Another way in which the reasonableness of the observed energy levels may be seen (in addition to the good agreement of the combination differences and calculations of the type first mentioned) is in the arrangement of the energy levels, or of the observed lines, in series that show regular trends with J and $(J+\tau)$. Two such arrays will be demonstrated; others can readily be assembled from the data of table 1. In table 7 the lines of the R_{01} branch, for $J \geqq 8$, are tabulated. Regularities may be noted for all the values of $(J+\tau)$, and the way in which the various $(J+\tau)$ series diverge and converge is characteristic. There is an obvious perturbation of the $(J+\tau)=8$ series at $J=12$, as mentioned above; similar perturbations of $(J+\tau)=6$ and $(J+\tau)=4$ occur at lower J values. The highest J entries in table 7 are rather uncertain, inasmuch as they cannot be confirmed by combination differences; on the basis of the series regularities and intensities they appear plausible however. Note that at frequencies greater than 5,560 cm^{-1} practically all of the identified lines belong to this branch, and that the array

TABLE 6. *Rotational energies for $J=12$*

τ	011			000		
	Calculated	Observed	Δ	Calculated	Observed	Δ
	cm^{-1}	cm^{-1}	cm^{-1}	cm^{-1}	cm^{-1}	cm^{-1}
−12, −11	1553.26	1525.29	7.97	1565.62	1558.07	7.55
−10	1773.43	1761.20	12.23	1787.22	1774.75	12.47
−9	1773.53	1761.20	12.33	1787.29	1774.88	12.41
−8	1983.12	1949.50	23.62	1981.36	1960.38	20.98
−7	1985.12	1962.20	22.92	1982.24	1962.60	19.64
−6	2150.24	2112.86	37.38	2138.02	2106.70	31.32
−5	2169.78	2134.91	34.87	2153.31	2124.84	28.47
−4	2264.04	2223.27	40.77	2245.29	2205.95	39.34
−3	2342.16	2296.19	45.97	2310.81	2275.65	35.16
−2	2371.52	2319.54	51.98	2341.38	2300.94	40.44
−1	2528.39	2464.76	63.63	2478.72	2434.14	44.58
0	2532.38	2468.80	63.58	2483.18	2437.84	45.34
1	2747.47	2659.50	87.97	2675.37	2613.26	62.11
2	2747.74	2659.50	88.24	2675.70	2613.49	62.21
3, 4	3004.33	2871.10	133.23	2906.07	2813.94	92.13
5, 6	3258.49	3101.40	197.09	3170.48	3033.17	137.31
7, 8	3029.13	3346.30	282.83	3467.84	3267.20	200.64
9, 10	3985.78	3699.30	386.48	3797.67	3512.80	284.87
11, 12	4398.15	3877.50	520.65	4159.71	3767.10	392.61

of table 7 includes most of the strong lines in that region.

Table 8 shows the series regularities of the strongest P_{01}^{01} branches, those with $J+\tau=0$, for all the bands; it will be noted that there are also regularities in the vibration sequences. In addition to the line frequencies, the line intensities are tabulated; when overlapping occurs, the intensities are given in parentheses. The theoretical rotational and vibrational intensity factors are also given.

Table 8 also demonstrates the second criterion, by which it is believed that the correct assignment has been made, namely, the agreement between the observed and calculated intensities. Both for the lines in table 8 and throughout the assignments there is gratifying parallelism between those quantities. Better agreement could hardly be expected, since it must be realized that the observed intensities are often irregualrly disturbed by weak neighboring lines (not to mention the large disturbances by atmospheric absorption of many lines, including all those of band a, between 5,100 and 5,600 cm^{-1}), and that the analysis is incomplete, so that unidentified transitions of higher J may be making additional contributions. The necessary condition for a satisfactory analysis, that no lines of high and medium intensity are predicted where there is no emission, has been met.

The agreement between the observed intensities of unblended lines and those calculated for 2,877° K shows that there is a possibility of using the H_2O emission for temperature determination. This cannot be done with complete confidence, however, until an even more complete analysis, or better resolution, has been achieved. On the basis of the present results it would appear that in the flames studied there is equilibrium within both the rotational and vibrational degrees of freedom, and that the temperature is within perhaps 500° of 2,877° K. While it is gratifying that an assignment can be given to nearly 90 percent of the lines observed, and that this accounts for all the predicted lines of intensity greater than 10 and about 75 percent of the total predicted intensity, there are no clear-cut criteria, as there are in the spectra of diatomic molecules, for determining whether a weak unassigned line may not be contributing to the observed intensity. Hence, although it is tempting to use the observed relative intensities of two lines that lie close in frequency but come from widely different energy levels, such as 5,600.65 cm^{-1}, ($E''=8{,}920$) and 5,602.55 cm^{-1} ($E''=7{,}193$) as a "thermometric pair", it may lead to error unless still higher resolution reveals the lines to be truly single.

The analysis also shows that there is no simple correlation between the frequency and the upper-state energy. In general, it is the case that the emission comes from higher and higher levels as one goes toward the wings of the band, but there are frequent exceptions inasmuch as the various bands, and the various sub-branches of a given band, overlap in a complicated manner. Hence it is questionable whether measurements with low-resolution spectrometers, comparing the relative intensity and emissivity in frequency intervals 10 to 20 cm^{-1} wide, could yield temperature determinations of high accuracy. There is no doubt however that measurements of this kind would be useful in a rough way, particularly if the present results are used to choose frequency ranges where the radiation comes principally from levels of nearly the same E''.

It was stated earlier that the empirical evidence indicated that the maximum emissivity did not exceed 0.2 to 0.4 at the cores of the strongest lines. This is a condition that is necessary if self-absorption effects are not to vitiate intensity measurements and temperature determinations [16, 17]. The emissivity of the strongest line, at 4,999.9 cm^{-1}, may be calculated approximately from the following data. The relative line intensity (sum of the three components listed in table 1) is 52. The total integrated intensity of the band, as determined from absorption measurements, is equivalent to 20 cm^{-2} atm^{-1} (atmosphere here refers to standard temperature and pressure). The fraction of this in the 5,000 cm^{-1} line is $20 \times 52/Q_rQ_v$, where the Q values are the rotational and vibrational partition functions, respectively 5,550 and 2.62 at 2,877° K. Hence the integrated absorption coefficient of the line is 0.072 cm^{-2} atm^{-1}. If the path length is 2 cm and the H_2O content of the outer-cone gas 80 percent, there are $0.80 \times 273/2877 = 0.152$ cm atm of H_2O in the line of sight. Hence the total line strength, S, is $0.072 \times 0.152 = 1.1 \times 10^{-3}$ cm^{-1}. The line shape will probably be Lorentzian, with a half-width γ_L of the order of 0.05 cm^{-1}. (The half-width of pure H_2O vapor at 100° C and 1 atm is about 0.4 cm^{-1}; its variation with temperature and pressure is uncertain, but the above estimate is of the correct order of magnitude, and is somewhat

TABLE 7. *Series regularities in the $R_{0,1}$ branch of 011–000*

	$J'+\tau$																
J'	0-1	2	3	4	5	6	7	8	9	10	11	12	13	14	15-16	17-18	19-20	21-22
8	.....	5507.50	5505.32	5535.95	5527.89	5571.82	5543.70	5548.96	5555.99	5556.13	5567.13		5580.59					
9	5489.50	5523.20	5521.74	5554.19	5547.10	5574.61	5564.83	5574.61	5577.88	5580.15	5580.06		5602.55		5614.99			
10	5503.19	5538.03	5537.20	5570.07	5564.83	5595.42	5584.87	5599.04	5599.77	5603.44	5612.26	5612.60	5624.95		5637.18	5649.30		
11	5516.73	5552.45		5584.87	5582.07	5614.47	5604.50	5621.43	5620.94	5627.49	5633.98	5634.92	5645.77		5658.91	5671.34	5683.70	
12	5529.05	5566.68		5599.77	5598.19	5630.59	5623.37	5654.80	5641.21	5651.68	5657.30	5655.50	5668.35		5679.80	5691.55	5704.06	5716.21
13	5541.18	5580.50		5614.90	5613.51	5646.86	5642.02	5674.04	5656.78	.....	5671.34	.....	5689.14	.....	5700.92	5712.80	5724.80	5736.73
14	5551.82	5594.30		5629.11	5628.35	5662.89	5659.75	5694.78	5673.29	5702.51	.....	5690.55	.....	5711.79	5722.43	5733.80	5745.85	5758.32
15	5562.96	5607.85		5644.65		5679.80	5679.80	.....	5690.14	.....	5707.54	.....	5727.49	.....	5743.26	5753.54	5765.96	5778.66
16	5573.30	5618.89		5659.75		5689.55	.....	5738.29	5705.35	5747.54	.....	.....	.....	5757.67	.....	.....	5785.97	
17	5582.94	5630.59		5674.82		.....	5717.13	.....	5719.34	.....	.....	.....	.....	.....	.....	.....	5806.12	
18	5592.03	5642.02		5687.77		5734.90		5773.75										
19	5600.65	5653.30		5700.23		5750.51												
20	5608.83	5663.63		5711.79		5763.75												
21	5616.52	5674.04		5722.43														
22	5623.37	5683.76		5731.82														
23	5630.29	5693.32																
24	5636.07																	

TABLE 8. *$J+\tau=0$ series in the P_{01} branches of 10 bands in the 011–000 sequence*

	Band...	a		b		c		d		h		e		j		k		f		g	
	v'.....	011		021		031		041		051		012		022		032		111		121	
	v''.....	000		010		020		030		040		001		011		021		100		110	
J'	vif [a]	100		90		62		39		23		28		25		16		16		15	
	rif [b]	ν	I	ν	I	ν	I	ν	I	ν	I	ν	I	ν	I	ν	I	ν	I	ν	I
7	23	5163.86	15	5110.84	41	5059.45	40	5005.18	35	.....	...	5078.75	(36)								
8	24	41.95	30	5089.05	45	37.91	32	4985.36	25	.....	...	57.35	18	5001.55	17	4945.71	20	4963.83	30	4910.80	(35)
9	25	19.63	48	67.91	45	16.86	35	65.39	37	4915.83	22	34.99	16	4980.12	14	25.35	19	42.49	25	4860.00	55
10	25	5096.57	45	45.79	45	4995.23	25	44.76	30	4906.02	11	12.39	(21)	58.84	(33)	05.13	20	20.25	20	68.81	15
11	24	73.35	65	23.07	44	73.16	(66)	24.05	(50)	75.86	10	4960.00	25	36.65	30	4884.72	20	4897.49	11	47.14	20
12	23	49.65	(85)	4999.99	(90)	51.28	55	02.86	(60)	55.74	10	66.60	18	14.62	25	63.34	15	73.87	16	24.50	14
13	22	25.47	45	76.72	55	28.11	50	4881.10	17	35.32	9	43.75	30	4892.12	20	41.30	15	49.25	27		
14	21	4999.99	(90)	51.77	45	03.87	20	39.80	15	.....	..	18.74	15	67.81	95	19.02	15	24.30	14		
15	19	75.66	50	27.77	56	4880.27	30	37.78	12	.....	..	4893.22	(35)	42.70	16	4797.56	10	4799.96	13		
16	18	50.46	45	02.86	(60)	56.75	25	.....	..	.....	..	67.00	30	16.60	12	73.85	7				
17	16	24.08	40	4878.40	40	32.89	22	.....	..	.....	..	41.30	15	4789.45	12						
18	14	4898.51	50	53.12	30	08.66	20	.....	..	.....	..	15.42	13								
19	13	72.21	28	27.59	27	4784.66	15														
20	11	45.34	40	01.75	18	60.71	10														
21	9	18.41	24	4776.02	17																
22	8	4791.47	15	50.05	16																
23	7	64.34	23	23.66	10																
24	6	35.54	10																		

[a] vif, vibrational intensity factor. [b] rif, rotational intensity factor.

greater than the Doppler half-width, $\gamma_D = 0.023$ cm^{-1}). Hence the maximum emissivity, given by $1 - e^{-S/\pi\gamma_L}$, would be 0.07, which is of the observed order of magnitude and definitely well below unity. This rough agreement also tends to confirm that the excitation of the H_2O vibrational states is predominantly thermal. In the 2.7-μ fundamental, where the integrated intensity of the band is an order of magnitude greater, self-absorption effects would begin to be encountered.

5. References

[1] E. K. Plyler and C. J. Humphreys, J. Research NBS **40,** 449 (1948) RP1890.

[2] G. Herzberg, Infrared and raman spectra of polyatomic molecules, p. 280 (D. Van Nostrand & Co., Inc., New York, N. Y., 1945).

[3] W. S. Benedict, unpublished data.

[4] NBS Symposium on Energy Transfer in Hot Gases, NBS Circular 523, especially papers by W. S. Benedict and E. K. Plyler; H. P. Broida; S. S. Penner; G. Dieke and H. M. Crosswhite; and A. G. Gaydon. Also A. G. Gaydon, Spectroscopy and combustion theory (Chapman & Hall, Ltd., London, 1948).

[5] R. C. Nelson, Atlas and wavelength tables showing the absorption of water vapor in the regions 1.33 to 1.48 and 1.77 to 1.98 microns (Department of Physics, Northwestern University, Evanston, Ill., 1949).

[6] W. S. Benedict and E. K. Plyler, J. Chem. Phys. **21,** 498 (1953).

[7] G. A. Hornbeck and R. C. Herman, Ind. Eng. Chem. **43,** 2739 (1951).

[8] J. Taylor, W. S. Benedict, and J. Strong, J. Chem. Phys. **20,** 1884 (1952).

[9] O. C. Mohler, R. R. McMath, A. K. Pierce, and L. Goldberg, Photometric atlas of the near infrared solar spectrum, (University of Michigan, Ann Arbor, 1951).

[10] P. C. Cross, R. M. Hainer, and G. W. King, J. Chem. Phys. **12,** 210 (1949).

[11] D. F. Eggers and B. L. Crawford, Jr., J. Chem. Phys. **19,** 1554 (1951).

[12] B. T. Darling and D. M. Dennison, Phys. Rev. **57,** 128 (1940).

[13] G. H. Dieke, Phys. Rev. **60,** 523 (1941).

[14] W. S. Benedict and E. K. Plyler, J. Research NBS **46,** 246 (1951) RP2194.

[15] W. S. Benedict, H. H. Claassen, and J. H. Shaw, J. Research NBS **49,** 91 (1952) RP2347.

[16] R. D. Cowan and G. H. Dieke, Rev. Mod. Phys. **20,** 418 (1948).

[17] S. S. Penner, J. Chem. Phys. **21,** 31 (1953).

WASHINGTON, August 12, 1953.

U. S. GOVERNMENT PRINTING OFFICE: 1954